

Critical properties of the Bose-Hubbard model

Von der Fakultät für Mathematik und Naturwissenschaften
der Carl von Ossietzky Universität Oldenburg
zur Erlangung des Grades und Titels eines
Doktors der Naturwissenschaften (Dr. rer. nat.)
angenommene

Dissertation

von Herrn Diplom-Physiker

Dennis Hinrichs

geboren am 27. Juli 1982 in Sögel

Erstgutachter:

Prof. Dr. Martin Holthaus

Zweitgutachter:

Priv.-Doz. Dr. Axel Pelster (HWK Delmenhorst und TU Kaiserslautern)

Tag der Disputation: 10. September 2012

für Anke

Zusammenfassung

Diese Dissertation behandelt im Wesentlichen zwei Themen: ultrakalte Atome und kritische Phänomene. Dabei liegt der Schwerpunkt aller Untersuchungen auf dem Bose-Hubbard Modell, das ein Vielteilchensystem von ultrakalten Bosonen auf einem optischen Gitter beschreibt. Obwohl die entscheidenden Merkmale dieses Modells nur durch zwei Terme bestimmt werden, einen Tunnel- und einen kurzreichweitigen Wechselwirkungsterm, weist es sehr komplexe Eigenschaften auf, die sich nur unter vergleichsweise großem Aufwand bestimmen lassen. Die wichtigste Eigenschaft ist die Existenz eines Quantenphasenübergangs vom Mott-Isolator hin zu einem superfluiden Zustand. Dieser Phasenübergang ist das Resultat der Konkurrenz zwischen dem Tunneln und der Wechselwirkung. Der Mott-Isolator wird charakterisiert durch lokalisierte Teilchen, da in diesem Zustand der Wechselwirkungsterm dominiert, während im superfluiden Zustand das Tunneln dominiert und die Teilchen über viele Gitterplätze delokalisiert sind.

Der Phasenübergang wird begleitet durch das Auftreten sowohl einer Kondensatdichte, die den Anteil von Teilchen im Grundzustand des Systems angibt, als auch einer Superfluiddichte, die entsprechend den Anteil von superfluiden Teilchen angibt. Ziel dieser Arbeit ist das Berechnen dieser Größen und die Untersuchung ihres kritischen Verhaltens hinsichtlich kritischer Exponenten. Obwohl diese kritischen Exponenten über die Zugehörigkeit des Bose-Hubbard Modells zu einer genau untersuchten Universalitätsklasse prinzipiell bekannt sind, steht die direkte Berechnung der korrekten kritischen Exponenten noch aus.

Die Einleitung im ersten Kapitel soll einen Überblick über die Physik ultrakalter Atome und speziell die des Bose-Hubbard Modells aus der Perspektive eines sogenannten Quantensimulators geben, welcher im Prinzip die Eigenschaften eines perfekt kontrollierbaren physikalischen Systems innehat. Der

Quantensimulator stellt in dieser Hinsicht eine große Motivation für die Untersuchung ultrakalter Atome dar. Weiterhin gibt dieses Kapitel einen Überblick über einige der wichtigsten Konzepte und Experimente, die zum Beispiel zur Realisierung der Bose-Einstein Kondensation oder des Quantenphasenübergangs vom Mott-Isolator zum Superfluid des Bose-Hubbard Modells geführt haben. Am Ende des Kapitels wird zudem das Bose-Hubbard Modell theoretisch eingeführt und zusätzlich werden wesentliche Eigenschaften dieses Modells diskutiert.

Das zweite Kapitel bietet einen Überblick über das Gebiet kritischer Phänomene. Als erstes werden Phasenübergänge phänomenologisch diskutiert. Nachdem im zweiten Abschnitt einige Ansätze zur quantitativen Analyse von Phasenübergängen eingeführt wurden, erläutert der dritte Abschnitt die Konzepte der Universalitätsklasse und der kritischen Exponenten. Am Ende werden einige Experimente vorgestellt, mit denen die wichtigsten dieser kritischen Exponenten gemessen wurden.

Da ein großer Teil der Rechnungen und damit auch der Resultate auf Störungstheorie beruhen, bietet das dritte Kapitel am Anfang eine detaillierte Erläuterung von Katos Formulierung der störungstheoretischen Reihe. Anschließend werden grundlegende Eigenschaften dieses Ansatzes diskutiert, der exemplarisch zur Berechnung der Grundzustandsenergie des Bose-Hubbard Modells genutzt wird. Diese Störungstheorie kann auch diagrammatisch interpretiert werden, und führt so zum sogenannten Prozesskettenansatz, der am Ende des Kapitels wiederum am Beispiel der Grundzustandsenergie des Bose-Hubbard Modells näher erläutert wird.

Um auch Zugang zum Superfluid zu Mott-Isolator Phasenübergang und damit zu dessen kritischen Exponenten zu bekommen, werden auch Methoden zur Resummation benötigt, um die für endliche Ordnungen erhaltenen Resultate der Störungstheorie in ein nicht-perturbatives Regime zu überführen. Die Einführung dieser Methoden erfolgt im vierten Kapitel. Der erste Abschnitt behandelt die Methode des effektiven Potentials, die eine Berechnung des oben erwähnten Phasenübergangs erlaubt. Dieses Verfahren erlaubt zudem einen Zugang zu bestimmten Größen, die allein für das Superfluid charakteristisch sind, obgleich die störungstheoretischen Rechnungen startend im Mott-Isolator durchgeführt werden. Darüber hinaus wird mit dem Ziel, die kritis-

chen Exponenten der Kondensatdichte sowie der Superfluidichte mit Hilfe der störungstheoretischen Resultate zu berechnen, im zweiten Abschnitt die Variationsstörungstheorie eingeführt. Mit Hilfe dieser Theorie können Schwachkopplungsreihen zu Starkkopplungsreihen transformiert werden, die einen direkten Zugang zu den kritischen Exponenten bieten.

Im letzten Kapitel werden die neu gewonnenen Resultate dieser Arbeit präsentiert. Im ersten Abschnitt wird eine leicht modifizierte Methode zur Bestimmung der Phasengrenze eingeführt. Nach einer Diskussion der Eigenschaften des effektiven Potentials wird die Teilchenzahl innerhalb des superfluiden Regimes ausgewertet. Diese weisen Linien konstanter Dichte auf, die mit Hilfe des effektiven Potentials berechnet werden können. Im vierten Abschnitt werden Resultate für die Kondensatdichte und für die Superfluidichte vorgestellt. Dort wird auch der Einfluss der Koeffizienten des effektiven Potentials für gerade bzw. ungerade Ordnungen erörtert, und es wird demonstriert, dass dieser bei der Berechnung der kritischen Exponenten berücksichtigt werden muss. Schlussendlich werden im letzten Abschnitt zwei Methoden eingeführt, die die Bestimmung der kritischen Exponenten erlauben. Die erste Methode basiert auf den störungstheoretischen Ergebnissen für ungerade Ordnungen und benötigt die Anwendung der Variationsstörungstheorie. Die zweite Methode bietet einen direkten Zugang zu den kritischen Exponenten über die Resultate der geraden Ordnungen, verlangt jedoch einen erhöhten numerischen Aufwand.

Abstract

This thesis concerns two topics: ultracold atoms and critical phenomena. The focus of all studies presented herein lies on the Bose-Hubbard model which describes a many-body system of ultracold atoms in an optical lattice. Although the main features of this model are defined by only two terms, a tunneling term and a short-range interaction term, its properties are very complex and hard to study. The most important feature is the occurrence of a quantum phase transition from a Mott insulator to a superfluid. This phase transition is the result of the competition of tunneling and interaction. The Mott insulator is characterized by localized particles since in this state the repulsive interaction term dominates, while in the superfluid state the tunneling term dominates and the particles are delocalized over many lattice sites.

This phase transition to the superfluid state is accompanied by the emergence of both a condensate density, which indicates the number of particles in the ground state, and a superfluid density, which gives accordingly the fraction of superfluid particles. The aim of this thesis is to calculate these quantities, and to study their behavior in terms of critical exponents. Although these critical exponents are known in principle because the Bose-Hubbard model belongs to a well-known universality class, a direct calculation of the correct critical exponents remains to be done.

The introduction in the first chapter is meant to view the physics of ultracold atoms and especially of the Bose-Hubbard model from the perspective of a quantum simulator which is basically a perfectly controllable physical system. The quantum simulator is, therefore, an important stimulus for the field of ultracold atoms. An overview is given of the most important concepts and experiments which led to, e.g., the measurement of the Bose-Einstein condensation, or of the superfluid-to-Mott insulator phase transition of the Bose-Hubbard model. At the end of this chapter the Bose-Hubbard model is theoretically

introduced and its basic properties are discussed.

The second chapter gives an overview over the field of critical phenomena. First the phenomenology of phase transitions is discussed. After introducing some ansatzes for a quantitative approach to phase transitions, the concept of universality classes and their critical exponents is treated. At the end some experiments are discussed, which have measured the most important of these critical exponents.

Since a major part of the calculations and therefore of the results are based on perturbation theory, the third chapter provides a detailed description of Kato's formulation of the perturbation series. After that some basic properties of this approach are discussed, and it is applied exemplarily to the Bose-Hubbard model in order to calculate the ground-state energy up to the third order. This perturbation theory can be interpreted diagrammatically and leads to the process-chain approach, which again is explained by using the example of the calculation of the ground-state energy of the Bose-Hubbard model at the end of this chapter.

To gain access to the superfluid-to-Mott insulator phase transition and, therewith, its critical properties, one also needs various non-perturbative methods for processing the finite-order results of the perturbational calculations, which are introduced in the fourth chapter. The first section treats the method of effective action which allows the calculation of the phase boundary of the afore-mentioned phase transition and which permits access to certain quantities characterizing the superfluid phase, although the perturbative calculations are done starting from the ground state of the Mott insulator. Moreover, with the aim to extract the critical exponents of the condensate and the superfluid density from the perturbational results, the variational perturbation theory is introduced in the second section. With this theory, weak-coupling series are transformed to strong-coupling series which provide a direct access to the critical exponents.

In the last chapter the new results obtained in this thesis are presented. In the first section a slightly modified method for determining the phase boundary is introduced. After a discussion of the properties of the effective potential, the particle number inside the superfluid regime is evaluated. It shows lines of constant density which can be calculated from the effective action. In the fourth

section the results for the condensate and the superfluid density are presented. There also the influence of the odd- and even-order coefficients of the effective potential are discussed and it is demonstrated that the calculation of the critical exponents of both densities has to account for this distinction. Finally, in the last section two methods are established which enable the determination of the critical exponents. The first method is based on the odd-order results of the perturbational calculations and requires the use of the variational perturbation theory. The second method yields a direct access to the critical exponents via the even-order results but it also requires a greater numerical effort.

Contents

List of Figures	XI
List of Tables	1
1 Introduction	3
1.1 Quantum simulators	3
1.2 Cooling methods	4
1.3 Bose-Einstein condensation	6
1.4 Bose-Hubbard model	11
2 Critical phenomena	17
2.1 Phase transitions	20
2.1.1 Discontinuous phase transitions	22
2.1.2 Continuous phase transitions	22
2.1.3 Thermodynamic limit	24
2.2 Theories for describing phase transitions	24
2.2.1 Mean-field theory	25
2.2.2 Landau theory and ϕ^4 -theory	26
2.3 Critical exponents	31
2.3.1 ϕ^4 -theory	33
2.3.2 Scaling relations	38
2.3.3 Experimental measurements	39
3 Perturbation theory	43
3.1 Kato's perturbation theory	43
3.2 Properties and applications	49
3.2.1 Standard form of matrix elements	49

3.2.2	Calculation of correlation functions	51
3.2.3	Energy eigenvalues in third-order perturbation theory . .	53
3.2.4	Process-chain approach	55
4	Non-perturbative methods	61
4.1	Method of effective action	62
4.2	Variational perturbation theory	68
4.2.1	Strong-coupling transformation	69
4.2.2	Application to the Bose-Hubbard model	74
5	Results	79
5.1	Phase boundary	79
5.2	Properties of effective potential	86
5.3	Particle number	95
5.4	Condensate and superfluid density	95
5.5	Critical exponents	104
5.5.1	$ \psi ^4$ -approach	105
5.5.2	$ \psi ^6$ -approach	110
6	Summary	115
	Bibliography	117

List of Figures

1.1	Schematic illustration of laser cooling and evaporative cooling	5
1.2	Bose-Einstein condensation explained via de Broglie wavelength	8
1.3	Image of Bose-Einstein condensate	9
1.4	Scattering length depending on Feshbach resonances	10
1.5	Phase diagram of Bose-Hubbard model	14
2.1	Phase diagram of water	18
2.2	Illustration of the universality of a phase transition	19
2.3	Free energy and its derivatives at critical point	23
2.4	Landau theory of continuous and discontinuous phase transitions	29
2.5	Vortices appearing at Kosterlitz-Thouless phase transition and Mexican hat potential	36
2.6	Specific heat and superfluid density of λ -transition	40
2.7	Condensate density and the correlation length of λ -transition	41
3.1	One-dimensional energy diagrams	57
4.1	Diagrams for calculating effective potential	65
4.2	Radius of convergence of condensate density	75
5.1	Extrapolation schemes for determination of phase boundary	81
5.2	Phase boundary for $D = 2$ and $D = 3$	83
5.3	Triangular and hexagonal lattices	85
5.4	Even order coefficients of effective potential for $D = 2$	90
5.5	Odd order coefficients of effective potential for $D = 2$	92
5.6	Coefficients of effective potential for $D = 3$	94
5.7	Lines of constant particle number inside superfluid region	96

5.8	Properties of condensate density for $D = 2$	98
5.9	Condensate density for $D = 2$ and $D = 3$	99
5.10	Influence of twist on superfluid density	101
5.11	Superfluid and condensate density for $D = 2$ and $D = 3$	103
5.12	Logarithmic derivatives of condensate and superfluid density	106
5.13	Determination of variational parameter q for the condensate density	108
5.14	Logarithmic derivative of condensate density	111
5.15	Intervals used for extrapolating the logarithmic derivative	113

List of Tables

2.1	Universality classes of phase transitions	31
2.2	Definition of critical exponents	33
2.3	Critical exponents of ϕ^4 -theory for $D = 2$ and $D \geq 4$	34
2.4	Critical exponents of ϕ^4 -theory for $D = 3$	35
3.1	Energy diagrams and their weight factors	59
5.1	Critical values of superfluid-to-Mott insulator phase transition	84
5.2	Critical exponents of $ \psi ^4$ -approach for $D = 2$	109
5.3	Critical exponents of $ \psi ^6$ -approach for $D = 2$	112

1 Introduction

At the moment the research area of ultracold quantum gases is one of the liveliest fields in physics. The promising fusion of atomic physics and quantum optics has led to various fascinating developments in the last 30 years. In this introduction some milestones leading to remarkable experiments are presented. In particular, we deal with the first realization of a Bose-Einstein condensate in 1995 [1, 2], honored with the physics noble price in 2001, the measurement of Fermi degeneracy [3–5], and the observation of the superfluid-to-Mott insulator quantum phase transition in an optical lattice [6].

1.1 Quantum simulators

To start with, the latter experiment can be connected to something at first sight completely different. In 1982 R. Feynman proposed an entirely new approach to study physics [7]. Instead of looking for solutions of complicated systems by using analytical or numerical methods, he suggested to simulate physics with computers which “*will do exactly the same as nature*”. Today this approach is known under the keyword “quantum simulator” and is the objective of many research branches. The effort becomes understandable if one estimates how large a quantum system maximally can be in order to be simulable on a classical computer. For a quantum system with N spin-1/2 particles, 2^N possible states exist and the density matrix has 2^{2N} entries. Already for about 30 particles such systems are not accessible anymore with present-day computers.

One can separate quantum simulators into analog and digital quantum simulators considering the way the original quantum system is simulated [8]. The analog quantum simulator, also known as a quantum emulator, mimics the evolution of the original quantum system. That means one has a simulating

system which is able to reproduce the dynamics of the original system. The main advantage in mapping the evolution of one system to another is that generally one has a far better control over the simulating than over the original system.

The digital quantum simulator is in fact a quantum computer and also known as the universal quantum simulator. In contrast to the analog quantum simulator this quantum simulator should be able to simulate any finite-dimensional local Hamiltonian. A local Hamiltonian can be written as $H = \sum_i H_i$ where each H_i acts on a finite number of particles. The time-evolution is then performed by applying repeatedly the infinitesimal time evolution operator $U_i = e^{-i\Delta t H_i/\hbar}$ [9, 10]. In quantum computing, however, the Hamiltonian is acting on qubits representing the quantum version of bits. Whereas a classical bit is always in one of the two states 0 or 1, a qubit can also exist in any superposition of these states. Generally for simulating a system with N particles the required time scales polynomially on a quantum computer, whereas it scales exponentially for a classical computer as described above [11]. Many candidates for the realization of qubits are under study. An overview of possible physical systems is given in the supplementary material of Ref. [8] and in Ref. [12].

1.2 Cooling methods

Both kinds of quantum simulators have in common that one needs a very good control over all relevant system parameters. One promising candidate for an extensively controllable system consists of ultracold atoms in optical lattices [15, 16].

To realize such a control needed for these experiments, the number of degrees of freedom must be reduced or even frozen out. This also allows one to trap atoms so that one can prevent the atomic gas from heating and to manipulate them in order to perform experiments. Cooling techniques were mainly developed in the 1980s and early 1990s which culminated in the award of the physics noble price in 1997 [17–19]. Most of the cooling techniques depend on the use of lasers.

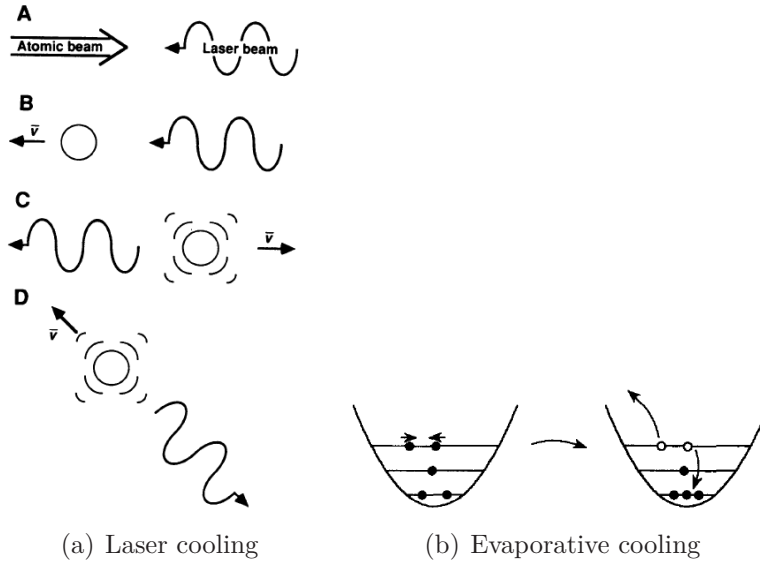


Figure 1.1: Schematic illustration of laser cooling and evaporative cooling. (a) Sketch of the laser cooling process. (A) Laser cooling of an atomic beam with a counter-propagating laser beam. (B) The velocity change of an atom caused by the absorption of a photon from the laser. (C) The velocity change that results from stimulated emission of a photon. (D) The random recoil caused by spontaneous emission [13]. (b) Schematic diagram illustrating the principle of evaporative cooling. Two atoms, with the same initial energies, collide and scatter into different vibrational states. If the hotter atom escapes, the net effect, after rethermalisation, is to leave the remaining sample colder [14].

The first step of a whole ladder of cooling methods is usually Doppler cooling. An atom moving in the direction of a counterpropagating laser beam as depicted in Fig. 1.1(a) absorbs photons and also the momentum of the photons. After one absorption process the atom is excited and is able to emit photons itself. Stimulated emission would not lead to a momentum decrease since these photons are emitted in the same direction as the laser beam and so they would accelerate the atom again. But for spontaneous emission the momentum transfer is zero on the average, leading to a deceleration of the atom. In order to let only fast-moving atoms absorb photons, the laser beam is slightly off-resonant so the absorption rate is higher for atoms moving towards the laser beam than in the other direction due to the Doppler effect. This effect leads to a fric-

tional force $dp/dt = -\gamma v$ on the atoms which can be interpreted as a radiation pressure. To consider the deceleration, laser cooling is often performed in a setup called Zeeman slower. Here the atoms pass through a magnetic field to change the energy level separation of the atoms so as to keep them in resonance with the fixed-frequency laser [13]. A setup consisting of several laser beams propagating in different directions is known as an optical molasses. It cools an atomic gas down to millikelvins in only a few microseconds. E.g., to cool down a sodium atom from room temperature to this temperature circa 10^4 photons must be absorbed and emitted. Every photon leads to a velocity change of 3 cm/s [13]. But due to the emission of photons the atoms can only be cooled down to an equilibrium temperature which is called the Doppler limit.

The last step in order to achieve temperatures of less than 1 μK is evaporative cooling as sketched in Fig. 1.1(b). In this cooling process the hottest atoms are removed purposefully so that the rest cools down by reaching a new thermal equilibrium with a lower total energy and entropy, respectively. This process requires a sufficiently high density since an equilibrium can only be reached by elastic collisions. Many other cooling techniques are known today allowing temperatures down to circa 100 nK and below. Furthermore, the cold atoms must be trapped. For this purpose different concepts such as optical, magnetic or magneto-optical traps have been established [14, 20–22].

1.3 Bose-Einstein condensation

What happens to bosons, if such low temperatures are reached, is predicted by the Bose-Einstein statistics. The foundations of this theory, valid for quantum particles with an integer spin, were laid by S. Bose in 1924 [23] and further interpreted by A. Einstein [24, 25]. He predicted a new state of matter for very low temperatures which is today called a Bose-Einstein condensate. According to the spin-statistics theorem [26] quantum particles with an integer spin are allowed to occupy the same state. If the temperature of a system is lowered, the bosons tend to occupy lower energy states until the state with the lowest energy is occupied with a macroscopic number $N \gg 1$ of particles. Furthermore the thermal de Broglie wave length $\lambda_{\text{dB}} = h/\sqrt{2\pi mk_B T}$ increases during the

cooling process until the point is reached where the thermal de Broglie wave length is equal to or greater than the mean spacing between particles. One would expect the critical temperature to be at that temperature where the system contains at least one particle within the volume λ_T^3 as indicated in Fig. 1.2. That means the onset of the phase transition depends on both the temperature and the density n of the system. The quantity $\varpi = n\lambda_T^3$ is called phase space density and more precise calculations reveal that $\varpi = \zeta(3/2) \approx 2.612$ must hold in order to observe a phase transition, where $\zeta(z)$ is the Riemann zeta function. The critical temperature depends strongly on boundary conditions and scales, e.g., as $T_c \propto [n/\zeta(3/2)]^{2/3}$ for a system in a rigid container and as $T_c \propto [N/\zeta(3)]^{1/3}$ for harmonically trapped atoms [27, 28].

While a Bose-Einstein condensate must occur even for a non-interacting system because of the Bose-Einstein statistics, systems with interaction also show this kind of phase transition. For repulsive interactions one can show this relatively straightforward [28] but for a long time it was unclear if a Bose-Einstein condensate could exist with attractive interactions. But it was shown that this is also possible in certain circumstances which will be briefly described here.

Because the atoms have such a small energy, scattering processes of two atoms can be described by one parameter only, the so-called s-wave scattering length a [22]. For large r the scattering wave function is given by $\psi = e^{ikr} + f(\theta)e^{ikr}/r$. For very low energies and thus $k \rightarrow 0$ the scattering amplitude approaches a constant $-a$ and the scattering wave function is given by $\psi = 1 - a/r$ in this limiting case. The total cross section for bosons is $\sigma = 8\pi a^2$ and zero for identical fermions.

Now, Bose-Einstein condensation for atoms with attractive interaction, for which $a < 0$, is possible if the number of particles in a condensate in a trap potential does not exceed a limiting value $N_m \approx l/|a|$, where N_m is of the order of 10^3 [30–35]. Here l denotes the size of the condensate in the absence of interactions.

In 1995 two groups observed the phase transition to a Bose-Einstein condensate of alkali atoms with repulsive interactions [1, 2]. The two groups used rubidium and sodium, respectively, and reached densities of $10^{12} - 10^{14} \text{ cm}^{-3}$ with $10^4 - 10^6$ condensed atoms, while the transition temperatures were be-

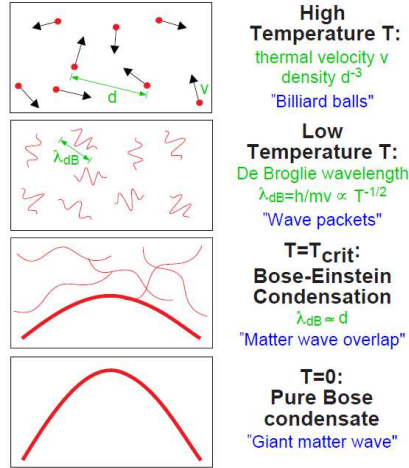


Figure 1.2: At high temperatures, a weakly interacting gas can be treated as a system of “billiard balls”. In a simplified quantum description, the atoms can be regarded as wavepackets with an extension Δx , approximately given by Heisenberg’s uncertainty relation $\Delta x = h/\Delta p$. Here Δp denotes the width of the thermal momentum distribution which is related via $\Delta p^2/2m = k_B T$ to the temperature T . The resulting Δx is approximately equal to the thermal de Broglie wavelength $\lambda_{dB} = h/\sqrt{2\pi m k_B T}$, the matter wavelength for an atom moving with the thermal velocity. At the BEC transition temperature, λ_{dB} becomes comparable to the distance between atoms, and the Bose-Einstein condensate forms which is characterized by a macroscopic population of the ground state of the system. As the temperature approaches absolute zero, the thermal cloud disappears leaving a pure Bose condensate [29].

tween 170 nK and 200 nK. Fig. 1.3 shows absorption images of an experimental observation of a Bose-Einstein condensate at different times after switching off the magnetic trap together with the original caption [29]. The width of the peaks is directly related to the velocity distribution and thus to the temperature of the condensate. The colder the atoms are, the less kinetic energy they possess, so that for a pure condensate one would expect a very narrow peak at the center indicating the condensed particles with momentum $\mathbf{k} = \mathbf{0}$. This situation is almost realized in the last picture of Fig. 1.3.

Today Bose-Einstein condensation has been observed in many other elements ([36, 37] and references therein) and it is already possible to reach tem-

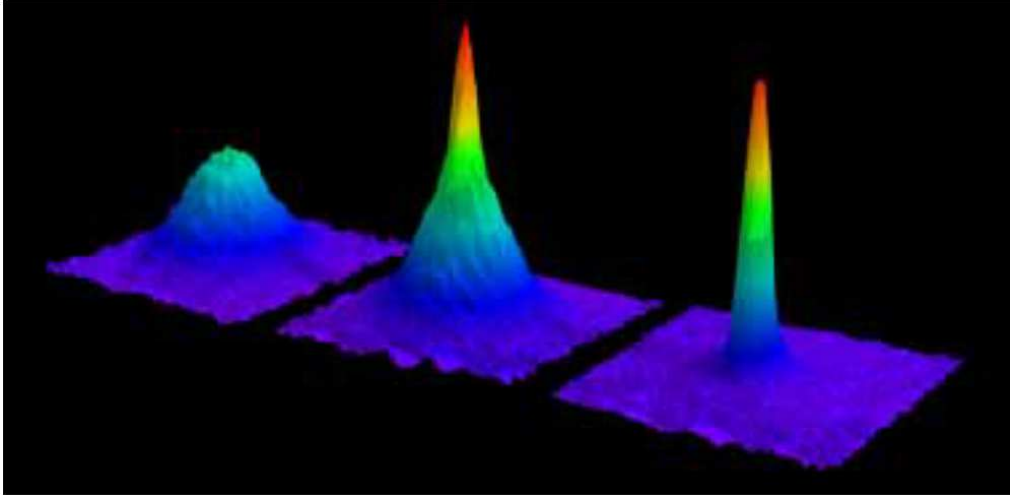


Figure 1.3: Observation of Bose-Einstein condensation of sodium atoms by absorption imaging. Shown is absorption vs. two spatial dimensions. The Bose-Einstein condensate is characterized by its slow expansion observed after 6 ms time of flight. The left picture shows an expanding cloud cooled to just above the transition point; middle: just after the condensate appeared; right: after further evaporative cooling has left an almost pure condensate. The width of the images is 1 mm. The total number of atoms at the phase transition is about $7 \cdot 10^5$, the temperature at the transition point is $2 \mu\text{K}$ [29].

peratures of a few hundred picokelvin [38]. Even the condensation of photons was observed recently in a microcavity [39, 40] which is impossible for a free photon gas since photons have a vanishing chemical potential and so the particle number is not conserved as one varies the temperature [28]. However in the experiment this was circumvented by bringing a photon gas into a dye-filled optical microcavity acting as an effective confining potential. The photons thermalize to the temperature of the dye solution by multiple scattering with the dye molecules. By increasing the number of the photons the phase space density increases until a Bose-Einstein condensation can be observed for approximately 77000 photons. The whole three-dimensional system is equivalent to an ideal gas of harmonically confined, massive bosons in two spatial dimensions.

The next step in the study of ultracold atoms was the realization of Fermi

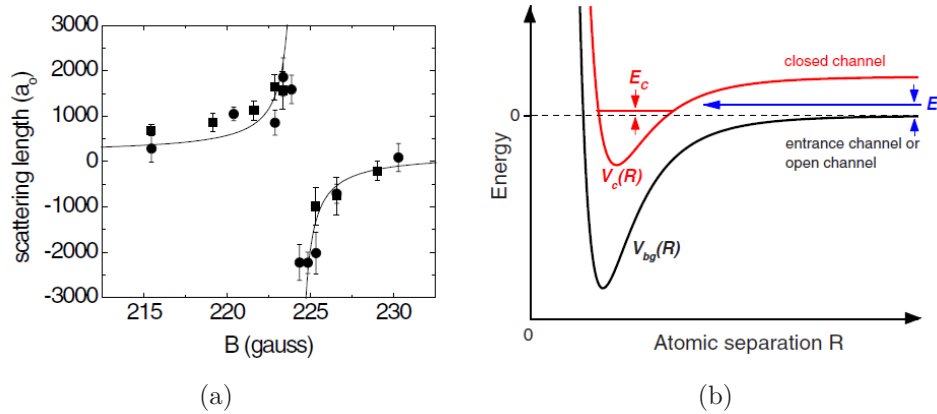


Figure 1.4: (a) Measurement of the scattering length a , given here in multiples of the Bohr radius a_0 , depending on an external magnetic field B near a Feshbach resonance [44]. The interaction can be attractive ($a < 0$) or repulsive ($a > 0$). (b) Schematic illustration of a Feshbach resonance [45]. An open channel is coupled to a closed channel by the variation of the energy difference dependent on a magnetic field.

degeneracy [3–5]. This degeneracy is reached when the temperature of the system is equal to or less than the Fermi temperature T_F . The main problem here is the cooling below the Fermi temperature. Since s-wave scattering dominates at very low temperatures, fermions are nearly non-interacting particles because of the Pauli exclusion principle. But evaporative cooling relies strongly on scattering processes so new cooling mechanisms had to be established. E.g., one of these methods is sympathetic cooling [41, 42], during which two species of atoms are brought together which are allowed to interact so that one species can give its energy to the other. In the first experiments temperatures of circa $0.3 T_F$ were reached but today also temperatures of approximately $0.03 T_F$ are possible [43].

Quantum degeneracy opened also another interesting field. By controlling the interaction strength between fermions, basically given by the scattering length a , the so-called BEC-BCS crossover [46–48] can be induced. The scattering length can be controlled by Feshbach resonances. They allow one to adjust the scattering length by varying an external magnetic field as depicted

in Fig. 1.4(a). For $a > 0$, called the BEC-side, a weakly bound molecular state [49–51] exists, so that in this case two fermions could form a bosonic molecule and thus a Bose-Einstein condensate for sufficiently low temperatures [52–54]. For $a < 0$, the BCS-side, the fermions can be described by weakly bound Cooper pairs and a BCS-like state [55, 56] can be observed ([48] and references therein).

At Feshbach resonances [45] a bound molecular state is coupled to a scattering state of two atoms. This is depicted in Fig. 1.4(b). The open channel represents the scattering potential V_{bg} and the closed channel the potential V_c of a bound state. A Feshbach resonance occurs when the closed channel approaches the open channel energetically due to a variation of E_c . The energy difference E_c depends on an external magnetic field B due to the Zeeman effect. The resulting scattering length can then be described by $a(B) = a_{\text{bg}} \left(1 - \frac{\Delta}{B - B_0}\right)$. The background scattering length a_{bg} is the scattering length of V_{bg} , B_0 stands for the position of the Feshbach resonance, and Δ denotes the width of the resonance.

1.4 Bose-Hubbard model

Whereas Bose-Einstein condensation and Fermi degeneracy deal mainly with dilute gases and weak interactions, another research field studies the opposite limit. In 2002 Greiner et al. measured the superfluid-to-Mott insulator phase transition [6] of a strongly correlated system.

An effect of strong correlations among electrons was observed in the late 1930s, when some metals were shown to exhibit a poorly conducting or even an insulating behavior despite their band structure which proposed a conducting behavior [57]. It was assumed that this could be explained by strong Coulomb repulsion between electrons preventing them from moving at all [58]. This led to the formulation of the Hubbard model [59] in the formalism of the second quantization, given by

$$H = -J \sum_{\langle i,j \rangle} c_{i,\sigma}^\dagger c_{j,\sigma} + U \sum_i n_{i,\uparrow} n_{i,\downarrow} - \mu \sum_i (n_{i,\uparrow} + n_{i,\downarrow}) . \quad (1.1)$$

This model is a simplified description of a solid but despite this, it can correctly

render the transition from a Mott insulator to a metal. It only takes two degrees of freedom into account: The electrons are allowed to move from one lattice site i to a neighboring site j with the tunneling energy J and they interact if two electrons with opposite spin σ occupy the same lattice site penalized by the interaction energy U . The last term controls the total number of particles by adjusting the chemical potential μ .

In 1989 a similar model was proposed by Fisher et al. describing bosons in a lattice [60]. This model is known as the Bose-Hubbard model and its second-quantization formulation reads

$$H = -J \sum_{\langle i,j \rangle} b_i^\dagger b_j + \frac{U}{2} \sum_i n_i (n_i - 1) - \mu \sum_i n_i . \quad (1.2)$$

It describes bosons at temperature $T = 0$ but it also shows the superfluid-to-Mott insulator phase transition. This means that the phase transition is purely driven by quantum fluctuations instead of thermal fluctuations and therefore it falls into the category of quantum phase transitions [61].

Jaksch et al. realized that this Hamiltonian could be simulated with great accuracy by ultracold bosons in an optical lattice [62]. An optical lattice is basically a standing wave of laser beams forming a lattice because of interference. They adopted trapped bosons in a trapping potential V_T interacting with an optical lattice potential V_0 confining the bosons to individual lattice sites. Because the atoms are ultracold, interactions between them are mostly given by s-wave scattering processes generally determined by the scattering length a . The resulting many-body Hamiltonian then reads

$$H = \int d^3x \psi^\dagger(\mathbf{x}) \left(-\frac{\hbar^2}{2m} \nabla^2 + V_0(\mathbf{x}) + V_T(\mathbf{x}) \right) \psi(\mathbf{x}) + \frac{1}{2} \frac{4\pi a \hbar^2}{m} \int d^3x \psi^\dagger(\mathbf{x}) \psi^\dagger(\mathbf{x}) \psi(\mathbf{x}) \psi(\mathbf{x}) . \quad (1.3)$$

By expanding the boson field operator in the localized Wannier basis [63, 64],

$$\psi(\mathbf{x}) = \sum_i w(\mathbf{x} - \mathbf{x}_i) b_i , \quad (1.4)$$

under the assumption that no excitations are present in the system, one gets the Bose-Hubbard Hamiltonian (1.2). The interaction strength is then given

by

$$U = \frac{4\pi a\hbar^2}{m} \int d^3x |w(\mathbf{x})|^4 \quad (1.5)$$

and the hopping matrix element between adjacent sites i and j is

$$J = - \int d^3x w^*(\mathbf{x} - \mathbf{x}_i) \left[-\frac{\hbar^2}{2m} \nabla^2 + V_0(\mathbf{x}) \right] w(\mathbf{x} - \mathbf{x}_j). \quad (1.6)$$

The energy offset on each lattice site $\mu_i = \int d^3x V_T(\mathbf{x}) |w(\mathbf{x} - \mathbf{x}_i)|^2$ is generally spatially varying, but for the case of a homogeneous lattice its site dependence vanishes. Then it is allowed to drop the index i by setting $\mu_i = \mu$ so that one arrives at the Hamiltonian (1.2).

The main benefit to simulate (1.2) with ultracold bosons in an optical lattice is the control over all important parameters in such an experiment. If an atom interacts with an electromagnetic field $\mathbf{E}(\mathbf{r}, t) = \mathbf{E}(\mathbf{r})e^{-i\omega t} + c.c.$ of laser light, a dipole moment $\mathbf{p}(\mathbf{r}, t) = \mathbf{p}(\mathbf{r})e^{-i\omega t} + c.c.$ is induced. The amplitude $\mathbf{p} = \alpha\mathbf{E}$ depends on the polarizability α of the atoms. This leads to an interaction potential

$$V_{\text{dip}} = -\frac{1}{2\epsilon_0 c} \text{Re}(\alpha) I \quad (1.7)$$

of the induced dipole moment in the electric field with $I = 2\epsilon_0 c |E(\mathbf{r})|^2$ being the intensity of the laser beam of the optical lattice [65]. That means by changing the intensity of the laser beams one has direct control over both the tunneling energy J and the on-site energy U of the Bose-Hubbard Hamiltonian. By using in addition a Feshbach resonance one can even control the interaction strength U alone so that one has control over both parameters J and U of the system.

The phase transition is easy to understand if one studies two physical limiting cases. In the atomic limit $J/U \rightarrow 0$ all particles are localized and on a lattice with N particles and M sites every site is occupied by $g = \langle n_i \rangle = N/M$ particles. The filling is denoted by the filling factor g which is supposed to be integer. This localization of particles and the corresponding incompressibility, expressed by $\partial \langle n_i \rangle / \partial \mu = 0$, defines the Mott insulator and, therefore, the ground state is given by

$$|\Psi_{\text{MI}}\rangle = \prod_{i=1}^M \frac{(b_i^\dagger)^g}{\sqrt{g!}} |0\rangle. \quad (1.8)$$

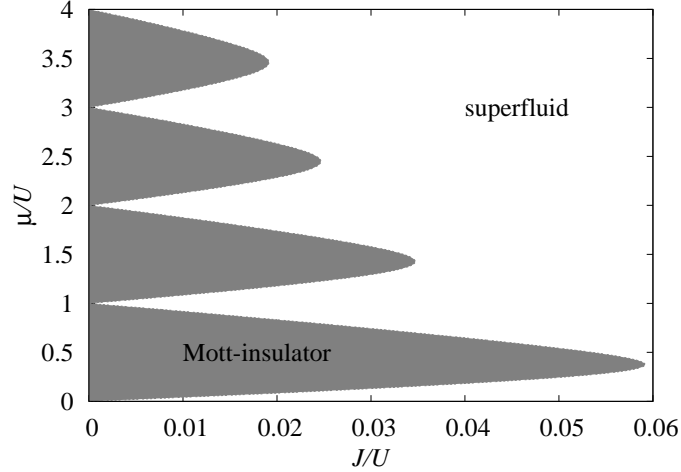


Figure 1.5: Phase diagram of the Bose-Hubbard model. Shown are four Mott lobes for different filling factors $\langle n_i \rangle = g$ and for the dimension $D = 2$. In the filled areas the system is in the Mott-insulator state. Outside of these areas lies the superfluid regime. The maximal value of J/U for which the system is still in a Mott insulator defines the critical chemical potential $(\mu/U)_c$ and the critical hopping $(J/U)_c$ of the respective Mott lobe.

The local creation operator b_i^\dagger acts g times on the vacuum state $|0\rangle$ without particles. In this phase the spectrum shows a gap between the ground-state energy and the energy of the first excitation.

In the opposite limit $J/U \rightarrow \infty$ the interaction energy is very small compared to the tunneling energy, leading to a delocalization of the particles. All particles are condensed into the ground state

$$|\Psi_{\text{SF}}\rangle = \frac{1}{\sqrt{N!}} \left(\frac{1}{\sqrt{M}} \sum_{i=1}^M b_i^\dagger \right)^N |0\rangle \quad (1.9)$$

with $\mathbf{k} = \mathbf{0}$. In this phase one has an uncertain number of particles on each lattice site but a long-range phase coherence emerges [66].

The two phases can also be classified by the concept of the off-diagonal long range order [67]. For this one has to define the one-particle density matrix

$$\rho_1 = \langle b_i^\dagger b_j \rangle \quad (1.10)$$

of the sites i and j at the positions \mathbf{r}_i and \mathbf{r}_j , respectively. In the Mott-insulator state this matrix vanishes in the limit $|\mathbf{r}_i - \mathbf{r}_j| \rightarrow \infty$. In the superfluid state, however, the density matrix converges to a finite value. If one considers the one-particle density matrix in momentum space, one gets

$$\rho_1 = \sum_{\mathbf{k}} n_{\mathbf{k}} e^{i\mathbf{k}(\mathbf{r}_i - \mathbf{r}_j)} = f_c + \sum_{\mathbf{k} \neq 0} n_{\mathbf{k}} e^{i\mathbf{k}(\mathbf{r}_i - \mathbf{r}_j)} \quad (1.11)$$

due to a Fourier representation of (1.10). The part with a nonzero momentum vanishes and only the condensed fraction f_c of all particles in the state with $\mathbf{k} = 0$ remains.

Between these two limiting cases lies the phase boundary defined by the values $(J/U)_{\text{pb}}$ and $(\mu/U)_{\text{pb}}$ as depicted in Fig. 1.5. Between every pair of integer values of the chemical potential one has a so-called *Mott lobe*. These Mott lobes are the shaded areas in Fig. 1.5 in which the system is in the Mott-insulator state. Everywhere outside of these areas the system is a superfluid. For each Mott-lobe a critical hopping $(J/U)_c$ and a critical chemical potential $(\mu/U)_c$ is defined by the maximal value of J/U for which the system is still a Mott insulator.

2 Critical phenomena

The state of a thermodynamic system is characterized by macroscopic state variables as, e.g., temperature, pressure or chemical potential. Depending on the adjustment of these variables the state is in a specific phase. Classical examples for such phases are solid, liquid or gaseous. But also “exotic” phases exist which escape the classical world of experience entirely. Examples for this are the Bose-Einstein condensation of bosonic particles at very low temperatures of circa 10^{-7} K near the absolute zero point [1, 2, 68] or the quark-gluon plasma [69] which appears not until temperatures of circa 10^{12} K [70, 71].

If a system changes its phase, for instance because of the increase of temperature, a phase transition takes place. During such a phase transition determining properties of the system change in such a characteristic way, that also the macroscopic behavior of the system changes dramatically. Such a property can be the symmetry of the system. E.g., whereas liquid water possesses continuous rotational and translational degrees of freedom, it loses these freedoms during the transition to the solid phase. In this latter phase water exists as ice and has a crystalline structure with a discrete rotational and translational symmetry.

If one knows all phases of a system one also knows the phase diagram. In Fig. 2.1 the phase diagram of water with its three phases solid, liquid, and gaseous or the three states of aggregation ice, water and, steam, respectively, can be seen as a function of temperature and pressure. These phases are separated by phase boundaries, so a phase transition must happen if the system crosses one of the boundaries. Along the phase boundaries two phases coexist in an equilibrium state. Actually all three phases coexist at the triple point, where the three branches meet each other.

The beginnings of the theory of phase transitions can roughly be traced back to the works of van der Waals [72]. For the first time also the behavior of real

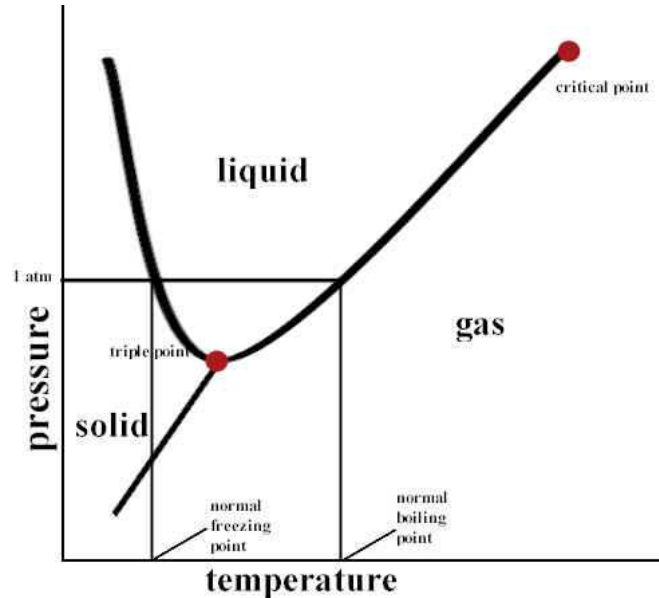


Figure 2.1: Schematic, simplified phase diagram of water. The three phases solid, liquid and gaseous of water and the phase boundaries as a function of pressure and temperature are shown. Further phases like, e.g., amorphous or overcritical phases are not shown for reasons of clarity. Water has a critical point at 647 K (373,9° C) and 218 atm behind which water exists as an overcritical fluid.

gases could be predicted with the van der Waals equation. With the help of this theory also critical parameters can be calculated which indicate the point of the phase transition in the phase diagram. However this theory is only a mean-field theory since the interaction of a particle with the rest of the system is approximated by an average interaction potential.

Mean-field theories usually render the critical parameters with good accuracy but the averaging of the interaction leads to the problem, that the approach of specific system variables to the critical point is described wrongly. This approach to the critical point is universal for many systems, which means that different systems behave identically in the vicinity of the critical point. It is often described by an algebraic equation, e.g., a variable X approaches the critical point as a function of the temperature as $X \propto (T - T_c)^\sigma$. Here σ is a so-called critical exponent and T_c is the critical temperature denoting the point

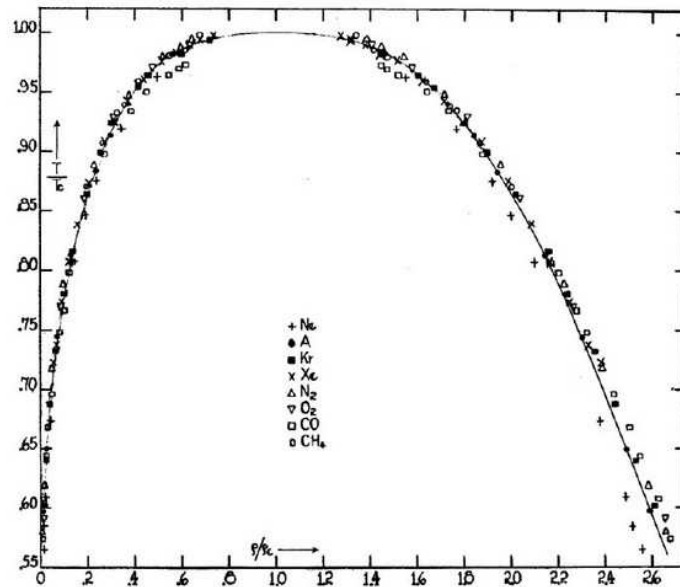


Figure 2.2: This graph strikingly demonstrates the universality of a phase transition [73]. The scaled temperature T/T_c is plotted as a function of the scaled density ρ/ρ_c , with the critical temperature T_c and the critical density ρ_c for each individual gas. All scaled temperatures are almost identical after the scaling.

of the phase transition. The exponent σ is then a universal parameter which is identical for a whole class of systems.

In Fig. 2.2 one of the first measurements revealing the universality of the solid-liquid phase transition of different substances is shown. With the help of the critical temperature T_c and the critical density ρ_c one can plot the scaled temperature T/T_c as a function of the scaled density ρ/ρ_c so that the scaled temperatures of all gases approximately coincide. This was also the first hint that the van der Waals theory is wrong because these data predict a critical exponent $1/3$ of the density whereas the theory of van der Waals predicts $1/2$.

The universality of a phase transition is one of the most important concepts of the theoretical description of critical phenomena. It is obvious that phase transitions mainly depend on interaction effects, however at the point of the

phase transition many features of these interactions seem to be unimportant since different systems show a very similar behavior at this point. The explanation of this behavior is that near the phase transition correlation effects dominate the behavior of the system. It turns out that these correlation effects and the fluctuations of them take place on all length scales so that certain microscopic features like the mass of the particles or the nature of the interaction between them are no longer important.

This chapter presents a brief introduction into the field of critical phenomena and introduces some concepts and results. In the first section the distinction of discontinuous and continuous phase transitions is explained. The focus lies on the definition and the qualitative study of important thermodynamic quantities. The second section introduces the Ginzburg-Landau and the ϕ^4 -theory and shows, how discontinuous and continuous phase transitions can be quantitatively studied using these concepts. The last chapter presents theoretical and experimental results of critical exponents and states important scaling relations.

2.1 Phase transitions

An important concept for the description of phase transitions is the order parameter. This parameter is defined in such a way that it is identical to zero in the “disordered” phase and unequal zero in the “ordered” phase. These phases are also called high-temperature and low-temperature phase, respectively.

Hamiltonians describing a many-body system are usually symmetric under miscellaneous transformations. In the disordered phase these symmetries are also fulfilled by the respective ground state while in the ordered phase the system has a lower symmetry than the corresponding Hamiltonian.

A good example for this issue is the phase transition of a magnet from the ferro- to a paramagnetic phase. For temperatures less than the Curie temperature a major fraction of elementary magnets are parallel, so that a macroscopic net magnetization is measurable. This parallel alignment of the elementary magnets breaks the symmetry of the Hamiltonian which does not favor a certain direction. Only after a spontaneous symmetry breaking one direction is

chosen. As one increases the temperature, the elementary magnets fluctuate more and more until the Curie temperature is reached, where the ferromagnet becomes a paramagnet. For this phase transition the order parameter is the net magnetization which is zero in the paramagnetic phase if no external magnetic field is present. The ordered phase is in this example the ferromagnetic phase and the disordered phase is the paramagnetic phase.

If $\mathcal{F}_0[\psi]$ is the free energy of the system expressed as a function of the order parameter [74], one can perform a Legendre transformation by introducing a new variable

$$\eta[\psi] = -\frac{\partial \mathcal{F}_0[\psi]}{\partial \psi} \quad (2.1)$$

and constructing the function

$$\mathcal{F}[\eta] = \mathcal{F}_0[\psi] + \eta\psi. \quad (2.2)$$

This corresponds to coupling an external field to the system which induces the spontaneous breaking of the symmetry. The order parameter ψ and the external field η are conjugated variables, since according to the Legendre transformation the order parameter can be calculated via

$$\psi[\eta] = \frac{\partial \mathcal{F}[\eta]}{\partial \eta}. \quad (2.3)$$

Furthermore one can calculate the isothermal susceptibility

$$\chi_T = \left(\frac{\partial^2 \mathcal{F}[\eta]}{\partial \eta^2} \right)_T = \left(\frac{\partial \psi[\eta]}{\partial \eta} \right)_T \quad (2.4)$$

and the specific heat

$$c_\eta = -T \left(\frac{\partial^2 \mathcal{F}[\eta]}{\partial T^2} \right)_\eta. \quad (2.5)$$

The coupling of an external field in (2.2) is crucial for the observation of spontaneous symmetry breaking since otherwise the system would stay in the state with the higher degree of symmetry. The occurrence of spontaneous symmetry breaking can be defined by the non-commutativity of the two limits $N \rightarrow \infty$ with N being the particle number and $\eta \rightarrow 0$:

$$0 = \lim_{N \rightarrow \infty} \lim_{\eta \rightarrow 0} \psi[\eta] \neq \lim_{\eta \rightarrow 0} \lim_{N \rightarrow \infty} \psi[\eta] \neq 0. \quad (2.6)$$

The role of the thermodynamic limit $N \rightarrow \infty$ is discussed in more detail in Sec. 2.1.3.

During a phase transition these observables show a characteristic behavior depending on the kind of the phase transition. On the basis of this behavior phase transitions are divided into discontinuous and continuous phase transitions.

2.1.1 Discontinuous phase transitions

Discontinuous phase transitions are defined by the absorption and release of latent heat

$$l = T\Delta S = T(S_1 - S_2) \quad (2.7)$$

during the phase transition from phase 1 to phase 2. The temperature T does not change during the phase transition according to the definition of latent heat. Since the entropy S is connected to the thermodynamic potential, here the free energy \mathcal{F} , via

$$S = - \left(\frac{\partial \mathcal{F}}{\partial T} \right)_\eta, \quad (2.8)$$

the first derivative shows a discontinuity at the critical point. This discontinuity of the first derivative is also responsible for the name first-order phase transition. Since the specific heat and the susceptibility are also connected to the free energy via (2.4) and (2.5), they likewise show a singularity at the critical point. The order parameter given by a derivative of the free energy with respect to the external field also shows a discontinuity.

2.1.2 Continuous phase transitions

Continuous phase transitions do not show a discontinuity in the first derivative but in higher derivatives. That means that also no latent heat takes part in this kind of phase transition. Continuous phase transitions can even be further divided into n th order phase transitions, depending on the order of the derivative which shows a discontinuity. However this so-called Ehrenfest classification is not sufficient for the description of all phase transitions. E.g., many systems with logarithmic divergences, i.e., with critical exponents equal

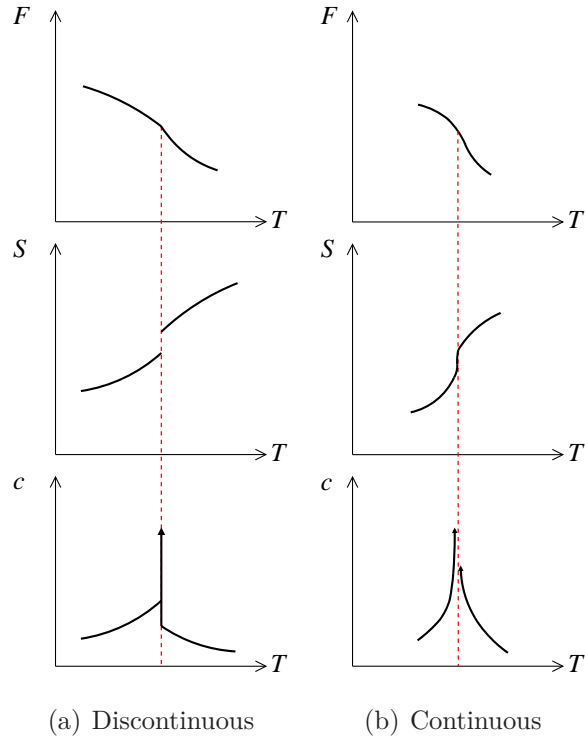


Figure 2.3: Schematic illustration of the difference between a discontinuous and a continuous phase transition. In the first case the entropy $S = -\partial F/\partial T$ shows a discontinuity which does not exist for continuous phase transitions. Correspondingly the heat capacity $c = -T\partial^2 F/\partial T^2$ of the discontinuous phase transition has a singularity at the critical point. It also diverges at the critical point of a continuous phase transition but the approach is continuous.

to zero, are known which are not taken into account in the Ehrenfest classification. One well-known example is the Ising model in two dimensions where the specific heat with its critical exponent $\alpha = 0$ shows a logarithmic divergence (see Tab. 2.3). Also the question arises if the distinction of two phases for a high-order phase transitions makes physical sense. Therefore the differentiation of discontinuous and continuous phase transitions seems to be the better classification. For orientation Fig. 2.3 shows the two kinds of phase transitions in comparison with each other.

A continuous phase transition can be observed in Fig. 2.1 if one moves along

the phase boundary between liquid water and steam in the direction towards the critical point. In this case the order parameter is the difference between the density of the liquid water and the density of the steam. This corresponds to the horizontal distance of the left and the right branch in Fig. 2.2. It is unequal zero along the phase boundary and becomes zero at the critical point characterized by ρ_c and T_c . Then water exists as a fluid for which one cannot distinguish between steam and liquid. Instead, one has steam bubbles and drops of liquid water on all length scales.

2.1.3 Thermodynamic limit

As already mentioned, the properties of thermodynamic potentials and of their derivatives are of great importance for the classification of phase transitions. A phase transition occurs at that point, where the system behaves non-analytically. These non-analytic features can only be observed in the thermodynamic limit $N, V \rightarrow \infty$ with the ratio N/V remaining constant. The grand-canonical equation of state reads

$$\frac{pV}{k_B T} = \ln \mathcal{Z} \quad (2.9)$$

and connects the pressure p and the volume V to the grand canonical partition function \mathcal{Z} . Thus one can expect a non-analytic behavior where the partition function has zeros. But the partition function of finite systems has no real zeros so that divergences and discontinuities cannot occur. Only in the thermodynamic limit one observes real-valued zeros defining the critical parameters [75, 76].

2.2 Theories for describing phase transitions

Up to now the role of the order parameter has been discussed only qualitatively. In this chapter it will be explained how discontinuous and continuous phase transitions can be modeled quantitatively with the help of the order parameter.

The section starts with the introduction of the mean-field ansatz since this is usually the first approach to the description of phase transitions because of its

simplifications. Then the Ginzburg-Landau theory is explained which is based fundamentally on the order parameter concept. Starting from this theory the Landau theory is deduced and an example, which shows how the Landau theory models continuous and discontinuous phase transitions, is discussed briefly.

2.2.1 Mean-field theory

As already mentioned at the beginning of this chapter, the first attempts to describe phase transitions are based on mean-field theories [77]. The conceptual basic principles were laid during the first tries to explain ferromagnetism [78, 79]. Before the discovery of the spin and the corresponding interaction a mean field was postulated which should be responsible for the alignment of the magnetic moments. Therefore this theory is also known as a molecular-field approximation. The success of this theory could be explained later by the finding that the molecular field corresponds to a mean field which simulates the interaction of one component (spin, particle, etc.) of the system with the whole rest of it. That means such a theory approximates a hard- or non-solvable Hamiltonian by one which is easier to solve because it does not contain the full interaction of all particles with each other but only the interaction of single particles with the mean-field.

For a Hamiltonian H one can use the Bogoliubov inequality [80]

$$\mathcal{F} \leq \Phi = \mathcal{F}_0 + \langle H - H_0 \rangle_0 \quad (2.10)$$

for the calculation of the free energy of the mean-field system [74]. Here \mathcal{F} is the free energy of the full Hamiltonian H , H_0 is a Hamiltonian which may depend on a variational parameter λ , and \mathcal{F}_0 is the free energy of this Hamiltonian. The expectation value $\langle \dots \rangle_0$ means the expectation value of that ensemble which is given by H_0 . The best approximation

$$\mathcal{F}_{\text{mf}} = \min_{\lambda} \Phi \quad (2.11)$$

to the full system is then given by the minimization of the function Φ with respect to λ .

This procedure corresponds to the decoupling of two operators O_1 and O_2 via

$$O_1 O_2 \longrightarrow O_1 \langle O_2 \rangle_0 + \langle O_1 \rangle_0 O_2 - \langle O_1 O_2 \rangle_0 . \quad (2.12)$$

The last term of the right-hand side makes sure that the expectation value of the left- and of the right-hand side coincide, if one neglects correlations.

Mean-field theories offer a very general ansatz for the treatment of interacting systems. However the quality of the predictions depends strongly on the distance from the critical parameter and the dimensionality of the system. Generally mean-field theories get worse the more one approaches the critical point since there fluctuations dominate the system which are not taken into account in these theories because of the averaging of the interactions. The range in which the mean-field theory gives reliable results is given by the Ginzburg criterion. Also there exists an upper critical dimension which states when a mean-field theory describes phase transitions exactly [81]. In general the critical exponents predicted by mean-field theories are wrong if the dimension of the system is less than the upper critical dimension. The existence of an upper critical dimension can be roughly led back to the number of neighbors one component has in the system. The higher the dimension of the system is, the more neighbors one component has and the better the averaging of the interaction approximates the real interaction.

2.2.2 Landau theory and ϕ^4 -theory

The Ginzburg-Landau theory is an extension of the Landau theory and was developed over the course of the understanding of superconductivity [82]. Landau knew that a phase transition comes always along with a breaking of symmetry [83]. Therefore one needs in the ordered phase one parameter more than in the disordered phase to describe the system completely. This parameter is the N -component order parameter $\boldsymbol{\psi} = (\psi_1(\mathbf{x}), \dots, \psi_N(\mathbf{x}))$ which is zero in the disordered phase and increases in the ordered phase. Every component $\psi_i(\mathbf{x})$ is a scalar, the argument \mathbf{x} of which is an element of the D -dimensional space \mathbb{R}^D . Since the order parameter is small nearby the critical parameter, so that $|\boldsymbol{\psi}| \ll 1$ holds, it is assumed that the free energy can be expanded in powers of $|\boldsymbol{\psi}|$.

Should the system break the symmetry spontaneously, no certain value of the order parameter should minimize the free energy without the presence of an external field. That indicates that the power series must be invariant under a rotation of $\boldsymbol{\psi}$. This is only fulfilled if the power series contains just even orders of $|\boldsymbol{\psi}|$.

Furthermore, to permit fluctuations, the order parameter must depend on the location. However fast fluctuations of the order parameter, whose increase signal the approach to the critical point of the phase transition [81] and thus tend to destroy the ordered phase, must lead to an energy increase. Since only even orders of $|\nabla\boldsymbol{\psi}(\mathbf{r})|$ are allowed, in first order a term proportional to $|\nabla\boldsymbol{\psi}(\mathbf{r})|^2$ describes location-dependent changes correctly. The neglect of higher order derivatives means that this theory is a local theory. If i denotes the sites of a one-dimensional lattice and by using the central difference quotient, the first derivative

$$\nabla\boldsymbol{\psi}(i) = \frac{\boldsymbol{\psi}(i+1) - \boldsymbol{\psi}(i-1)}{2} \quad (2.13)$$

connects the site $i+1$ and $i-1$. The next order would already involve the sites $i+2$ and $i-2$ and even higher order derivatives would gradually lead to a nonlocal theory.

If one also wants to consider spontaneous symmetry breaking, the order parameter must be coupled to an external field $\boldsymbol{\eta}$ having the same dimensionality as the order parameter $\boldsymbol{\psi}$. This field determines a preferred direction, which breaks the original symmetry of the system. The external field $\boldsymbol{\eta}$ and the order parameter $\boldsymbol{\psi}$ are conjugated variables since the order parameter is given by the derivative of the free energy with respect to the field $\boldsymbol{\eta}$ via (2.3). Here the sign of this term is negative since the direction chosen by the external field is supposed to be favored.

By summarizing these considerations one gets the energy of the Ginzburg-Landau theory in form of the functional

$$\mathcal{F}_{\text{GL}}[\boldsymbol{\psi}] = \int d\mathbf{r} \left\{ a_0 + a_2 |\boldsymbol{\psi}(\mathbf{r})|^2 + a_4 |\boldsymbol{\psi}(\mathbf{r})|^4 + a_6 |\boldsymbol{\psi}(\mathbf{r})|^6 + \gamma |\nabla\boldsymbol{\psi}(\mathbf{r})|^2 - \boldsymbol{\eta}\boldsymbol{\psi}(\mathbf{r}) \right\} . \quad (2.14)$$

To calculate the partition sum

$$Z = \int \mathcal{D}\psi e^{-\mathcal{F}_{\text{GL}}[\psi]/(k_B T)} \quad (2.15)$$

one has to integrate over all possible realizations of the order parameter.

Starting with this functional one can also derive the free energy of the Landau theory. In this approximation one favors that state with the highest probability which is the equilibrium state of the system minimizing the functional (2.14). A constant function in space $\boldsymbol{\psi}(\mathbf{r}) = \boldsymbol{\psi}_c$ minimizes the gradient term since then $\nabla\boldsymbol{\psi}_c = 0$. Furthermore the order parameter should be parallel to the external field $\boldsymbol{\eta}$ since then the interaction term, which must be subtracted, is maximized. With this condition the order parameter can be chosen to point in the same direction as the external field, so that both become scalars η and ψ_c . Under these conditions one gets the free energy density

$$f_{\text{L}}(\psi_c) = a_0 + a_2\psi_c^2 + a_4\psi_c^4 + a_6\psi_c^6 - \eta\psi_c \quad (2.16)$$

of the Landau theory. Because this theory ignores fluctuations, the Landau theory is a mean-field theory.

For simplicity let us set $\eta \equiv 0$ and $a_0 = 0$. Depending on the other coefficients, f_{L} has different solutions for its minimum. If all coefficients are positive, only the trivial solution $\psi_0 \equiv 0$ exists which guarantees a minimum. The system is then located in the disordered phase. One can now study continuous and discontinuous phase transitions by considering different values of the coefficients a_2 , a_4 , and a_6 .

For a continuous phase transition one must have $a_4 > 0$. Because a positive a_4 guarantees a minimum one does not need the term $a_6\psi_c^6$ and the free energy is given by

$$f_{\text{L}}(\psi_c) = a_2\psi_c^2 + a_4\psi_c^4. \quad (2.17)$$

A new minimum is only possible if a_2 changes its sign. As soon as a_2 is less than zero a new minimum $\psi_0 \neq 0$ does exist. Then one has the solution

$$|\psi_0| = \sqrt{\frac{-a_2}{2a_4}} \quad (2.18)$$

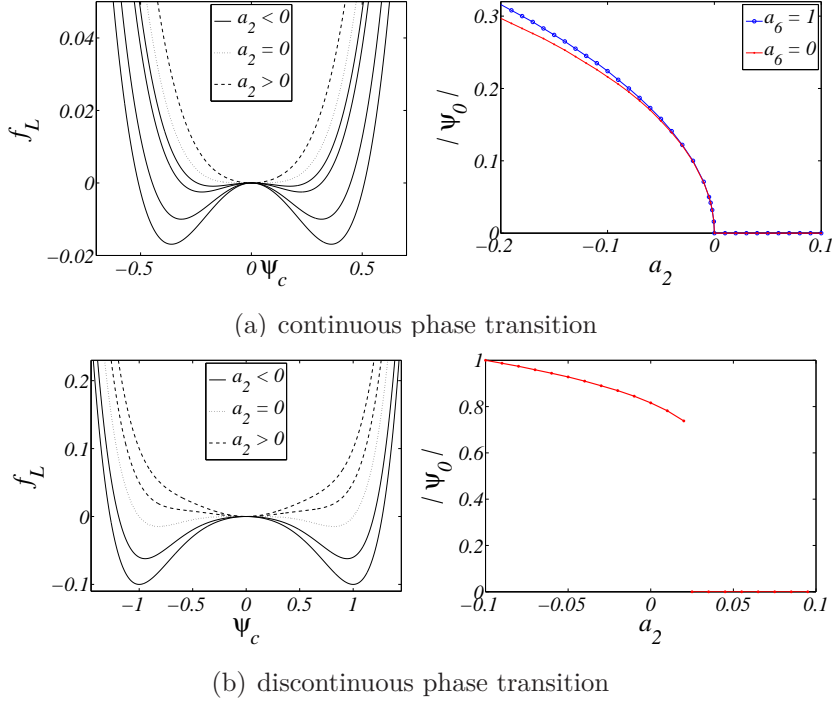


Figure 2.4: The behavior of the free energy and the order parameter of the Landau theory for (a) continuous and (b) discontinuous phase transitions. In the first case one has a continuous transition from the trivial minimum at $\psi_0 = 0$ to another minimum with $\psi_0 \neq 0$. It is also shown that the coefficient a_6 influences the curve only marginally in the immediate vicinity of the transition point if a_4 is greater zero. In the second case a new minimum develops, separated from the trivial minimum in a discontinuous way.

for a real-valued order parameter. By verifying the condition

$$\frac{d^2 f_L(\psi_c)}{d\psi_c^2} > 0, \quad (2.19)$$

one can easily show that this solution is indeed a minimum for $a_2 < 0$ and $a_4 > 0$.

For a complex order parameter one has an uncountable set of solutions since the free energy has the shape of the Mexican-hat potential of Fig. 2.5(a). Fig. 2.4(a) shows the free energy and the order parameter during a continuous phase transition attaining values greater zero at the point of the phase

transition given by $a_2(\psi_c) = 0$. The left picture shows the free energy for different values of a_2 with $a_4 = 1$ and $a_6 = 0$. In the right picture the minimum of this free energy is plotted as a dotted line. Additionally the minimum of the free energy f_L with $a_6 = 1$ is plotted with circles on a line. The point of the phase transition is not changed by a_6 , only the shape of the curve differs.

For discontinuous phase transitions the coefficient a_4 is less than zero and so the coefficient a_6 has to be considered for the free energy

$$f_L(\psi_c) = a_2\psi_c^2 + a_4\psi_c^4 + a_6\psi_c^6 \quad (2.20)$$

and it must be greater than zero. In this case the phase transition is discontinuous as it is shown in Fig. 2.4(b). There the coefficients are $a_4 = -0.1$ and $a_6 = 0.1$ and a_2 changes from -0.1 to 0.095 . The zeros are given by the trivial minimum $\psi_0 = 0$ and

$$|\psi_0^+| = \sqrt{\frac{-a_4 + \sqrt{a_4^2 - 3a_2a_6}}{3a_6}}, \quad |\psi_0^-| = \sqrt{\frac{-a_4 - \sqrt{a_4^2 - 3a_2a_6}}{3a_6}}. \quad (2.21)$$

The solution $|\psi_0^+|$ describes the phase transition whereas $|\psi_0^-|$ is a non-physical solution with an imaginary order parameter. Those values of $\psi_0^+ \neq 0$ minimizing the free energy according to the condition

$$a_2\psi_0^2 + a_4\psi_0^4 + a_6\psi_0^6 < 0 \quad (2.22)$$

define the new global minima. Already before a_2 changes its sign, another minimum develops apart from $\psi_0 = 0$ at $a_2 = 0.025$ here, which also fulfills (2.19). The order parameter has a discontinuity where this new minimum becomes the new global minimum.

If one generalizes the properties of the order parameter of the Ginzburg-Landau theory one gets the ϕ^4 -theory. In the original Ginzburg-Landau theory used for the description of superconductivity, the order parameter can be interpreted as the wave function of the superconducting electrons. So this order parameter consists of two components representing a real and a complex part, respectively. In general the order parameter $\boldsymbol{\psi} = (\psi_1(\mathbf{x}), \dots, \psi_N(\mathbf{x}))$ consists of N components with $\mathbf{x} \in \mathbb{R}^D$.

N	Universality class
∞	Spherical model [84, 85]
3	Heisenberg model
2	xy -model
1	Ising model
0	Polymers (self-avoiding walk) [86]
-2	Gauss model [84]

Table 2.1: For different values of N one gets different universality classes which are represented by another model [61, 87]. All models of a certain universality class possess the same critical exponents. The strange case $N = -2$ corresponds to an analytical continuation of a $1/N$ -expansion [88, 89].

The ϕ^4 -theory is used for the study of continuous phase transitions. Its energy functional has the form

$$\mathcal{F}[\psi] = \int d^D x \frac{1}{2} \{ [\partial_{\mathbf{x}} \psi(\mathbf{x})]^2 + m^2 \psi^2(\mathbf{x}) \} + \frac{\lambda}{4!} \psi^4(\mathbf{x}) . \quad (2.23)$$

The first term describes the kinetic energy, the second term represents the mass, and the last term stands for the interaction. The universality class of the phase transition is determined by the number N of components of the order parameter, and the dimensionality D [90, 91]. The best-known universality classes are shown in Tab. 2.1. The classes are usually named after one of the most important representatives of each class.

2.3 Critical exponents

The universality of different phase transitions can be explained by observing that near the critical point the behavior of the system is largely independent of specific details of the Hamiltonian. This can be further understood by the renormalization group approach [92]. This approach distinguishes between so-called relevant and irrelevant operators. Irrelevant operators vanish at the

critical point due to the large correlation length and only the relevant quantities define the critical behavior of the system. They depend mainly on the dimensionality D of the system, the number of the order parameters N and the range of the interactions. Therefore specific quantities of different systems or models behave nearly identically in the vicinity of the phase transition so that the behavior of them can be characterized with only a few parameters like critical exponents.

An important example of such an observable is the connected correlation function

$$G^{(n)}(\mathbf{x}_1, \dots, \mathbf{x}_n) = \langle \psi(\mathbf{x}_1) \dots \psi(\mathbf{x}_n) \rangle - \langle \psi(\mathbf{x}_1) \rangle \dots \langle \psi(\mathbf{x}_n) \rangle, \quad (2.24)$$

which measures the correlation of the fluctuations of the order parameter around its expectation value. Especially the 2-point correlation function of a translationally invariant and isotropic system,

$$G(x) := G^{(2)}(x) = \langle \delta\psi(\mathbf{x}_1) \delta\psi(\mathbf{x}_2) \rangle, \quad (2.25)$$

where $\delta\psi(\mathbf{x}_1) := \psi(\mathbf{x}_1) - \langle \psi(\mathbf{x}_1) \rangle$ and the correlation function only depends on the distance $x = |\mathbf{x}_1 - \mathbf{x}_2|$ of the points \mathbf{x}_1 and \mathbf{x}_2 , is of great relevance. Near the phase transition this correlation function shows the characteristic behavior [81]

$$G(x) \propto \frac{1}{x^{D-2+\eta}} e^{-x/\xi} \quad (2.26)$$

with the correlation length ξ indicating on which length scale correlations exist in the system. In addition the correlation function depends only on the dimensionality D and on the critical exponent η . At the critical point the correlation length ξ diverges and the correlation function (2.26) reduces to

$$G(x) \propto \frac{1}{x^{D-2+\eta}}. \quad (2.27)$$

Which critical exponent is assigned to which quantity and how they behave near the phase transition depending on the temperature $\tau = T_c - T$ can be seen in Tab. 2.2. Except for the exponents β and δ , which are only defined for $T < T_c$, since the order parameter is equal to zero in the disordered phase, the renormalization group theory [90, 93, 94] says that all critical exponents

physical quantity		behavior	regime
correlation length	ν	$\xi \propto \tau^{-\nu}$	$T \rightarrow T_c, \tilde{\eta} = 0$
correlation function	η	$G(x) \propto x^{-(D-2+\eta)} e^{-x/\xi}$	$T \rightarrow T_c, \tilde{\eta} = 0$
		$G(x) \propto x^{-(D-2+\eta)}$	$T = T_c, \tilde{\eta} = 0$
specific heat	α	$c \propto \tau^{-\alpha}$	$T \rightarrow T_c, \tilde{\eta} = 0$
order parameter	β	$\psi \propto \tau^\beta$	$T \rightarrow T_c, \tilde{\eta} = 0$
	δ	$\psi \propto \tilde{\eta}^{1/\delta}$	$T = T_c, \tilde{\eta} \rightarrow 0$
susceptibility	γ	$\chi \propto \tau^{-\gamma}$	$T \rightarrow T_c, \tilde{\eta} = 0$

Table 2.2: Definition of the critical exponents using the example of a temperature dependent phase transition with $\tau = T_c - T$. The critical exponents determine the behavior of the physical quantities in the vicinity of the phase transition at $T = T_c$. Here, the external field introduced in (2.1) is denoted by $\tilde{\eta}$ in order to distinguish it from the critical exponent η .

are equal above and below the critical temperature at least in the vicinity of the phase transition [81]. However this does not hold for the prefactors a^\pm of a quantity

$$X \propto a^\pm |\tau|^\sigma, \tau \rightarrow \pm 0. \quad (2.28)$$

They differ from each other depending on whether the system is in the ordered or disordered phase. On the other hand one can find ratios of these prefactors which are called universal amplitude ratios. They show a universal behavior like the critical exponents [95, 96].

2.3.1 ϕ^4 -theory

In Tab. 2.3 and Tab. 2.4 some chosen values of critical exponents for dimensionalities $D = 2, 3$ and 4 are shown. For the ϕ^4 -theory $D = 4$ is the upper critical dimension. Starting from this dimension the mean-field exponents become exact, and thus they do not depend on the number of order parameters N anymore.

For $D = 3$ two independent values for each critical exponent are quoted by way of comparison in Tab. 2.4. All exponents computed in Refs. [97, 98] except

$$D = 2$$

N	ν	η	α	β	γ
1	1	0.25	0 (log)	0.125	1.75

$$D \geq 4 \text{ ([87])}$$

ν	η	α	β	γ	δ
0.5	0	0 (dis)	0.5	1	3

Table 2.3: Critical exponents of the ϕ^4 -theory for dimensionalities $D = 2$ and $D \geq 4$. For $D = 2$ the exact exponents of the two-dimensional Ising model are stated. In $D = 4$ the mean-field theory is exact. The abbreviation “(log)” refers to a logarithmic singularity, and “(dis)” indicates a discontinuous transition.

for α result from an ϵ -expansion in $D = 4 - \epsilon$ dimensions. The exponent α of Ref. [98] is the result of an expansion with fixed dimension $D = 3$ [81, 92, 96]. Since the accessible power series are finite, one needs to extrapolate these series. In Ref. [97] the weak-coupling series was transformed into a strong-coupling series by the use of a variational perturbation theory [81, 99–101]. The critical exponents of Ref. [98] result from a Borel-Leroy transformation [96, 98]. Where no source is quoted, the hyperscaling relations (2.36a) and (2.36b), respectively, were used to calculate the respective missing exponent. Ref. [102] provides α as listed in the upper row with $N = 2$. (For further reference data, see [103].)

For $D = 2$ only the critical exponents for the Ising model with $N = 1$ are stated in Tab. 2.3. This model is one of the very few non-trivial models which can be solved analytically [104, 105]. Therefore the stated exponents are exact. For $D \leq 2$ and $N \geq 2$, i.e., for a system with a continuous symmetry, no spontaneous symmetry breaking with a long-range order can be observed according to the Mermin-Wagner theorem [106–108].

This theorem does not hold for the Ising model since this model possesses a discrete symmetry (spin “up” or “down”) and thus the Hamiltonian is only invariant under a simultaneous 180° rotation of all spins. Despite this the one-dimensional Ising model does not show a phase transition, either. This is because for the rotation of one spin an energy E must be spent, since a domain

	Ref.	0	1	2	3
ν	[97]	0.5874	0.6292	0.6697	0.7081
	[98]	0.5875 ± 0.0025	0.6290 ± 0.0025	0.6680 ± 0.0035	0.7045 ± 0.0055
η	[97]	0.0316	0.0373	0.0396	0.0367
	[98]	0.0300 ± 0.005	0.0360 ± 0.005	0.0380 ± 0.005	0.0375 ± 0.0045
α		0.2378	0.1124	$-0,01126 \pm 0.001^\dagger$	-0.1243
	[98]	0.235 ± 0.003	0.109 ± 0.004	-0.011 ± 0.004	-0.122 ± 0.01
β		0.3030	0.3263	0.3481	0.3670
	[98]	0.3025 ± 0.0025	0.3257 ± 0.0025	0.3465 ± 0.0035	0.3655 ± 0.0035
γ	[97]	1.1576	1.2349	1.31045	1.3830
	[98]	1.1575 ± 0.006	1.2355 ± 0.005	1.3110 ± 0.007	1.3820 ± 0.009

Table 2.4: Critical exponents of the ϕ^4 -theory for $D = 3$ and $N = 0, 1, 2, 3$. The exponents are results of an ϵ -expansion together with different following extrapolation methods. The references for the respective exponents are stated in the second column. The explanation for exponents without a reference is given in the text. (\dagger [102]: α for $N = 2$)

wall is created. But no further energy must be spent for the rotation of every other spin belonging to this domain, because the surface area of the domain does not change in a one-dimensional system. In order to create M domains a finite energy ME must be spent, independent of the number of involved spins. On the other hand the entropy increases with M . Now the free energy of the system is given by

$$F = ME - TS(M) , \quad (2.29)$$

and one can show that in the thermodynamic limit the entropy increases faster than the expended energy. Therefore, the system tends to split into a macroscopic number of domains for all temperatures $T > 0$ [109, 110]. A phase transition is therefore only possible for $T = 0$.

By contrast the systems for $N \geq 2$ are invariant under every infinitesimal simultaneous rotation of all spins. That means that the system can be excited by an infinitesimal amount of energy. These excitations with the properties of

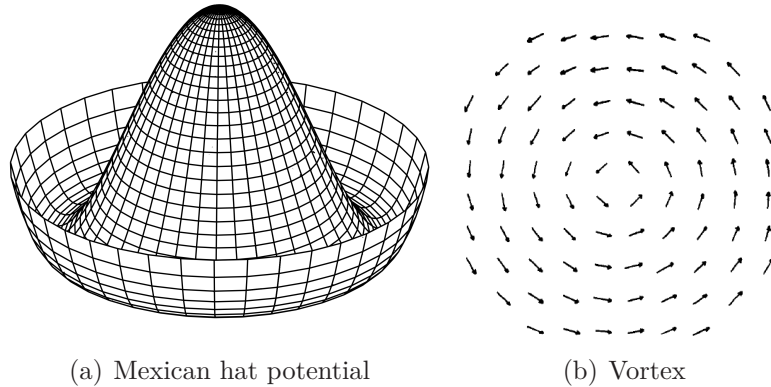


Figure 2.5: (a) Potential of the free energy (2.17). For the order parameter to attain a value $\psi_0 \neq 0$ the symmetry must be spontaneously broken. (b) A vortex of spins. Such vortices are the prime cause the Kosterlitz-Thouless phase transition has unique features.

spin- and massless particles are named Goldstone modes [111]. They occur in all systems with a broken continuous symmetry and prevent a long-range order for all systems with $D \leq 2$. Descriptively, Goldstone modes can be figured as vertical excitations in the Mexican-hat potential of Fig. 2.5(a). After a phase transition the system has chosen one of the minima because of the spontaneous symmetry breaking, however fluctuations along the minima are possible with an infinitesimal amount of energy because the gradient in this direction is zero. An example for Goldstone modes are spin waves or magnons, respectively.

In two dimensions and $N = 2$ another phase transition takes place because of this missing long-range order. This is the so-called Kosterlitz-Thouless (KT) phase transition [112, 113]. The xy -model is one of the first models with which the KT phase transition was studied [114]. In this model the correlation length is $\xi = \infty$ for $T < T_c$ and

$$\xi \propto e^{-b/(T-T_c)^{1/2}} \quad \text{for } T > T_c \quad (2.30)$$

with $b \approx 1.5$. Physically this phase transition can be traced back to the existence of vortices as depicted in Fig. 2.5(b). That means the spins are arranged in such a way, that for the spin field $\theta(\mathbf{x})$, which gives the angle of the spin at

the position \mathbf{x} [87], one has

$$\oint_C d\mathbf{x} \nabla\theta(\mathbf{x}) = 2\pi q, \quad (2.31)$$

where q is the quantum number of the so-called charge of the vortices. These vortices couple mainly to vortex-antivortex pairs during the decrease of temperature. For distances large enough the integral (2.31) over a vortex-antivortex leads to $q = 0$. The unbounded vortices are responsible for the exponential decay of the correlation length and the likewise exponentially decaying correlation function

$$G(x) \propto e^{-x/\xi} \quad \text{for } T > T_c. \quad (2.32)$$

Because of the paired vortices a quasi long-range order exists in the low-temperature phase, which is also named topological long-range order, with

$$G(x) \propto x^{-\eta} \quad \text{for } T < T_c. \quad (2.33)$$

The exponent $\eta = \eta(T)$ depends itself on the temperature. The critical value is $\eta(T_c) = 0.25$ [114, 115]. The singular part of the free energy, which contains the thermodynamics of the vortices, scales with

$$F \propto \xi^{-2}. \quad (2.34)$$

That means that the KT phase transition is in the sense of the Ehrenfest classification a phase transition of infinite order because all derivatives are continuous. The susceptibility shows a similar behavior as the correlation length as it yields $\chi = \infty$ for $T < T_c$ and

$$\chi \propto \xi^{2-\eta} \quad \text{for } T > T_c. \quad (2.35)$$

This kind of phase transition has no order parameter because, e.g., the magnetization for the xy -model is zero for all temperatures because of the spin waves and Goldstone modes, respectively. To sum up, the mechanisms of this phase transition are entirely different from that of the ϕ^4 -theory. This phase transition is of great interest in the theory of two-dimensional melting processes [116] and for the explanation of phenomena important in the field of superconductivity [117].

For a two-dimensional system with $N > 2$ there exists no definite proof for or against the existence of a phase transition. However there are many indications that for such systems no phase transition exists for $T > 0$ ([118, 119] and references therein).

2.3.2 Scaling relations

The critical exponents are not independent of each other as they are related via the hyperscaling relations

$$\alpha = 2 - \nu D , \quad (2.36a)$$

$$\beta = \frac{\nu}{2}(D - 2 + \eta) , \quad (2.36b)$$

$$\gamma = \nu(2 - \eta) , \quad (2.36c)$$

$$\delta = \frac{D + 2 - \eta}{D - 2 + \eta} , \quad (2.36d)$$

depending explicitly on the dimensionality D . Thus if one knows the value of two of these critical exponents all other exponents can then be calculated. These relations follow from the renormalization group theory [96].

One can also find scaling relations which neither do depend on the dimensionality nor include the critical exponents ν and η of the order parameter. The first one reads [120]

$$\alpha + 2\beta + \gamma = 2 , \quad (2.37)$$

and can be derived from the two relations

$$\alpha + \beta(1 + \delta) = 2 , \quad (2.38a)$$

$$\gamma + \beta(1 - \delta) = 0 . \quad (2.38b)$$

Quite another relation holds for superfluid density ρ_{sf} and its critical exponent ν . The superfluid density also emerges at the critical point as $\rho_{\text{sf}} \propto \tau^\nu$, similar to the quantities stated in Tab. 2.2. For the critical exponent ν one has the Josephson relation [121–123]

$$\nu = 2\beta - \eta\nu , \quad (2.39)$$

which in the case of the Bose-Hubbard model directly connects the critical exponent of the superfluid density to the critical exponent $\beta_c = 2\beta$ of the condensate density.

2.3.3 Experimental measurements

To support the theoretical predictions of Tab. 2.3 and Tab. 2.4 one also needs experimental results for comparison. This section reports some experimental measurements of certain critical exponents. The main focus lies on the λ -transition of helium which is in the universality class of $D = 3$ and $N = 2$ [124]. This universality class is of peculiar interest because the D -dimensional Bose-Hubbard model is a member of the universality class of the $(D+1)$ -dimensional xy -model [60, 61].

By decreasing the temperature helium shows a second-order phase transition from so-called He-I to He-II at the λ -point. This point marks the critical pressure-dependent transition temperature $T_\lambda \approx 2.17$ K. Whereas He-I is just liquid helium without unusual properties, He-II is a superfluid. Characteristic features of this state are a very large thermal conductivity [125, 126] as well as a very small viscosity. The viscosity can be explained with the two-fluid model [68, 127]. This model states, that the density $\rho = \rho_s + \rho_n$ of He-II is given by one component called the superfluid density ρ_s and one component called the normal density ρ_n . Whereas the normal component acts as a classical liquid, the superfluid component has zero viscosity, zero entropy, and an infinite thermal conductivity. This can be observed conclusively in the Hess-Fairbank effect [128]. If one has a rotating container filled with liquid He-I at a temperature $T > T_\lambda$, the angular momentum of He-I is $L_{\text{cl}} = I_{\text{cl}}\omega$, where I_{cl} is the classical moment of inertia. Now if one cools down the system while the angular velocity is less than a critical angular velocity, the superfluid fraction will not contribute to the angular momentum. With the normal fraction $f_n(T) = \rho_n(T)/\rho$ the non-classical angular momentum is then given by $L(T) = f_n(T)I_{\text{cl}}\omega$.

The superfluid density is closely related to the condensate density ρ_c which is defined as that part of the system which is Bose-Einstein condensed. The superfluid density is proportional to the condensate density but up to date it

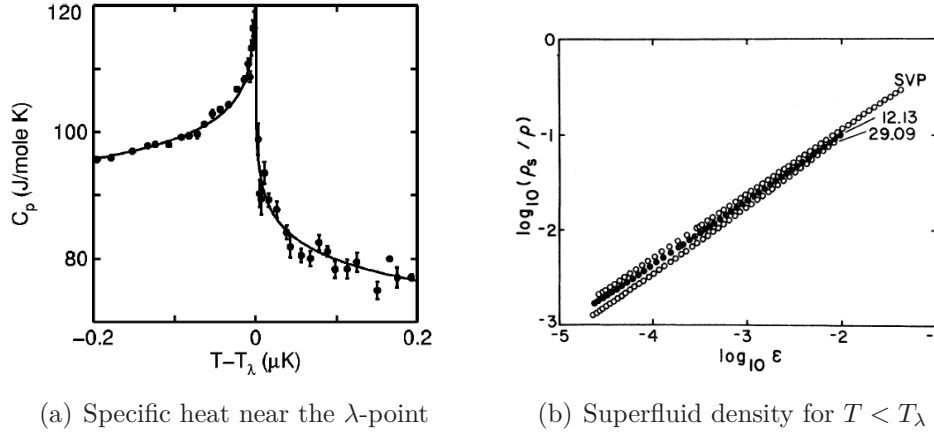


Figure 2.6: (a) Specific heat of liquid helium measured during a zero-gravity experiment [129]. The dots are the measured data and the line is a fit according to (2.40) with a critical exponent $\alpha = -0.01264$. (b) The superfluid density of ${}^4\text{He}$ determined by a measurement of the second sound leading to a critical exponent $\nu = 0.674$ [130].

is not quite clear how they are connected exactly. But it seems clear that in the limit $T \rightarrow 0$ one has $\rho_s \rightarrow \rho$ and simultaneously $\rho_c/\rho \approx 0.1$ [131]. It also follows from the Josephson relation (2.39) that $\rho_s > \rho_c$ must hold.

Furthermore the specific heat as a function of the temperature has the eponymous shape of the Greek letter λ as depicted in Fig. 2.6(a). The points are measured data [129] from a microgravity experiment [132] and the line is a fit with the function

$$c_p = \begin{cases} \frac{A^-}{\alpha} t^{-\alpha} (1 + a_c^- t^\Delta + b_c^- t^{2\Delta}) + B & , T < T_\lambda \\ \frac{A^+}{\alpha} |t|^{-\alpha} + B & , T > T_\lambda \end{cases} \quad (2.40)$$

and $t = 1 - T/T_\lambda$. The most important quantities are the universal amplitude ratio $A^+/A^- = 1.05251$ and the critical exponent $\alpha = -0.01264$. This fit function is a truncated version of the theoretically predicted specific heat [133]

$$c_p = \frac{A^\pm}{\alpha} |t|^{-\alpha} (1 + a_c^\pm |t|^\Delta + b_c^\pm |t|^{2\Delta} + \dots) + B. \quad (2.41)$$

One of the first measurements of the superfluid density ρ_s is depicted in Fig. 2.6(b). There the superfluid fraction $f_s = \rho_s/\rho$ is plotted versus the

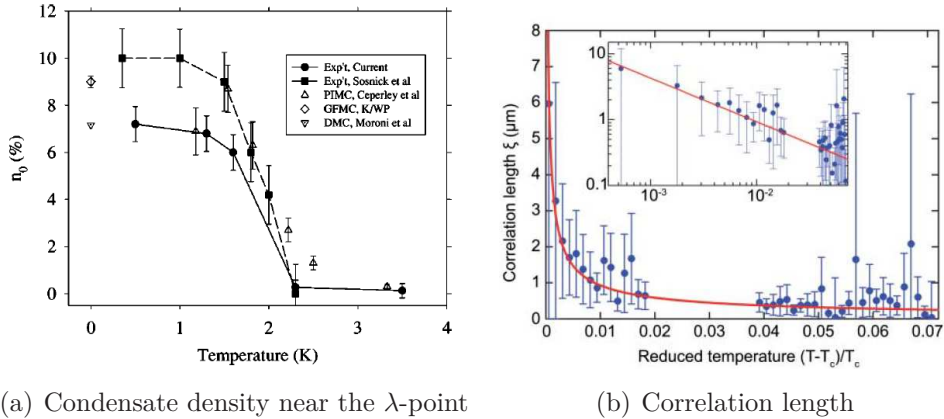


Figure 2.7: (a) Condensate density determined experimentally by neutron scattering measurements (dotted lines) and theoretically with Monte-Carlo simulations (points) [134]. (b) Correlation length of a Bose-Einstein condensed sample of ^{87}Rb [135].

reduced temperature $\epsilon = 1 - T/T_\lambda$ on logarithmic scales. This experiment is based on the measurement of the second sound c_2 , which is connected to the superfluid and normal density via

$$c_2^2 \propto \frac{\rho_s}{\rho_n c_p}, \quad (2.42)$$

and leads to the critical exponent $\nu = 0.674 \pm 0.001$ of the superfluid density [130].

The experimental determination of the critical exponent of the condensate density of He-II is pending. Even the challenge of an unambiguous identification of a condensate in liquid ^4He and an accurate determination of the condensate fraction f_c is not completed. Reasons for this are that liquid ^4He is a strongly interacting fluid and the condensate fraction is small. However in Fig. 2.7(a) experimental as well as theoretical results are shown for the condensate fraction denoted here as n_0 [134]. The points refer to results of Monte-Carlo simulations and the dotted lines to experimental data of neutron scattering experiments ([134] and references therein). The condensate fraction at $T = 0$ K lies between 7% and 10%. For $T > T_\lambda$ the condensate fraction is zero according to Ref. [134] which emphasizes the link between the condensate

and the superfluid fraction.

Another remarkable experiment determined the critical exponent of the correlation length of a Bose-Einstein condensed sample of ^{87}Rb [135]. The 2-point correlation function (2.25) was determined by the measurement of the visibility of the interference pattern of two atomic beams [136]. The correlation length is depicted in Fig. 2.7(b). Only the correlation length for temperatures $T > T_c$ was measured. It is clearly visible how the correlation length diverges at the critical temperature T_c . The phase transition of Bose-Einstein condensation should also be in the same universality class as the xy -model and the λ -transition of He-II with $N = 2$. But in this case the atoms were located in a trap so it was neither theoretically nor experimentally clear which value the critical exponent should attain. However the measured critical exponent of the correlation length is $\nu = 0.67 \pm 0.13$, which agrees with the theoretical result of the ϕ^4 -theory in Tab. 2.4 quite well.

Great prospects for the measurement of critical exponents offer Bose-Einstein condensates and ultracold atoms in optical lattices [62, 137]. In these experiments a Bose-Einstein condensate or a gas of ultracold atoms interact with a light-induced periodic potential leading to the interaction potential (1.7), which acts as the optical lattice. These systems are free of impurities and one has full control over various parameters such as the interaction strength. With such a controllable system it is possible to realize different models experimentally, such as the Bose-Hubbard model with its superfluid-to-Mott insulator quantum phase transition [6]. The opportunity to address and manipulate single sites of the lattice [138–141], which has emerged only recently, can be used, e.g., to directly measure correlation functions [142].

3 Perturbation theory

In physics one has often models which cannot be solved analytically. This means one has to use either approximations or perturbation theory. When using approximations there is always the danger of ignoring important physical features so that many problems do not allow to be treated with approximations. But on the other hand perturbational methods cannot always be used and the computational effort is often immense so that one is usually restricted to calculations up to the second order. Several approaches have been developed over the last hundred years as, e.g., the Rayleigh-Schrödinger [143] or Brillouin-Wigner perturbation theory [144]. In the first section of this chapter another formulation, which is called Kato's perturbation theory [145], will be introduced. It has the major advantage that this theory allows one to formulate the contributions to every order in a closed form, that means one needs no information about the preceding orders. In the second section this perturbation theory is applied to the Bose-Hubbard model. This leads to a tremendous speed-up of the calculations so that calculations up to the 10th order can be done on an average PC. It will be shown how this theory can be adapted to the treatment of the Bose-Hubbard model and how it can be implemented numerically by a diagrammatic approach.

3.1 Kato's perturbation theory

Starting point of the perturbation theory by Kato is the resolvent of an operator H which is defined as

$$R(\ell) = (\ell - H)^{-1} := (\ell I - H)^{-1} \quad (3.1)$$

with the identity operator I . All $\ell \in \mathbb{C}$ are allowed for which the resolvent exists, i.e., for which $(\ell I - H)$ is invertible. They define the resolvent set

$\rho(R)$ and the spectrum $\sigma(H) = \mathbb{C}/\rho(R)$ of an operator H . Because H is from now on the linear operator of a quantum mechanical system, the spectrum consists of all eigenvalues. In the following it is assumed that all operators are well-behaved in the sense that no pathological cases have to be considered. Ref. [146] presents a more precise definition of the operators treated here.

We assume that the spectrum of H is a point spectrum. That means this spectrum consists of discrete eigenvalues $\sigma(H) = \{\lambda_i, i \in \mathbb{N}\}$. The Hamiltonian can then be written as

$$H = \sum_i \lambda_i P_i, \quad (3.2)$$

with the projection operator P_i on the eigenspace of the corresponding eigenvalue λ_i . These projection operators fulfill the properties

$$P_i P_j = \delta_{ij} P_i, \quad (3.3)$$

which means that they are idempotent and orthogonal, as well as the completeness relation

$$\sum_i P_i = I. \quad (3.4)$$

The resolvent can then be spectrally decomposed into

$$R(\ell) = \sum_i (\ell - \lambda_i)^{-1} P_i. \quad (3.5)$$

If one applies Cauchy's integral formula to this equation one gets

$$\frac{1}{2\pi i} \oint_C d\ell R(\ell) = \frac{1}{2\pi i} \oint_C d\ell \sum_i (\ell - \lambda_i)^{-1} P_i = \sum_C P_i, \quad (3.6)$$

with a sum over all projection operators with eigenvalues λ_i lying inside the closed curve C in the complex plane.

Now a perturbed operator

$$H_x = H_0 + xV \quad (3.7)$$

is considered with a perturbation V , which is linearly coupled to the unperturbed part H_0 with a coupling strength $x \ll 1$. The eigenvalues of the unperturbed operator H_0 are denoted here as λ_i . Without loss of generality it

is assumed that the eigenvalue λ_i is not degenerate and, therefore, has the multiplicity one. For the resolvent $R_x(\ell)$ of H_x one has

$$P_x = \frac{1}{2\pi i} \oint_C d\ell R_x(\ell) \quad (3.8)$$

on the supposition of a regular perturbation, meaning that the projection operator on the eigenspace of the eigenvalues λ_x of H_x fulfills the condition

$$P_x \xrightarrow{\lim_{x \rightarrow 0}} P_0 . \quad (3.9)$$

Here it is assumed that the curve C encircles both the perturbed eigenvalue λ_x and the unperturbed eigenvalue λ_0 but no other eigenvalues.

Furthermore, for the resolvent one finds

$$\begin{aligned} R_x(\ell) &= (\ell - H_x)^{-1} = (\ell - H_0 - xV)^{-1} \\ &= \left([1 - xV \cdot R_0(\ell)] \frac{1}{R_0(\ell)} \right)^{-1} \\ &= R_0(\ell) \sum_{n=0}^{\infty} [V \cdot R_0(\ell)]^n \cdot x^n , \end{aligned} \quad (3.10)$$

where in the last step $[1 - xV \cdot R_0(\ell)]^{-1}$ was expanded into a Taylor series about $x = 0$. Inserting this into (3.8) one gets the expansion

$$\begin{aligned} P_x &= \frac{1}{2\pi i} \oint_C d\ell R_0(\ell) + \frac{1}{2\pi i} \sum_{n=1}^{\infty} \oint_C d\ell R_0(\ell) [V \cdot R_0(\ell)]^n \cdot x^n \\ &= P_0 + \sum_{n=1}^{\infty} A^{(n)} \cdot x^n \end{aligned} \quad (3.11)$$

for the projection operator on the eigenspaces of the full Hamiltonian H_x as a Taylor expansion about $x = 0$ with coefficients

$$A^{(n)} = \frac{1}{2\pi i} \oint_C d\ell R_0(\ell) [V \cdot R_0(\ell)]^n . \quad (3.12)$$

At this point the reduced resolvent

$$S_0(\ell) = \sum_{i \neq 0} (\ell - \lambda_i)^{-1} P_i \quad (3.13)$$

is introduced, given by the sum over all projection operators P_i with eigenvalues $\lambda_i \neq \lambda_0$. With this the unperturbed resolvent can be split into

$$R_0(\ell) = (\ell - \lambda_0)^{-1} P_0 + S_0(\ell) . \quad (3.14)$$

The reduced resolvent $S_0(\ell)$ is regular for $\ell = \lambda_0$ and the derivatives with respect to ℓ fulfill

$$\begin{aligned} S_0^{(k)}(\ell) &:= \frac{d^k}{d\ell^k} S_0(\ell) = \frac{d^k}{d\ell^k} \sum_{i \neq 0} (\ell - \lambda_i)^{-1} P_i \\ &= (-1)^k k! \sum_{i \neq 0} (\ell - \lambda_i)^{-(k+1)} P_i = (-1)^k k! S_0(\ell)^{k+1} , \end{aligned} \quad (3.15)$$

where the last identity holds because of the orthogonality of the projection operators in (3.3). After an expansion about $\ell = \lambda_0$ one gets together with (3.15)

$$\begin{aligned} S_0(\ell) &= \sum_{k=0}^{\infty} \frac{1}{k!} S_0^{(k)}(\lambda_0) \cdot (\ell - \lambda_0)^k \\ &= \sum_{k=0}^{\infty} (-1)^k S_0(\lambda_0)^{k+1} \cdot (\ell - \lambda_0)^k . \end{aligned} \quad (3.16)$$

With (3.16) the full unperturbed resolvent (3.14) can be written as

$$\begin{aligned} R_0(\ell) &= (\ell - \lambda_0)^{-1} P_0 + \sum_{k=0}^{\infty} (-1)^k S_0(\lambda_0)^{k+1} \cdot (\ell - \lambda_0)^k \\ &= \sum_{k=-1}^{\infty} (-1)^k S^{k+1} \cdot (\ell - \lambda_0)^k . \end{aligned} \quad (3.17)$$

Here, the short-hand notation

$$S^0 := -P_0 , \quad (3.18a)$$

$$S^k := S_0(\lambda_0)^k, \quad k > 0 \quad (3.18b)$$

was introduced. Equation (3.17) corresponds to the Laurent series of $R_0(\ell)$. That means that for the integrand $R_0(\ell) [V \cdot R_0(\ell)]^n$ of (3.12) there also exists

a Laurent series, whose principal part consists only of that part which is proportional to $(\ell - \lambda_0)^{-1}$. Because of the integral equation (3.12) and the residue theorem, $A^{(n)}$ is identical with the residue of the integrand. For the evaluation of the integral in (3.11) only those summands in the sum $\sum_{n=1}^{\infty} R_0(\ell) [V \cdot R_0(\ell)]^n$ have to be considered for which the factors $(\ell - \lambda_0)^k$ multiply to $(\ell - \lambda_0)^{-1}$. Introducing new exponents α_k ($k = 1, \dots, n+1$) and numerating the occurring factors according to

$$\left[(-1)^{\alpha_1-1} S^{\alpha_1} (\ell - \lambda_0)^{\alpha_1-1} \right] V \dots V \left[(-1)^{\alpha_{n+1}-1} S^{\alpha_{n+1}} (\ell - \lambda_0)^{\alpha_{n+1}-1} \right], \quad (3.19)$$

one gets therefore the condition

$$(\alpha_1 - 1) + \dots + (\alpha_{n+1} - 1) = -(n+1) + \sum_{k=1}^{n+1} \alpha_k \stackrel{!}{=} -1. \quad (3.20)$$

It is exactly fulfilled if

$$\sum_{k=1}^{n+1} \alpha_k = n \quad (3.21)$$

holds for the respective exponents α_k . Because of this condition the prefactors $(-1)^{\alpha_i-1}$ of the particular factors in (3.19) result in a prefactor -1 and, therefore, (3.12) becomes

$$A^{(n)} = - \sum_{\alpha_1 + \dots + \alpha_{n+1} = n} S^{\alpha_1} V S^{\alpha_2} V \dots V S^{\alpha_{n+1}}. \quad (3.22)$$

Thus, the projection operator is finally given by

$$P_x = P_0 - \sum_{n=1}^{\infty} x^n \sum_{\alpha_1 + \dots + \alpha_{n+1} = n} S^{\alpha_1} V S^{\alpha_2} V \dots V S^{\alpha_{n+1}}. \quad (3.23)$$

The derivation of a scheme for the perturbative calculation of the eigenvalues proceeds in a similar way. With the identity $H_x R_x(\ell) = -I + \ell R_x(\ell)$ and (3.8)

one has

$$\begin{aligned}
(H_x - \lambda_0)P_x &= \frac{1}{2\pi i} \oint_C d\ell (H_x - \lambda_0) \cdot R_x(\ell) \\
&= \frac{1}{2\pi i} \oint_C d\ell (\ell - \lambda_0) \cdot R_x(\ell) \\
&= \frac{1}{2\pi i} \oint_C d\ell (\ell - \lambda_0) \cdot R_0(\ell) \sum_{n=0}^{\infty} [V \cdot R_0(\ell)]^n \cdot x^n \\
&= \sum_{n=1}^{\infty} B^{(n)} \cdot x^n,
\end{aligned} \tag{3.24}$$

where the expression (3.10) was used in the third row. The summand for $n = 0$ vanishes and only the analytic integrand P_0 remains. For the calculation of the integral

$$B^{(n)} = \frac{1}{2\pi i} \oint_C d\ell (\ell - \lambda_0) \cdot R_0(\ell) [V \cdot R_0(\ell)]^n \tag{3.25}$$

all arguments leading to the condition (3.21) in the calculation of the integral (3.12) can also be used here. The only difference is that in the integrand one more factor $(\ell - \lambda_0)$ exists so that the condition for the exponents reads here

$$1 + (\alpha_1 - 1) + \dots + (\alpha_{n+1} - 1) = -n + \sum_{k=1}^{n+1} \alpha_k \stackrel{!}{=} -1, \tag{3.26}$$

leading to

$$\sum_{k=1}^{n+1} \alpha_k = n - 1. \tag{3.27}$$

Since the requirement on the exponents α_k differs from that for the projection operator, here the prefactor, which stems from the particular factors $(-1)^{\alpha_k - 1}$ in (3.19), is one.

For the following it is useful to define the set

$$\Lambda_n := \left\{ (\alpha_1, \dots, \alpha_{n+1}) \mid \sum_{k=1}^{n+1} \alpha_k = n - 1 \right\}, \tag{3.28}$$

containing all integers $(\alpha_1, \dots, \alpha_{n+1})$ which obey the condition (3.27).

After the application of the trace operator on (3.24) the desired eigenvalue of the full Hamiltonian H_x is given by

$$\begin{aligned}\lambda_x &= \lambda_0 + \sum_{n=1}^{\infty} x^n \cdot \text{tr} \{B^{(n)}\} . \\ &= \lambda_0 + \sum_{n=1}^{\infty} x^n \sum_{\Lambda_n} \text{tr} \{S^{\alpha_1} V S^{\alpha_2} V \dots V S^{\alpha_{n+1}}\} .\end{aligned}\tag{3.29}$$

For the evaluation of the matrix elements $n + 1$ exponents α_i must be determined. This is a purely combinatorial problem and can be solved irrespective of the concrete form of the perturbation V . So only the combinations $(\alpha_1, \dots, \alpha_{n+1})$ are of interest for this problem. The determination of all combinations can be done numerically up to very high orders. For instance up to the 20th order the computation time on a 2GHz PC stays under a minute [147, 148].

3.2 Properties and applications

As already mentioned in the introduction of this chapter, one can adapt Kato's perturbation theory to the Bose-Hubbard model in order to speed up the calculations provided one is given a unique ground state $|m\rangle$. Furthermore, the calculation of correlation functions with this perturbation theory will be explained. Finally, the implementation of Kato's perturbation theory is shown by using the example of the calculation of the ground-state energy.

3.2.1 Standard form of matrix elements

The operators of (3.18) are superpositions of weighted projection operators and fulfill, due to (3.3) and (3.4), the useful relations

$$S^0 S^0 = -S^0 , \tag{3.30a}$$

$$S^0 S^\alpha = S^\alpha S^0 = 0 \quad \text{for } \alpha > 0 , \tag{3.30b}$$

$$S^\alpha S^\beta = S^{\alpha+\beta} \quad \text{for } \alpha, \beta > 0 . \tag{3.30c}$$

From now on they are called *chain operators* because they connect the single perturbation operators to a chain as can be seen in (3.29).

The following considerations allow one to convert the seemingly complicated matrix elements $\text{tr} \{S^{\alpha_1} V S^{\alpha_2} V \dots V S^{\alpha_{n+1}}\}$, which are necessary for the calculation of the eigenvalues, to the so-called standard form which enables a significantly simpler evaluation.

If one of the conditions

$$\alpha_1 = 0 \wedge \alpha_{n+1} \neq 0 \quad \text{or} \quad \alpha_1 \neq 0 \wedge \alpha_{n+1} = 0 \quad (3.31)$$

holds for the first or last exponent in (3.29) the corresponding matrix element vanishes, since then orthogonal states appear on the left and right side because of the trace operator and cancel each other according to (3.30b). Therefore, only matrix elements with $\alpha_1 \neq 0 \neq \alpha_{n+1}$ have to be considered.

Furthermore, condition (3.27) requires that at least two exponents have to be zero since $n + 1$ non-negative integers must be summed up to $n - 1$. That means a matrix elements consists always of at least two chain operators S^0 .

In addition the trace is invariant under cyclic permutations, i.e.,

$$\text{tr}(ABC) = \text{tr}(CAB) = \text{tr}(BCA) . \quad (3.32)$$

If one combines the two latter properties, the matrix elements can always be turned into

$$\begin{aligned} & \text{tr} \{S^{\alpha_1} V \dots S^{\alpha_{i-1}} V S^0 V S^{\alpha_{i+1}} \dots V S^{\alpha_{n+1}}\} \\ \stackrel{(3.30c)}{=} & \text{tr} \{S^0 V S^{\alpha_{i+1}} \dots V S^{\alpha_1 + \alpha_{n+1}} V \dots S^{\alpha_{i-1}} V\} \\ \stackrel{(3.30a)}{=} & - \text{tr} \{S^0 S^0 V S^{\alpha_{i+1}} \dots V S^{\alpha_1 + \alpha_{n+1}} V \dots S^{\alpha_{i-1}} V\} \\ = & - \text{tr} \{S^0 V S^{\alpha_{i+1}} \dots V S^{\alpha_1 + \alpha_{n+1}} V \dots S^{\alpha_{i-1}} V S^0\} \end{aligned} \quad (3.33)$$

with S^0 at the first and last position. Therefore, assuming that the projection operator P_0 is given by the projection on the unique ground state $|m\rangle$ with the corresponding chain operator

$$S^0 = -P_0 = -|m\rangle \langle m| , \quad (3.34)$$

all matrix elements can always be turned into the standard form

$$\pm \langle m| V S^{\alpha_1} V S^{\alpha_2} V \dots V S^{\alpha_{n-1}} V |m\rangle \quad (3.35)$$

independent of their explicit structure.

Matrix elements already in standard form can be further summed up. A matrix element in standard form with one or more chain operators S^0 can be split up in so-called submatrix elements:

$$\begin{aligned}
 &= \langle \mathbf{m} | VS^{\alpha_1} \dots S^{\alpha_{i-1}} VS^0 VS^{\alpha_{i+1}} \dots S^{\alpha_{n-1}} V | \mathbf{m} \rangle \\
 &\stackrel{(3.18a)}{=} - \langle \mathbf{m} | VS^{\alpha_1} \dots S^{\alpha_{i-1}} V | \mathbf{m} \rangle \langle \mathbf{m} | VS^{\alpha_{i+1}} \dots S^{\alpha_{n-1}} V | \mathbf{m} \rangle \\
 &= - \langle \mathbf{m} | VS^{\alpha_{i+1}} \dots S^{\alpha_{n-1}} V | \mathbf{m} \rangle \langle \mathbf{m} | VS^{\alpha_1} \dots S^{\alpha_{i-1}} V | \mathbf{m} \rangle \\
 &= \langle \mathbf{m} | VS^{\alpha_{i+1}} \dots S^{\alpha_{n-1}} VS^0 VS^{\alpha_1} \dots S^{\alpha_{i-1}} V | \mathbf{m} \rangle .
 \end{aligned} \tag{3.36}$$

If the submatrix elements of different standard forms are identical, which may be achieved in some cases only after cyclic permutation, then also the standard forms are identical. They can be summed up, and yield a corresponding weight factor.

So far the considerations were independent of the concrete form of the perturbation V . But in some cases the evaluation of matrix elements can be further simplified if the explicit structure of the perturbation operator is considered. E.g., in many cases the first-order contribution

$$\langle \mathbf{m} | V | \mathbf{m} \rangle = 0 \tag{3.37}$$

vanishes. This holds often for the dipole operator $\mathbf{d} = -e\mathbf{r}$ and the interaction operator $V = -\mathbf{d} \cdot \mathcal{E}$, respectively, of a charge in an electromagnetic field, which changes the parity of the wave function. Another example is the tunneling operator $V = b_i^\dagger b_j$ of the Bose-Hubbard model, if the ground state $|\mathbf{m}\rangle$ is the Mott insulator (1.8). In these cases matrix elements with the factors $\dots S^0 VS^0 \dots$ can be neglected.

3.2.2 Calculation of correlation functions

Up to now only the calculation of the expectation value of the energy of a Hamiltonian has been addressed. Beyond that it is also necessary to calculate expectation values of other operators as, for instance, correlation functions.

Starting with the perturbative calculation of energy eigenvalues, there also exists a general approach to the calculation of these [149].

If one wants to calculate the expectation value of an operator H_2 of a system described by a Hamiltonian $H_x = H_0 + xH_1$, the first step is to couple the operator to this Hamiltonian. Should H_2 not be Hermitian, one could choose the superpositions $H_2^{(+)} = \frac{1}{2}(H_2 + H_2^\dagger)$ or $H_2^{(-)} = \frac{1}{2i}(H_2 - H_2^\dagger)$.

Now the energy of the new Hamiltonian

$$H_{x,y} = H_0 + xH_1 + yH_2 \quad (3.38)$$

can be calculated for the perturbation $V = xH_1 + yH_2$ with the formalism of Sec. 3.1. For the eigenstate $|m\rangle$ of the unperturbed part H_0 one gets according to (3.29)

$$\begin{aligned} \lambda_{x,y} &= \lambda_0 + \sum_{n=1}^{\infty} \sum_{\Lambda_n} \text{tr} \{ S^{\alpha_1} V S^{\alpha_2} V \dots V S^{\alpha_{n+1}} \} \\ &= \lambda_0 + \sum_{n=1}^{\infty} \sum_{\nu=0}^n x^\nu y^{n-\nu} D^{(\nu, n-\nu)}. \end{aligned} \quad (3.39)$$

Here $D^{(\nu, n-\nu)}$ is the sum over all traces which contain ν operators H_1 and $n - \nu$ operators H_2 fulfilling the condition $(\alpha_1, \dots, \alpha_{n+1}) \in \Lambda_n$. After using the Hellmann-Feynman theorem [150]

$$\frac{d}{dy} \langle H \rangle = \left\langle \frac{d}{dy} H \right\rangle, \quad (3.40)$$

where the left-hand side refers to the eigenvalue of (3.39) and the right-hand side to the extended Hamiltonian of (3.38), one gets

$$\langle H_2 \rangle = \lim_{y \rightarrow 0} \sum_{n=1}^{\infty} \sum_{\nu=0}^n (n - \nu) x^\nu y^{n-\nu-1} D^{(\nu, n-\nu)}. \quad (3.41)$$

In the limit of vanishing coupling $y \rightarrow 0$ only summands with $n - \nu - 1 = 0$ contribute, with $n = \nu + 1$ being the order of the perturbative calculation. That means the operator H_1 occurs $(n - 1)$ times and the operator H_2 occurs

($n - \nu = 1$) times. Therefore, the sum reduces to

$$\begin{aligned}
 \langle H_2 \rangle &= \sum_{\nu=0}^{\infty} x^\nu D^{(\nu,1)} \\
 &= \text{tr} \left\{ S^0 H_2 S^0 \right\} \\
 &\quad + x \text{tr} \left\{ S^0 H_1 S^1 H_2 S^0 + S^0 H_2 S^1 H_1 S^0 \right\} \pm \mathcal{O}(x^2) \\
 &= \langle \mathbf{m} | H_2 | \mathbf{m} \rangle \\
 &\quad + \left[\langle \mathbf{m} | H_1 S^1 H_2 | \mathbf{m} \rangle + \langle \mathbf{m} | H_2 S^1 H_1 | \mathbf{m} \rangle \right] x \pm \mathcal{O}(x^2) .
 \end{aligned} \tag{3.42}$$

3.2.3 Energy eigenvalues in third-order perturbation theory

Now Kato's perturbation theory will be demonstrated by using the example of the perturbative calculation of the ground-state energy λ_x in third order of a Hamiltonian $H = H_0 + xV$ in the state $|\mathbf{m}\rangle$ with the unperturbed energy given by

$$H_0 |\mathbf{m}\rangle = \lambda_m |\mathbf{m}\rangle . \tag{3.43}$$

The zeroth order delivers trivially the eigenvalue $\lambda_m^{(0)} = \lambda_m$ of H_0 .

According to (3.27), in first order the exponents must fulfill the condition $\alpha_1 + \alpha_2 = 0$ which is only possible for $(\alpha_1, \alpha_2) = (0, 0)$. Accordingly the perturbational contribution in this order is

$$\lambda_m^{(1)} = \text{tr} \left\{ S^0 V S^0 \right\} = \langle \mathbf{m} | V | \mathbf{m} \rangle . \tag{3.44}$$

In second order $\alpha_1 + \alpha_2 + \alpha_3 = 1$ must hold, leading to the set

$$\Lambda_2 = \{(1, 0, 0), (0, 1, 0), (0, 0, 1)\} \tag{3.45}$$

of 3-tuples. The corresponding matrix elements of the first and last term vanish according to (3.31). Only the diagonal matrix elements

$$\lambda_m^{(2)} = \text{tr} \left\{ S^0 V S^1 V S^0 \right\} = \langle \mathbf{m} | V S^1 V | \mathbf{m} \rangle = \sum_{i \neq m} \frac{\langle \mathbf{m} | V | i \rangle \langle i | V | \mathbf{m} \rangle}{\lambda_m - \lambda_i} \tag{3.46}$$

are left over.

In third order already ten combinations fulfilling $\alpha_1 + \alpha_2 + \alpha_3 + \alpha_4 = 2$ exist. Excluding non-contributing matrix elements as dictated by (3.31), one gets the set

$$\Lambda_3 = \{(1, 0, 0, 1), (0, 1, 1, 0), (0, 2, 0, 0), (0, 0, 2, 0)\} \quad (3.47)$$

of 4-tuples. The first term can be rearranged to read

$$\begin{aligned} (1, 0, 0, 1) &\cong \text{tr} \{S^1 V S^0 V S^0 V S^1\} \\ &= \text{tr} \{S^0 V S^0 V S^1 S^1 V\} = \text{tr} \{S^0 V S^0 V S^2 V\} \\ &= \text{tr} \{S^0 V S^2 V S^0 V\} = -\text{tr} \{S^0 V S^2 V S^0 V S^0\} \\ &\cong - (0, 2, 0, 0) . \end{aligned} \quad (3.48)$$

Similarly the term $(0, 0, 2, 0)$ can be rearranged to $(0, 2, 0, 0)$ so that after summarizing the three resulting terms, $(0, 2, 0, 0)$ has the weight one. The resulting set contains therefore the combinations $\{(0, 2, 0, 0), (0, 1, 1, 0)\}$. This leads to the third-order energy correction

$$\begin{aligned} \lambda_m^{(3)} &= \text{tr} \{S^0 V S^2 V S^0 V S^0\} + \text{tr} \{S^0 V S^1 V S^1 V S^0\} \\ &= - \sum_{i \neq m} \frac{\langle m | V | i \rangle \langle i | V | m \rangle \langle m | V | m \rangle}{(\lambda_m - \lambda_i)^2} \\ &\quad + \sum_{i, j \neq m} \frac{\langle m | V | i \rangle \langle i | V | j \rangle \langle j | V | m \rangle}{(\lambda_m - \lambda_i)(\lambda_m - \lambda_j)} . \end{aligned} \quad (3.49)$$

In total one gets

$$\begin{aligned} \lambda_x &= \langle m | H_0 | m \rangle + \langle m | V | m \rangle \cdot x + \sum_{i \neq m} \frac{\langle m | V | i \rangle \langle i | V | m \rangle}{\lambda_m - \lambda_i} \cdot x^2 \\ &\quad + \left[\sum_{i, j \neq m} \frac{\langle m | V | i \rangle \langle i | V | j \rangle \langle j | V | m \rangle}{(\lambda_m - \lambda_i)(\lambda_m - \lambda_j)} \right. \\ &\quad \left. - \sum_{i \neq m} \frac{\langle m | V | i \rangle \langle i | V | m \rangle \langle m | V | m \rangle}{(\lambda_m - \lambda_i)^2} \right] \cdot x^3 + \mathcal{O}(x^4) , \end{aligned} \quad (3.50)$$

which is equivalent to the well-known textbook result of Rayleigh-Schrödinger perturbation theory [143].

3.2.4 Process-chain approach

In this section the diagrammatical implementation of Kato's perturbation theory within a many-body context will be explained [149]. Since the focus of this thesis lies on the Bose-Hubbard model, this model is also used as a testing ground for the implementation of this perturbation theory. For reasons of simplicity all examples given in the following are calculated on a one-dimensional lattice with $z = 2$ nearest neighbors. All calculations can be easily adapted to other lattice geometries by considering the respective diagrams.

The process-chain approach can also be applied to other models, as it was recently done in Ref. [151] in order to calculate the ground-state energy of the Jaynes-Cummings lattice model.

The homogeneous Bose-Hubbard Hamiltonian has been introduced in (1.2). For reasons of numerical calculations the Hamiltonian is used in its dimensionless form

$$H_{\text{BH}} = \frac{1}{2} \sum_i n_i (n_i - 1) - \mu/U \sum_i n_i - J/U \sum_{\langle i,j \rangle} b_i^\dagger b_j. \quad (3.51)$$

Basically it consists of two parts. The first part

$$H_0 = \frac{1}{2} \sum_i n_i (n_i - 1) - \mu/U \sum_i n_i \quad (3.52)$$

is the on-site interaction together with the chemical potential. This part of the Hamiltonian is diagonal in the Fock space of site-occupation states. The second part is the tunneling term

$$V = -J/U \sum_{\langle i,j \rangle} b_i^\dagger b_j, \quad (3.53)$$

which is treated as the perturbation. The index $\langle i, j \rangle$ indicates that the tunneling is restricted to neighboring sites.

The ground state

$$|m\rangle = |\Psi_{\text{MI}}\rangle = \prod_{i=1}^M \frac{(b_i^\dagger)^g}{\sqrt{g!}} |0\rangle = |g\rangle \dots |g\rangle, \quad (3.54)$$

from which the perturbative calculations start, is given by the ground state (1.8) of the Mott insulator and has an integer number $g = N/M$ of particles on every site. Here N denotes the number of particles and M is the number of lattice sites. In this basis the ground-state energy is given by

$$\lambda_m := \lambda_m^{(0)} = \langle m | H_0 | m \rangle = \frac{M}{2}g(g-1) - M\frac{\mu}{U}g. \quad (3.55)$$

Central point of the diagrammatical representation of Kato's perturbation theory are the matrix elements in standard form

$$\lambda^{(n)} = \sum \kappa_{\{\alpha_\ell\}} \langle m | VS^{\alpha_1}VS^{\alpha_2}V \dots VS^{\alpha_{n-1}}V | m \rangle \quad (3.56)$$

as defined in (3.35). Here $\lambda^{(n)}$ denotes the n -th order energy correction and $\kappa_{\{\alpha_\ell\}}$ is the sign belonging to a specific $(n-1)$ -tuple $\{\alpha_\ell\}$, with the sum extending over all these tuples. The chain operator $S^0 = -|m\rangle\langle m|$ is defined by the ground state mentioned above and all other chain operators

$$S^\alpha = \sum_{i \neq m} \frac{|i\rangle\langle i|}{(\lambda_m - \lambda_i)^\alpha} \quad (3.57)$$

are therefore defined by the intermediate states $|i\rangle$ which form a complete basis of orthogonal Fock states with N particles.

Every summand of (3.56) can now be interpreted as a chain of processes V leading from the ground state $|m\rangle$ over various intermediate states given by S^α back to the ground state [152].

Formally one has to calculate the energy starting from every lattice site. But since the homogeneous Bose-Hubbard Hamiltonian (3.51) is isotropic and translationally invariant, it is sufficient to calculate the contribution to the energy of one lattice site. The contribution of the whole lattice is then given by a multiplication with the number M of lattice sites.

To visualize the diagrammatic perturbation theory, the perturbative calculation of energy corrections in a one-dimensional lattice will be presented. The number of nearest neighbors for $D = 1$ is given by $z = 2D = 2$ so that for every tunneling process $b_2^\dagger b_1$ with lattice sites 1 and 2 being nearest neighbors two directions are possible. Starting with the first order, the corresponding

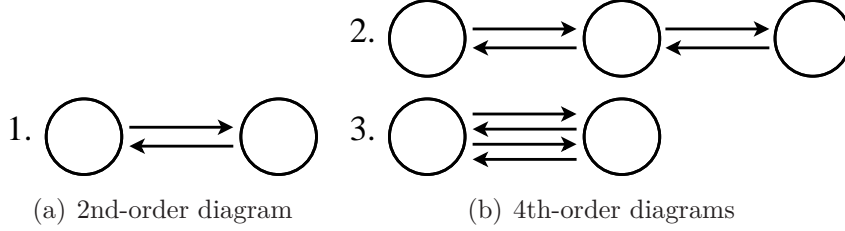


Figure 3.1: All three 2nd- and 4th-order diagrams contributing to the ground-state energy of the Bose-Hubbard model on a one-dimensional lattice. An arrow corresponds to a hopping process, a circle depicts a lattice site. All these diagrams are closed, i.e., in n th-order a particle would tunnel back to its starting site after n tunneling processes. Odd-order diagrams do not contribute to the ground-state energy since these are never closed.

contribution is given by (3.44). So one particle has to tunnel from site 1 to site 2 leading to an intermediate state

$$|i\rangle = \sqrt{g(g+1)} |g\rangle \dots |g\rangle \underbrace{|g-1\rangle}_1 \underbrace{|g+1\rangle}_2 |g\rangle \dots |g\rangle \quad (3.58)$$

with the prefactor coming from the creation and annihilation operators, respectively. Since $\langle m|i\rangle = 0$ the first-order energy contribution vanishes.

At this point it is beneficial to introduce a clear notation of diagrams. Since all lattice sites of the Bose-Hubbard Hamiltonian (3.51) are equivalent, it is not important which specific sites of the lattice are involved in the tunneling processes. Instead every diagram is uniquely defined by the way it connects the individual sites. For example the diagram, which is used for the calculation of the first-order energy correction, can be represented by the notation $\{^1_2\}$. Here a particle tunnels from site 1 to site 2. In general an n th-order diagram consisting of tunneling processes $\{b_{i_1}^\dagger b_{j_1} \ b_{i_2}^\dagger b_{j_2} \ \dots \ b_{i_n}^\dagger b_{j_n}\}$ can be represented by $\left\{ \begin{matrix} j_1 & j_2 & \dots & j_n \\ i_1 & i_2 & \dots & i_n \end{matrix} \right\}$.

The second order is given by (3.46) so that two tunneling processes have to be considered. For the same reasons stated above, two tunneling processes leading away from the starting site give rise to a state which is orthogonal to the ground state $|m\rangle$. So only two tunneling processes leading back and forth can contribute. This is only fulfilled by the diagram $\{^1_2, ^2_1\}$. Since there are two

possibilities to realize this diagram, given by tunneling first to the left or right nearest neighbor, this diagram must be provided with a weight factor 2. This diagram is shown in Fig. 3.1(a). The arrows symbolize the tunneling processes and the circles the lattice sites. Fig. 3.1(b) shows the respective diagrams of the 4th-order. Diagram number two is given by $\{\frac{1}{2} \frac{2}{3} \frac{3}{2} \frac{2}{1}\}$ and diagram number three by $\{\frac{1}{2} \frac{2}{1} \frac{1}{2} \frac{2}{1}\}$. Since odd orders always vanish for the same reason the first order vanishes, Fig. 3.1 shows all diagrams necessary to calculate the energy up to the 4th order.

As already mentioned it is possible to calculate the contribution of all lattice sites by calculating the contribution of one lattice site. The end result is then given after the multiplication with M . The easiest way to calculate the contribution of one site is to find all possible diagrams and to permute the sequence of tunneling processes, e.g. one has to calculate the contribution of $\{\frac{1}{2} \frac{2}{1}\}$ and $\{\frac{2}{1} \frac{1}{2}\}$. But this leads to a multiple counting since after the multiplication with M the sequence of tunneling processes $\{\frac{1}{2} \frac{2}{1}\}$ counts as a full contribution of both the sites 1 and 2, although both participate only half in this sequence. In order to avoid this, an additional correction factor must be assigned to every diagram. For diagrams necessary to calculate the energy this correction factor is the number of sites involved in the respective diagram. This is characteristic for diagrams which are closed, i.e., such diagrams which lead a particle back to the site where it started.

Summarizing these remarks, with the intermediate states

$$\begin{aligned} |i_1\rangle &= \sqrt{g(g+1)} |g\rangle \dots |g\rangle |g+1\rangle |g-1\rangle |g\rangle \dots |g\rangle, \\ |i_2\rangle &= \sqrt{g(g+1)} |g\rangle \dots |g\rangle |g-1\rangle |g+1\rangle |g\rangle \dots |g\rangle \end{aligned} \quad (3.59)$$

the second-order contribution is given by

$$\begin{aligned} \lambda_m^{(2)} &= M(J/U)^2 \underbrace{2}_{\text{weight factor}} \underbrace{0.5}_{\text{correction factor}} \\ &\cdot \left(\frac{\langle m | b_j^\dagger b_{j-1} | i_1 \rangle \langle i_1 | b_{j-1}^\dagger b_j | m \rangle}{\lambda_m - \lambda_{i_1}} + \frac{\langle m | b_{j-1}^\dagger b_j | i_2 \rangle \langle i_2 | b_j^\dagger b_{j-1} | m \rangle}{\lambda_m - \lambda_{i_2}} \right) \quad (3.60) \\ &= -2Mg(g+1)(J/U)^2. \end{aligned}$$

It does not depend on the chemical potential μ since for the energy differences one has $\lambda_m - \lambda_{i_1} = \lambda_m - \lambda_{i_2} = -1$.

diagram	weight factor
$\begin{Bmatrix} 1 & 2 \\ 2 & 1 \end{Bmatrix}$	$2D$
$\begin{Bmatrix} 1 & 2 & 3 & 2 \\ 2 & 3 & 2 & 1 \end{Bmatrix}$	$2D(2D - 1) + D(2D - 1)$
$\begin{Bmatrix} 1 & 2 & 1 & 2 \\ 2 & 1 & 2 & 1 \end{Bmatrix}$	$2D$
$\begin{Bmatrix} 1 & 2 & 3 & 4 \\ 2 & 3 & 4 & 1 \end{Bmatrix}$	$2D(2D - 2)$
$\begin{Bmatrix} 1 & 2 & 3 & 4 & 3 & 2 \\ 2 & 3 & 4 & 3 & 2 & 1 \end{Bmatrix}$	$4D(2D - 1)^2$
$\begin{Bmatrix} 1 & 2 & 1 & 2 & 1 & 2 \\ 2 & 1 & 2 & 1 & 2 & 1 \end{Bmatrix}$	$2D$
$\begin{Bmatrix} 1 & 2 & 3 & 4 & 1 & 5 \\ 2 & 3 & 4 & 1 & 5 & 1 \end{Bmatrix}$	$8D(2D - 2)^2 + 2D(2D - 2)(2D - 3) + 2D(2D - 2)$
$\begin{Bmatrix} 1 & 2 & 3 & 2 & 3 & 4 \\ 2 & 3 & 2 & 3 & 4 & 1 \end{Bmatrix}$	$8D(2D - 2)$
$\begin{Bmatrix} 1 & 2 & 3 & 4 & 5 & 6 \\ 2 & 3 & 4 & 5 & 6 & 1 \end{Bmatrix}$	$6D(2D - 2) + 8D(2D - 2)(2D - 4)$
$\begin{Bmatrix} 1 & 2 & 3 & 2 & 4 & 2 \\ 2 & 3 & 2 & 4 & 2 & 1 \end{Bmatrix}$	$\frac{4}{3}D(2D - 1)(2D - 2)$
$\begin{Bmatrix} 1 & 2 & 3 & 2 & 3 & 2 \\ 2 & 3 & 2 & 3 & 2 & 1 \end{Bmatrix}$	$6D(2D - 1)$

Table 3.1: Listed are all diagrams needed for the calculation of the ground-state energy of the Bose-Hubbard model up to the 6th order. The weight factors are valid for lattice geometries with $2D$ nearest neighbors, e.g., the square lattice for $D = 2$ or the cubic lattice for $D = 3$.

The next non-vanishing order is the 4th order. The two diagrams are shown in Fig. 3.1(b). The calculation of their contribution is by far more complex than that of the second-order diagram. The diagram number two, $\begin{Bmatrix} 1 & 2 & 3 & 2 \\ 2 & 3 & 2 & 1 \end{Bmatrix}$ in Fig. 3.1, consists of four different tunneling processes so that one has $4! = 24$ permutations to consider. Diagram number three $\begin{Bmatrix} 1 & 2 & 1 & 2 \\ 2 & 1 & 2 & 1 \end{Bmatrix}$ consists of the two different tunneling processes $\frac{1}{2}$ and $\frac{2}{1}$ which gives $\frac{4!}{2!2!} = 6$ permutations. If one considers lattices with a higher dimensionality, only the complexity of the diagrams changes. Tab. 3.1 shows all diagrams up to the 6th order including their weight factors. Some diagrams with weight zero like the fourth diagram do not exist for a one-dimensional lattice.

According to the linked-cluster theorem [153] it is sufficient to consider only process-chains which consist of one connected piece. That means every lattice site participating in the considered process has to be connected to all others

by a sequence of chain operators.

For the one-, two-, and three-dimensional square lattice the results of the perturbational calculation of the ground-state energy of the Bose-Hubbard model can be found in Ref. [154]. For the one-dimensional lattice these results agree accurately with the data of a linked-cluster expansion [155].

For this kind of numerical evaluation the number of permutations is the most severe limitation. Up to now the numerical implementation allows us to perform calculations up to the 12th order with a maximum of 12! permutations.

The diagrammatics introduced in this section can be ideally implemented numerically as is explained briefly in Ref. [156]. This formalism can also be easily generalized and used for the diagrammatic calculation of, e.g., correlation functions [149, 154].

4 Non-perturbative methods

In this chapter some methods are introduced to extend the perturbative results of the process-chain approach into a non-perturbative regime. These methods allow one to obtain results which are not directly accessible through the finite series of the perturbative calculations. This is necessary since the process-chain approach itself relies on the ground state of the Mott insulator so that the superfluid phase cannot be entered with this approach alone. Moreover some perturbative results apparently show a mean-field behavior which is quantitatively wrong for the critical exponents. Thus, a special treatment is required, in order to obtain results which are beyond mean field.

In the first section the method of the effective potential [157] is detailed briefly. This method allows one to enter the superfluid phase although all perturbational calculations start in the Mott-insulator state as stated in Sec. 3.2.4. The key point of this method is the implementation of a symmetry-breaking term and the Legendre transformation of the free energy of the Bose-Hubbard Hamiltonian to the effective potential which depends on the order parameter of the superfluid-to-Mott insulator phase transition. This method involves a resummation of the perturbative coefficients of the free energy, which are accessible as finite series. This resummation has the form of a Taylor expansion and transforms the perturbative data of the process-chain approach to beyond-perturbative results.

In the second section the variational perturbation theory of Hagen Kleinert [99, 100] is explained. It allows one to transform the divergent weak-coupling series of the process-chain approach to a convergent strong-coupling series which provides a direct access to the critical exponents of a considered quantity. Thus, variational perturbation theory basically acts as a resummation method which permits access to beyond-mean field results.

4.1 Method of effective action

The Bose-Hubbard Hamiltonian (3.51) possesses a $U(2) = O(1)$ symmetry which basically means that the Hamiltonian is invariant under a phase transformation $b_i \rightarrow e^{i\varphi} b_i$, $b_i^\dagger \rightarrow e^{-i\varphi} b_i^\dagger$ of the annihilation and creation operators, respectively. This also means that the Hamiltonian conserves the number of particles N in the lattice. On the other hand the phase transition from the Mott insulator to the superfluid explained in the introduction in Sec. 1.4 can only be observed if this symmetry is broken. This breaking of the symmetry occurs spontaneously and is modeled by introducing external source fields η , η^* as explained in Sec. 2.1. The natural choice for implementing the symmetry-breaking terms is the creation and annihilation operators, respectively, since they are not invariant under the transformation mentioned above on their own. So the symmetry-breaking terms read ηb_i^\dagger and the complex conjugated $\eta^* b_i$. They are coupled to the dimensionless Bose-Hubbard Hamiltonian (3.51) so that one gets a new Hamiltonian

$$\tilde{H}_{\text{BH}} = H_0 + V + \sum_i \left(\eta b_i^\dagger + \eta^* b_i \right) , \quad (4.1)$$

where H_0 represents the site-diagonal terms defined in (3.52) and V is the tunneling term defined in (3.53). These symmetry-breaking terms are also called source and drain terms since they create or annihilate particles, so \tilde{H}_{BH} does not conserve the number of particles.

The grand-canonical free energy of (4.1) at zero temperature is given by

$$\mathcal{F}(J/U, \mu/U, \eta, \eta^*) = \langle \tilde{H}_{\text{BH}} \rangle . \quad (4.2)$$

Since it depends explicitly on the fields η and η^* , one can rewrite the free energy in powers of them. As explained in Sec. 3.2.4 the ground state of the perturbative calculations is the ground state of the Mott insulator as defined in (3.54). Thus, all contributions with an odd number of source and drain terms vanish. Because all terms of the perturbation theory in the formalism of the process-chain approach are matrix elements in standard form like (3.35), an odd number of source and drain terms would change the particle number of the incoming state on the right-hand side in (3.35). So this state would meet

a state with a different number of particles on the left-hand side. Such states are orthogonal and, therefore, all such terms do not contribute. This leads to a power series in $|\eta|^2$ according to

$$\mathcal{F}(J/U, \mu/U, |\eta|^2) = M \left(f_0(J/U, \mu/U) + \sum_{i=1}^{\infty} c_{2i}(J/U, \mu/U) |\eta|^{2i} \right) \quad (4.3)$$

on a lattice with M sites.

The order parameter of this phase transition is given by

$$\psi = \frac{1}{M} \frac{\partial \mathcal{F}}{\partial \eta^*} = \langle b_i \rangle, \quad \psi^* = \frac{1}{M} \frac{\partial \mathcal{F}}{\partial \eta} = \langle b_i^\dagger \rangle \quad (4.4)$$

and describes the reaction of the system to the source and drain terms. In the Mott-insulator state the ground state is site-diagonal and, therefore, the order parameter is zero. In the superfluid state the particles delocalize and the order parameter starts to increase at the critical point. The effective potential is then given by the Legendre transform

$$\tilde{\Gamma}(J/U, \mu/U, \eta, \eta^*) = \mathcal{F} - M (\eta \psi^* + \eta^* \psi) . \quad (4.5)$$

The field η and the order parameter ψ constitute conjugated variables.

In order to expand the effective potential in powers of the order parameter, firstly this must be done for η and η^* . The crucial point for this expansion is up to which order the free energy of (4.3) is taken into account. Since later both expansions up to $\ell = 2$ and up to $\ell = 3$ are needed, both degrees of approximation will be discussed in this thesis.

For the following calculations we use the truncated free energy

$$\mathcal{F}(J/U, \mu/U, |\eta|^2) = M \left(f_0 + c_2 |\eta|^2 + c_4 |\eta|^4 + c_6 |\eta|^6 \right) \quad (4.6)$$

with $c_{2i} = c_{2i}(J/U, \mu/U)$ and $f_0 = f_0(J/U, \mu/U)$. By invoking (4.4) one gets

$$\begin{aligned} \psi &= c_2 \eta + 2c_4 |\eta|^2 \eta + 3c_6 |\eta|^4 \eta, \\ \psi^* &= c_2 \eta^* + 2c_4 |\eta|^2 \eta^* + 3c_6 |\eta|^4 \eta^*. \end{aligned} \quad (4.7)$$

These equations must be inverted and solved for η and η^* . This will be done successively order by order. In the first order one gets

$$\eta = \frac{\psi}{c_2}, \quad \eta^* = \frac{\psi^*}{c_2}. \quad (4.8)$$

Inserting this into the next-order approximation

$$\eta = \frac{\psi}{c_2 + 2c_4|\eta|^2}, \quad \eta^* = \frac{\psi^*}{c_2 + 2c_4|\eta|^2} \quad (4.9)$$

leads to

$$\eta = \frac{\psi}{c_2 + 2\frac{c_4}{c_2^2}|\psi|^2}, \quad \eta^* = \frac{\psi^*}{c_2 + 2\frac{c_4}{c_2^2}|\psi|^2}. \quad (4.10)$$

This expressions must be inserted into the still more accurate approximations

$$\eta = \frac{\psi}{c_2 + 2c_4|\eta|^2 + 3c_6|\eta|^4}, \quad \eta^* = \frac{\psi^*}{c_2 + 2c_4|\eta|^2 + 3c_6|\eta|^4}. \quad (4.11)$$

By ignoring terms with orders higher than $|\psi|^6$ and expanding the denominator about $|\psi| = 0$, the final result reads

$$\begin{aligned} \eta &= \psi \left[\frac{1}{c_2} - \frac{2c_4}{c_2^4}|\psi|^2 + \left(\frac{12c_4^2}{c_2^7} - \frac{3c_6}{c_2^6} \right) |\psi|^4 + \mathcal{O}(|\psi|^6) \right], \\ \eta^* &= \psi^* \left[\frac{1}{c_2} - \frac{2c_4}{c_2^4}|\psi|^2 + \left(\frac{12c_4^2}{c_2^7} - \frac{3c_6}{c_2^6} \right) |\psi|^4 + \mathcal{O}(|\psi|^6) \right]. \end{aligned} \quad (4.12)$$

With this expansion of η and η^* one is able to expand the effective action (4.5) in powers of $|\psi|^2$:

$$\begin{aligned} \frac{1}{M} \tilde{\Gamma}(J/U, \mu/U, |\psi|^2) &= f_0 - \frac{1}{c_2}|\psi|^2 + \frac{c_4}{c_2^4}|\psi|^4 + \left(\frac{c_6}{c_2^6} - \frac{4c_4^2}{c_2^7} \right) |\psi|^6 + \mathcal{O}(|\psi|^8) \\ &:= f_0 + \alpha_2|\psi|^2 + \alpha_4|\psi|^4 + \alpha_6|\psi|^6 + \mathcal{O}(|\psi|^8) \\ &= f_0 + \sum_{i=1}^{\ell} (\alpha_{2i}|\psi|^{2i}) + \mathcal{O}(|\psi|^{2(\ell+1)}). \end{aligned} \quad (4.13)$$

The introduction of the coefficients α_i implies a Taylor expansion, e.g., α_2 is given by the Taylor expansion of $-1/c_2$. This expansion is equivalent to a resummation of the underlying perturbative contributions.

As already mentioned the external field and the order parameter constitute conjugate variables. That means they are connected via the Legendre transformation and obey

$$\frac{1}{M} \frac{\partial \tilde{\Gamma}}{\partial \psi^*} = -\eta, \quad \frac{1}{M} \frac{\partial \tilde{\Gamma}}{\partial \psi} = -\eta^*. \quad (4.14)$$

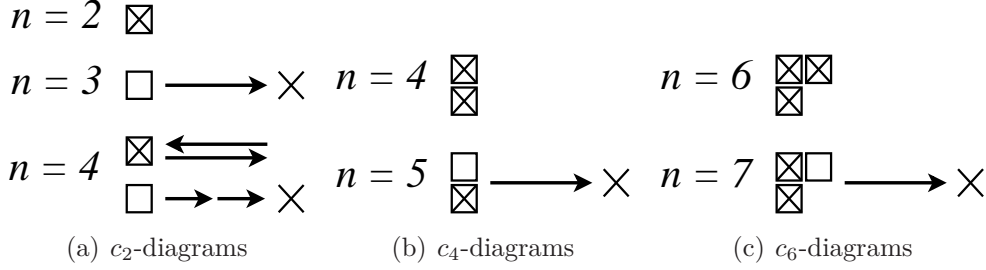


Figure 4.1: Shown are different n th-order diagrams necessary for the calculation of the coefficients c_{2i} . Tunneling processes are represented by arrows, a creation process by a square, and an annihilation process by a cross. Two adjacent lattice sites are always connected by an arrow.

The original Bose-Hubbard Hamiltonian (3.51) without source and drain terms is restored by setting $\eta = \eta^* = 0$. So one has to determine the order parameter $\psi_0(J/U, \mu/U)$ actually adopted by the system in such a way that it fulfills (4.14) for $\eta = \eta^* = 0$. This corresponds exactly to the condition discussed in Sec. 2.2.2. It implies that the effective potential has to have a trivial minimum at $\psi_0 = 0$ in the Mott-insulator state, which means that the effective action and the free energy of the original Bose-Hubbard Hamiltonian are equivalent there, and a non-trivial minimum when ψ_0 is non-zero in the superfluid phase.

The parameter c_2 can be interpreted as a susceptibility like (2.4) since, according to (4.7), one has

$$c_2 = \left(\frac{\partial \psi}{\partial \eta} \right)_{\eta \rightarrow 0} . \quad (4.15)$$

According to this and according to Landau's argument given in Sec. 2.2.2, the phase boundary is defined by that value $(J/U)_{\text{pb}}$ for which

$$\lim_{(J/U) \rightarrow (J/U)_{\text{pb}}} c_2(J/U, \mu/U) = \infty , \quad (4.16)$$

or rather for which the coefficient α_2 of the effective potential (4.13) vanishes:

$$\alpha_2((J/U)_{\text{pb}}, \mu/U) = 0 . \quad (4.17)$$

For each fixed value of μ/U , the coefficients c_{2i} can be expanded into a power series of J/U :

$$c_{2i} = \sum_{\nu=0}^{n-2i} \gamma_{2i}^{(\nu)} (J/U)^\nu . \quad (4.18)$$

In n th order of perturbation theory one has to consider i annihilation and i creation processes, respectively, and $\nu = n - 2i$ tunneling processes for the calculation of the coefficients $\gamma_{2i}^{(\nu)}$. They can be obtained from the process-chain approach by carrying out the strategy for the calculation of the ground-state energy of Sec. 3.2.4 with the small modification that one has two different kinds of perturbations. This leads to a new kind of diagram as depicted in Fig. 4.1. In these diagrams, tunneling processes are represented by arrows, a creation process by a square, and an annihilation process by a cross. The lattice sites are not shown since two adjacent lattice sites are always connected by an arrow. These diagrams do not have to be closed like the energy diagrams. This leads to a greater variety of diagrams, and a more rapid increase of the number of diagrams with the order of perturbation theory.

Another observation is that the lowest order of the different diagrams changes since one has a different number of creation and annihilation processes. This is a great disadvantage for the numerical calculation because the coefficients c_{2i} of the free energy must all exhibit the same number of tunneling processes in order to evaluate the effective potential. If one has six tunneling processes, the calculation of c_2 corresponds to 8th-order perturbation theory, which can be evaluated on an average PC in a few minutes. But for c_6 this already corresponds to 12th-order perturbation theory. Currently this requires a few weeks computation time on our ‘‘Hero’’-cluster.¹

Based on (4.14) and the condition $\eta = \eta^* = 0$, the equations

$$\frac{\partial \tilde{\Gamma}}{\partial \psi^*} = 0 , \quad \frac{\partial \tilde{\Gamma}}{\partial \psi} = 0 \quad (4.19)$$

allow one to determine the condensate density $\rho_c = |\psi_0|^2$. Here two cases regarding the order of the expansion of (4.3) will be taken into account.

¹For the specifications of the Hero (High-End Computing Resource Oldenburg) cluster see: <http://www.fk5.uni-oldenburg.de/45729.html>

In the first case the free energy is expanded up to $\ell = 3$. This means one has to use the effective action (4.13) leading to the condition

$$\alpha_2 + 2\alpha_4|\psi|^2 + 3\alpha_6|\psi|^4 = 0 \quad (4.20)$$

and finally to the condensate density

$$\rho_{c,3} = |\psi_{0,3}|^2 = \frac{1 - \alpha_4 + \sqrt{\alpha_4^2 - 3\alpha_2\alpha_6}}{\alpha_6}. \quad (4.21)$$

The second solution of the quadratic equation is unphysical as can be seen if the coefficients α_{2i} are known.

In the second case the free energy is expanded up to $\ell = 2$. Therefore the term proportional to $|\psi|^6$ in (4.13) can be ignored. This leads in the same way as described above to the condensate density

$$\rho_{c,2} = |\psi_{0,2}|^2 = -\frac{\alpha_2}{2\alpha_4}. \quad (4.22)$$

Finally one is also able to calculate the superfluid density ρ_{sf} . The underlying idea is the following: Let Ψ_0 be the spatially constant (or at most slowly varying) condensate wave function. A spatially varying condensate phase $\varphi(\mathbf{x})$ imposed on the wave function $\Psi_0(\mathbf{x}) = e^{i\varphi(\mathbf{x})}|\Psi_0|$ leads to the superfluid velocity

$$\mathbf{v}_s = \langle \mathbf{p}/m \rangle = \frac{\hbar}{m} \nabla \varphi(\mathbf{x}). \quad (4.23)$$

Moreover, the phase is considered to behave like $\varphi(\mathbf{x}) = \boldsymbol{\theta}\mathbf{x}/\tilde{L}$ where \tilde{L} is the total length of the system. With this the superfluid velocity is given by $\mathbf{v}_s = (\hbar/m)\boldsymbol{\theta}/\tilde{L}$ [158]. If we now consider a lattice with M sites, and with the dimensionless superfluid density ρ_{sf} specifying the number of superfluid particles (of mass m) per lattice site, the difference between the free energy $\mathcal{F}(\theta \neq 0)$ corresponding to a system with a moving superfluid fraction and the free energy $\mathcal{F}(0)$ for a system with vanishing momentum is equal to the kinetic energy of the superfluid:

$$\mathcal{F}(\theta) - \mathcal{F}(0) = \frac{1}{2}m\rho_{\text{sf}}Mv_s^2 = \frac{1}{2}m\rho_{\text{sf}}M \left(\frac{\hbar}{m}\right)^2 \left(\frac{\theta}{\tilde{L}}\right)^2. \quad (4.24)$$

The term $\rho_{\text{sf}}M$ can be interpreted as that fraction of the particles that is in a superfluid state.

Now the parameters have to be adapted to the Bose-Hubbard model. Inspecting its single-particle dispersion relation, one sees that the factor $\hbar^2/(2m)$ has to be replaced by Ja^2 , where a is the lattice constant. Moreover, the free energy \mathcal{F} is replaced by U times the reduced dimensionless effective action

$$\Gamma(\theta) = \tilde{\Gamma}(\theta) - f_0 . \quad (4.25)$$

Hence the superfluid density is finally given by

$$\rho_{\text{sf}}(J/U) = \lim_{\theta \rightarrow 0} \frac{1}{M(J/U)} \left(\frac{L}{\theta} \right)^2 [\Gamma(\theta) - \Gamma(0)] , \quad (4.26)$$

with the dimensionless length $L = \tilde{L}/a$ measuring distances in numbers of lattice sites.

The required “twisted boundary conditions” [159, 160]

$$\Psi(\dots, x_n, \dots) = e^{i\varphi(x)} \Psi(\dots, x_n + L, \dots) \quad (4.27)$$

are imposed on the wave function by adding a phase to the tunneling processes via [161]

$$b_i \rightarrow e^{ix\theta/L} b_i \quad \text{and} \quad b_i^\dagger \rightarrow e^{-ix\theta/L} b_i^\dagger . \quad (4.28)$$

Apart from this modification all calculations proceed as before.

4.2 Variational perturbation theory

The process-chain approach allows one to calculate various quantities up to very high orders. Nonetheless these series are often asymptotic series so that a further treatment is necessary in order to transform them into convergent strong-coupling series. This procedure is known as resummation [81, 96].

A series

$$f_L(x) = \sum_{\ell=0}^L a_\ell x^\ell \quad (4.29)$$

is called asymptotic to a function $f(x)$ if a bound $c_L|x|^L$ exists and one has

$$|f(x) - \sum_{\ell=0}^L a_\ell x^\ell| \leq c_{L+1}|x|^{L+1} \quad (4.30)$$

for all L and for all x where $f(x)$ is analytic, but the bound diverges like

$$c_L|x|^L \xrightarrow{L \rightarrow \infty} \infty. \quad (4.31)$$

If $|x|$ is small enough the bound first decreases with L and then finally increases. If one truncates the series at the minimum distance to $f(x)$ one gets the best possible estimate of $f(x)$. The divergence is connected to a radius of convergence which is zero so that the series diverges for all $|x| > 0$. The asymptotic behavior of a perturbatively calculated function usually stems from the factorial growth $a_\ell \propto \ell!$ of the perturbative coefficients.

The question is whether a mapping

$$\phi : f_L(x) \rightarrow f(x) \quad (4.32)$$

exists which maps the divergently calculated function $f_L(x)$ on the exact physical function $f(x)$. This mapping is then a so-called resummation. Prominent resummations are, e.g., Padé-approximants [162] or the Borel transformation [81, 96].

In this work the variational perturbation method [99, 100] is used which acts as a resummation of divergent weak-coupling series. This method will be introduced and then applied to certain quantities of the Bose-Hubbard model.

4.2.1 Strong-coupling transformation

Starting point is a weak-coupling series

$$f_L(x) = \sum_{\ell=0}^L a_\ell x^\ell \quad (4.33)$$

with a coupling parameter $x \ll 1$ and some coefficients a_ℓ . The purpose of the upcoming transformation is to transform this weak-coupling series into a

strong-coupling series

$$g_M(x) = x^{p/q} \sum_{m=0}^M b_m \left(x^{-2/q}\right)^m \quad (4.34)$$

with parameters p and q determined by the specific properties of the strong-coupling series. The ratio p/q is called the leading-power behavior in x and $2/q$ is the so-called approach to the leading-power behavior.

The first step is to extend the weak-coupling series with an auxiliary parameter ω to

$$h(x) = \omega^p \sum_{\ell=0}^L a_\ell \left(\frac{x}{\omega^q}\right)^\ell, \quad (4.35)$$

where ω will be set to one eventually. With the identity

$$\omega \rightarrow \sqrt{k^2 + \omega^2 - k^2} \quad (4.36)$$

a parameter k is introduced which acts as the variational parameter later on. For the sake of simplicity this substitution is written with new dimensionless quantities

$$\hat{x} := x/k^q \quad \text{and} \quad \hat{\omega} := \omega/k \quad (4.37)$$

leading to

$$\omega \rightarrow k(1 - \sigma\hat{x})^{1/2} \quad (4.38)$$

with

$$\sigma(x, \omega, k) = (1 - \hat{\omega}^2)/\hat{x}. \quad (4.39)$$

Since \hat{x} is dimensionless, one must have $[x] = [k]^q$.

This new substitution is now inserted in (4.35) so that one gets

$$h(x, k) = k^p \sum_{\ell=0}^L a_\ell (1 - \sigma\hat{x})^{(p-\ell q)/2} \hat{x}^\ell. \quad (4.40)$$

The expression $(1 - \sigma\hat{x})^{(p-\ell q)/2}$ is now expanded about $\hat{x} = 0$ leading to

$$(1 - \sigma\hat{x})^{(p-\ell q)/2} = \sum_{i=0}^{\infty} \frac{1}{i!} (-\sigma)^i \hat{x}^i \prod_{j=0}^{i-1} \left[\frac{p - \ell q}{2} - j \right], \quad (4.41)$$

where the empty product is defined as $\prod_{j>i}^i [\dots] := 1$. This expansion is now inserted into (4.40) but since the series is only known up to the order L , (4.41) is only allowed to be expanded up to the order $L - \ell$. That leads to

$$h_L(x, k) = k^p \sum_{\ell=0}^L a_\ell \hat{x}^\ell \sum_{i=0}^{L-\ell} \frac{1}{i!} (-\sigma)^i \hat{x}^i \prod_{j=0}^{i-1} \left[\frac{p - \ell q}{2} - j \right]. \quad (4.42)$$

This result is equivalent to

$$h_L(x, k) = k^p \sum_{\ell=0}^L \epsilon_\ell(\sigma) \hat{x}^\ell \quad (4.43)$$

with

$$\epsilon_\ell(\sigma) = \sum_{j=0}^{\ell} a_j \binom{(p - qj)/2}{\ell - j} (-\sigma)^{\ell-j} \quad (4.44)$$

of Ref. [100].

The k -dependency of (4.42) becomes apparent if one sets $\omega = 1$ as stipulated in the beginning. This turns (4.42) into

$$h_L(x, k) = \sum_{\ell=0}^L a_\ell k^{p-\ell q} x^\ell \sum_{i=0}^{L-\ell} \frac{1}{i!} \left(\frac{1}{k^2} - 1 \right)^i \prod_{j=0}^{i-1} \left[\frac{p - \ell q}{2} - j \right]. \quad (4.45)$$

This k -dependency stems from the Taylor expansion (4.41) which is truncated after the order $L - \ell$ in (4.42), and vanishes for $L \rightarrow \infty$. To minimize the influence of this parameter one has to use the *principle of minimal sensitivity* [163]. That means the first and second derivative with respect to k has to be calculated for (4.45). The optimal scaling parameter k_L is then given by smallest value k which belongs to an extremum or a turning point of $h_L(x, k)$ (see [81], p. 328). Then the function $h_L(x) = h_L(x, k_L)$ constitutes the L th variational approximation to the function $f(x)$ for finite x .

However, the crucial point is what happens in the strong-coupling limit $x \rightarrow \infty$. Then one resorts to a scaling argument: Since $[x] = [k]^q$, the optimal $k_L \approx x^{1/q} c_L$ is proportional to $x^{1/q}$ with some proportionality factor c_L . That means \hat{x} becomes asymptotically constant, $\hat{x} \rightarrow c_L^{-q}$. Since one has

$$\hat{\omega} = \omega/k \stackrel{x \gg 1}{\approx} \frac{\omega}{x^{1/q} c_L} \xrightarrow{x \rightarrow \infty} 0, \quad (4.46)$$

it follows that

$$\sigma = \frac{1}{\hat{x}} - \frac{\hat{\omega}^2}{\hat{x}} \xrightarrow{x \rightarrow \infty} c_L^q \quad (4.47)$$

becomes constant, too.

To get the full strong-coupling series, $(-\sigma\hat{x})^i = (\hat{\omega}^2 - 1)^i$ of (4.42) has to be expanded about

$$\hat{\omega}^2 = \left(\frac{x}{\omega^q \hat{x}} \right)^{\frac{-2}{q}} = 0 . \quad (4.48)$$

This leads to the expansion

$$(\hat{\omega}^2 - 1)^i = \sum_{m=0}^i \frac{1}{m!} (-1)^{i-m} \left(\frac{x}{\omega^q \hat{x}} \right)^{-2m/q} \prod_{j=0}^{m-1} [i - j] . \quad (4.49)$$

By inserting this expansion into (4.42) and by simultaneously going to the strong-coupling limit with $k^p = x^{p/q} \hat{x}^{-p/q}$ one gets an expansion of the form

$$h_L^\infty(x, \hat{x}) = x^{p/q} \sum_{\ell=0}^L \bar{b}_\ell(\hat{x}) \hat{x}^{(2\ell-p)/q} \left(\frac{x}{\omega^q} \right)^{-2\ell/q} . \quad (4.50)$$

The variable \hat{x} now is a variational parameter, to be determined by taking the derivatives with respect to \hat{x} as the optimal extremum or turning point, in accordance with the principle of minimal sensitivity. This optimal parameter is of the form

$$\hat{x} = c_L^{-q} \left[1 + \gamma_1 \left(\frac{x}{\omega^q} \right)^{-2/q} + \gamma_2 \left(\frac{x}{\omega^q} \right)^{-4/q} + \dots \right] . \quad (4.51)$$

Here also the optimal parameter c_L^{-q} has to be determined, which leads with $\omega = 1$ to the strong-coupling series

$$h_L^\infty(x) = x^{p/q} \sum_{\ell=0}^L b_\ell x^{-2\ell/q} . \quad (4.52)$$

The procedure for the explicit determination of the coefficients \bar{b}_ℓ , γ_ℓ and b_ℓ can be found in Ref. [81].

Later on one is only interested in the limit $x \rightarrow \infty$ for which the approach proportional to $x^{-2/q}$ vanishes. One does get this strong-coupling limit of (4.42)

for $\sigma \hat{x} \rightarrow 1$, which leads to

$$h_L^\infty(x, \hat{x}) \approx x^{p/q} \hat{x}^{-p/q} \sum_{\ell=0}^L a_\ell \hat{x}^\ell \sum_{i=0}^{L-\ell} \frac{1}{i!} (-1)^i \prod_{j=0}^{i-1} \left[\frac{p - \ell q}{2} - j \right]. \quad (4.53)$$

That means this function takes on the form

$$h_L^\infty(x, \hat{x}) \approx x^{p/q} \hat{x}^{-p/q} w_L(\hat{x}) \quad (4.54)$$

with

$$w_L(\hat{x}) = \sum_{\ell=0}^L a_\ell \hat{x}^\ell \sum_{i=0}^{L-\ell} \frac{1}{i!} (-1)^i \prod_{j=0}^{i-1} \left[\frac{p - \ell q}{2} - j \right]. \quad (4.55)$$

The variable \hat{x} is now a new variational parameter, again to be determined as the optimal extremum or turning point. This optimal point is defined as the smallest such \hat{x} according to the principle of minimal sensitivity.

Up to now the parameters p and q are unknown. They must be determined self-consistently from the strong-coupling expansion (4.53). To this end one defines the two logarithmic derivatives

$$F_1(x) = \frac{d \log f_L(x)}{d \log x} = \frac{x f_L'(x)}{f_L(x)} \quad (4.56)$$

and

$$F_2(x) = \frac{d \log F_1(x)}{d \log x} = \frac{x F_1'(x)}{F_1(x)} \quad (4.57)$$

of the original weak-coupling series (4.33).

After transforming these two functions to the strong-coupling limit, so that one gets two functions $F_1^\infty(x, \hat{x})$ and $F_2^\infty(x, \hat{x})$ of the form (4.53) and assuming that $f_L(x)$ is of the form (4.52), one gets two equations which can be used for the determination of the variational parameters p and q . The first of these conditions reads

$$\lim_{x \rightarrow \infty} F_1^\infty(x, \hat{x}) = \frac{p}{q}. \quad (4.58)$$

The second condition depends on the parameter p , on whether p is zero or not. The logarithmic derivative of (4.52) for $L = 1$ leads to

$$\lim_{x \rightarrow \infty} \frac{4b_0 b_1 (b_0 + b_1 x^{-2/q})}{q (x^{2/q} p b_0 + p b_1 - 2b_1) (b_0 + x^{-2/q} b_1)} = \begin{cases} 0, & p \neq 0 \\ -2/q, & p = 0 \end{cases}. \quad (4.59)$$

That means the second condition reads

$$\lim_{x \rightarrow \infty} F_2^\infty(x, \hat{x}) = \begin{cases} 0, & p \neq 0 \\ -2/q, & p = 0 \end{cases}. \quad (4.60)$$

These two equations constitute a system from which the two parameters can be determined self-consistently

4.2.2 Application to the Bose-Hubbard model

As will be explained in detail in Chapter 5, the variational perturbation theory can be used to calculate the critical exponents of both the condensate and the superfluid density of the Bose-Hubbard model. The process-chain approach yields a finite series of the form

$$f_L(x) = \sum_{\nu=0}^L a_\nu x^\nu \quad (4.61)$$

for both densities, with $x = J/U$. The variational approach is then applied to these series.

It cannot be clearly stated if the series of the condensate and superfluid density are divergent or convergent. Fig 4.2 shows the coefficients a_ν of the condensate density in 7th-order perturbation theory for $D = 2$. The data of the superfluid density look qualitatively similar. Two criteria are evaluated which should give the radius of convergence r . It is

$$r_1 = \lim_{\nu \rightarrow \infty} \left| \frac{a_\nu}{a_{\nu+1}} \right| \quad (4.62)$$

for the ratio test and

$$r_2 = \frac{1}{\limsup_{\nu \rightarrow \infty} \sqrt[\nu]{|a_\nu|}} \quad (4.63)$$

for the root test. Both tests fail to give a clear limit. But in both cases the data points are very small and have the tendency to decrease so the radius of convergence is at least smaller than the critical point of the Bose-Hubbard model which is approximately $(J/U)_c = 0.06$ for $D = 2$ [152]. Since the

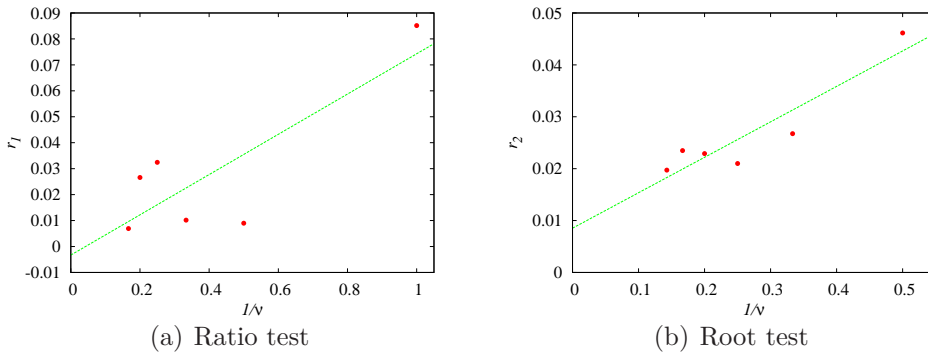


Figure 4.2: The root test and the ratio test are applied to the coefficients of the condensate density in 7th-order perturbation theory for $D = 2$. Plotted are (a) the ratios (4.62) and (b) the roots (4.63) versus $1/\nu$. The radius of convergence should be given by the limit $1/\nu \rightarrow 0$. The line depicts a linear fit of the data points. These data do not show clearly if the series has a finite radius of convergence.

variational perturbation theory is used to calculate the critical exponents of the phase transition of the Bose-Hubbard model, one enters the superfluid regime with $x > (J/U)_c$ which makes a resummation necessary.

The critical exponents of interest are β , quantifying the condensate density, and ν , quantifying the superfluid density. The procedure of their determination will be explained by considering the example of the condensate density ρ_c . After the calculation of ρ_c via the process-chain approach, it is given as a weak-coupling series

$$\rho_c(x) = \sum_{\ell=0}^L a_\ell x^\ell \quad (4.64)$$

with $x := J/U \ll 1$. On the other hand, in the strong-coupling regime the leading-power behavior of the condensate density is given by the critical exponent β , so that the strong-coupling expansion has to have the form

$$\rho_c^\infty(x) = x^\beta \sum_{m=0}^M b_m \left(x^{-2/q}\right)^m \quad (4.65)$$

with $\beta := p/q$. That means that one has to take the logarithmic derivative of

the weak-coupling series (4.64),

$$G(x) = \frac{d \log \rho_c(x)}{d \log x} = \frac{x \rho_c'(x)}{\rho_c(x)} = \sum_{\ell=0}^{L'} \tilde{a}_\ell x^\ell, \quad (4.66)$$

and transform the resulting series to the strong-coupling regime; it should then converge to the critical exponent in the limit $x \rightarrow \infty$. Generally one has $L' \leq L$.

Because one does not match the asymptotics of the original series (4.64), but rather that of its logarithmic derivative (4.66), the strong-coupling expansion of this latter series has to proceed with $p_G = 0$, leading according to (4.53) to a series

$$G^\infty(\tilde{x}) = \sum_{\ell=0}^{L'} \tilde{a}_\ell \tilde{x}^\ell \sum_{i=0}^{L'-\ell} \frac{1}{i!} \prod_{j=0}^{i-1} \left[\frac{\ell q_G}{2} + j \right] \quad (4.67)$$

depending on the parameter q_G . According to (4.58) and (4.60) this parameter must be determined self-consistently with the help of the functions

$$F_1(x) = \frac{d \log G(x)}{d \log x} = \frac{x G'(x)}{G(x)} = \sum_{\ell=0}^{L_1} f_\ell^{(1)} x^\ell \quad (4.68)$$

and

$$F_2(x) = \frac{d \log F_1(x)}{d \log x} = \frac{x F_1'(x)}{F_1(x)} = \sum_{\ell=0}^{L_2} f_\ell^{(2)} x^\ell. \quad (4.69)$$

Since $p_G = 0$, the conditions (4.58) and (4.60) become

$$F_1^\infty(\hat{x}) = 0 \quad \text{and} \quad F_2^\infty(\hat{x}) = -2/q_G \quad (4.70)$$

with

$$F_1^\infty(\hat{x}) = \sum_{\ell=0}^{L_1} f_\ell^{(1)} \hat{x}^\ell \sum_{i=0}^{L_1-\ell} \frac{1}{i!} \prod_{j=0}^{i-1} \left[\frac{\ell q_G}{2} + j \right] \quad (4.71)$$

and

$$F_2^\infty(\hat{x}) = \sum_{\ell=0}^{L_2} f_\ell^{(2)} \hat{x}^\ell \sum_{i=0}^{L_2-\ell} \frac{1}{i!} \prod_{j=0}^{i-1} \left[\frac{\ell q_G}{2} + j \right]. \quad (4.72)$$

First one has to determine the optimal variational parameter \hat{x} as described in Sec. 4.2.1 for (4.71) and (4.72), which also depends on q_G . Both equations

depend then only on q_G . Then these conditions allow one to determine the parameter q_G itself.

With the knowledge of this parameter q_G , the optimal variational parameter \hat{x} for (4.67) must be determined by the principle of minimal sensitivity in a next step. Inserting this \hat{x} in (4.67), one finally gets the critical exponent β .

The explicit results of this variational perturbation theory, when applied to the Bose-Hubbard model, will be discussed in detail in Chapt. 5.

5 Results

In this chapter the final results of this thesis will be presented. All data have been calculated for the two-dimensional square and the three-dimensional cubic lattice, respectively. That means if only the dimensionality is mentioned the results refer to one of these cases. The underlying model is always the dimensionless Bose-Hubbard model (3.51).

In the first section the determination of the phase boundary according to Ref. [152] will be recapitulated. But also a further method will be put forward, which gives similar but slightly different results for the phase boundary. In the second section the coefficients of the effective potential will be discussed. This is necessary because the behavior of these coefficients depends strongly on the order of the perturbation theory. In the third section the determination of the particle number will be discussed. This method not only gives the lines of constant density inside the superfluid region, but it also gives access to another method for determining the phase boundary whose results are identical to the method of the first section. The calculation of both the condensate and the superfluid density is performed in the fourth section. In two dimensions odd and even orders of the perturbation theory have to be treated differently. Based on these two cases the critical exponents of both densities will be calculated in the last section. For one case the use of the variational perturbation method is necessary, while the other case permits a direct access to the critical exponents.

5.1 Phase boundary

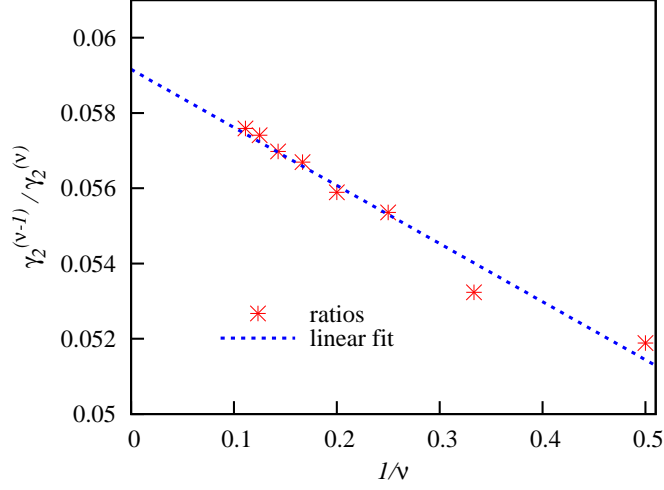
The precise determination of the phase boundary is a topic of great interest. The first solution was a mean-field approach which was presented by Fisher et al. [60] together with the proposal of the model. But the mean-field solution is

only exact in the limit $D \rightarrow \infty$ so that, e.g., the critical hopping (5.6) at the tip of the Mott lobe is about $(J/U)_c^{\text{mf}} \approx 0.043$ for $D = 2$ and $g = 1$ within the mean-field approach. This solution deviates from the more precise numerical solution $(J/U)_c \approx 0.06$ by approximately 30%. This example makes it clear that the mean-field solution is insufficient.

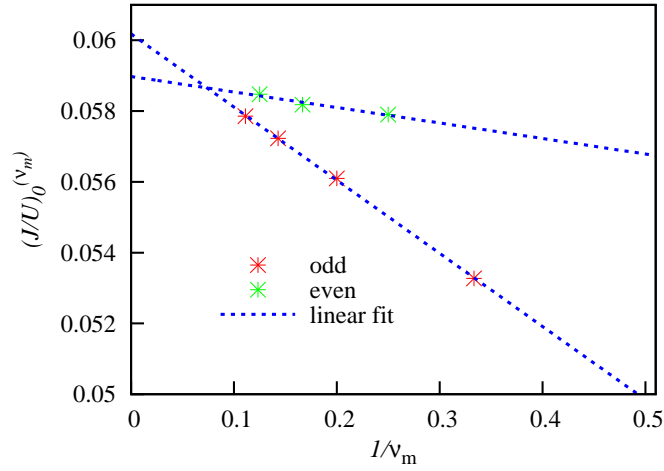
The phase boundary was therefore studied by many other methods like strong-coupling expansions [164, 165], quantum Monte Carlo simulations [166–169], the density matrix renormalization group [170–173] and recently by means of the variational cluster approach [174, 175]. In addition many different aspects were considered like various dimensionalities or additional disorder.

Here the determination of the phase boundary for the two- and the three-dimensional square and cubic lattice, respectively, with the method of the effective potential of Sec. 4.1 will be explained. Since the one-dimensional system lies in a different universality class than the Bose-Hubbard model with $D \geq 2$, it is not accessible with the method of the effective potential. Two- and three-dimensional lattices are therefore the most interesting cases for this method; for these dimensionalities various geometries like triangular, hexagonal or kagome lattices are experimentally realizable [176, 177]. The following methods are also valid for these and other lattice geometries. Only the diagrams of the process-chain approach used for the calculation of the effective potential change if one considers different lattice geometries but everything else is unaffected.

The phase boundary is determinable by solely the coefficient c_2 or rather by the coefficient $\alpha_2(J/U) = -1/c_2(J/U)$ arising in the effective potential (4.13). For fixed chemical potential μ/U the phase boundary is given by that value $(J/U)_{\text{pb}}$ for which c_2 diverges, or for which the coefficient α_2 vanishes.



(a)



(b)

Figure 5.1: Shown are the two extrapolation schemes for determining the phase boundary, exemplary for $D = 2$. In (a) the ratios $\gamma_2^{(\nu-1)}/\gamma_2^{(\nu)}$ of the coefficients of c_2 of (5.2) are plotted in order to determine the radius of convergence. In (b) the zeros $(J/U)_0^{(\nu_m)}$ of the series $\alpha_2^{(\nu_m)}$ defined in (5.3), which mark the phase boundary in $(\nu_m + 2)$ th order, are fitted linearly.

The first condition,

$$\lim_{(J/U) \rightarrow (J/U)_{\text{pb}}} c_2(J/U, \mu/U) = \infty, \quad (5.1)$$

already introduced in Ref. [152], requires a method to determine the radius of convergence of the n th-order perturbation series

$$c_2 = \sum_{\nu=0}^{n-2} \gamma_2^{(\nu)} (J/U)^\nu. \quad (5.2)$$

This is done by the already mentioned ratio test, as defined in (4.62). For this the ratios $\gamma_2^{(\nu-1)}/\gamma_2^{(\nu)}$ are plotted over the inverse order $1/\nu$. They are linearly fitted in order to determine the radius of convergence, which is then equal to the extrapolated value of the phase boundary $(J/U)_{\text{pb}}$ with $n \rightarrow \infty$. This procedure is depicted in Fig. 5.1(a) for $n = 11$ on a two-dimensional square lattice and filling factor $g = 1$. The chemical potential is the critical chemical potential at the tip of the Mott lobes, i.e. $(\mu/U)_c = 0.375$. The critical hopping for $n \rightarrow \infty$ is given by $(J/U)_c \approx 0.05920$. This differs by about 0.2% from the value 0.05909 stated in Refs. [152, 154], since this previous value was obtained for $n = 10$.

The second condition involves a Taylor expansion of $\alpha_2 = -1/c_2$ so that one gets a new series

$$\alpha_2^{(\nu_m)} = \sum_{\nu=0}^{\nu_m \leq n-2} a_2^{(\nu)} (J/U)^\nu. \quad (5.3)$$

The zeros $(J/U)_0^{(\nu_m)}$ for different values of ν_m mark the $(\nu_m + 2)$ th-order phase boundary. Here only the zero of the function $\alpha_2^{(\nu_m)}$ is of interest. These zeros are also fitted linearly, but here odd and even orders are fitted separately. This extrapolation scheme leads to two estimates for the phase boundary. This is shown in Fig. 5.1(b) for the same parameters as stated above with the exception that the critical chemical potential is now $(\mu/U)_c \approx 0.373$ for both the even and odd orders. The critical hopping also differs slightly from that of the first condition. One gets the critical hopping $(J/U)_c^{\text{even}} \approx 0.05898$ for the even and $(J/U)_c^{\text{odd}} \approx 0.06018$ for the odd orders.

The resulting phase boundaries provided by both schemes are shown in Fig. 5.2(a). One recognizes that the two phase boundaries of the second scheme

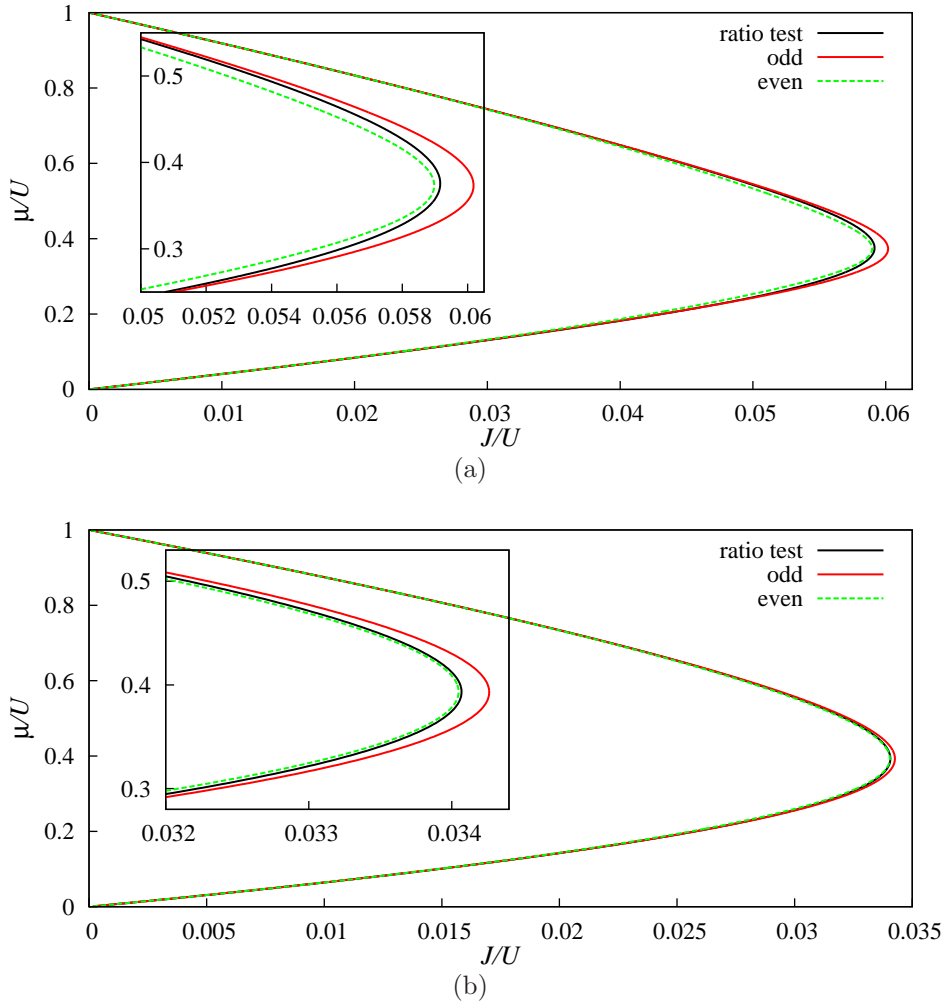


Figure 5.2: Shown are the phase boundaries of (a) the two-dimensional square lattice and (b) the three-dimensional cubic lattice. In both figures the extrapolated results of the ratio test applied to (5.2) and of the zeros of (5.3) are plotted. The insets show the tip of the Mott lobe. One recognizes that both methods converge to each other when μ/U becomes integer. Furthermore, the two phase boundaries determined by the zeros act as upper and lower bounds on the results of the ratio test.

ν_m	$D = 2$		$D = 3$	
	$(J/U)_c^{(\nu_m)}$	$(\mu/U)_c^{(\nu_m)}$	$(J/U)_c^{(\nu_m)}$	$(\mu/U)_c^{(\nu_m)}$
1	0.04289	0.414	0.02860	0.414
2	0.05557	0.382	0.03305	0.397
3	0.05333	0.387	0.03266	0.398
4	0.05791	0.376	0.03347	0.395
5	0.05612	0.380	0.03331	0.396
6	0.05818	0.375	0.03366	0.395
7	0.05724	0.377	0.03357	0.395
8	0.05847	0.374	0.03376	0.394
9	0.05786	0.376	-	-
∞ , odd	0.06018	0.373	0.03426	0.393
∞ , even	0.05898	0.373	0.03405	0.393

Table 5.1: Critical values of the hopping and the chemical potential depending on the maximal order ν_m defined in (5.3). The phase boundary is determined by the respective smallest non-negative zero $(J/U)_0^{(\nu_m)} = (J/U)_{\text{pb}}^{(\nu_m)}$ of (5.3) for each value of the chemical potential. The critical parameters are defined by the largest value of the hopping belonging to the phase boundary. The last two columns show the extrapolated critical parameters where odd and even orders are fitted separately.

act as upper and lower bounds of the phase boundary determined by the first scheme. All three phase boundaries converge when the chemical potential goes to one and zero, respectively. In Fig. 5.2(b) also the phase boundaries for $D = 3$ are shown. The procedure for the determination of these phase boundaries works in the same way. Here the critical chemical potential $(\mu/U)_c = 0.393$ is the same for both conditions. The critical hopping is $(J/U)_c \approx 0.03407$ for the first method as well as $(J/U)_c^{\text{even}} \approx 0.03405$ and $(J/U)_c^{\text{odd}} \approx 0.03426$, respectively, for the second method. Tab. 5.1 lists all critical values depending on the maximal order ν_m for the two- and three-dimensional square lattice. The accuracy of both schemes is very high and the error can be estimated to be

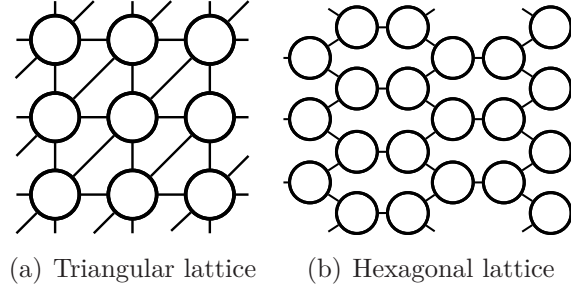


Figure 5.3: Shown are the triangular and the hexagonal lattice geometry studied in Ref. [178] regarding the phase boundary. A circle represents a lattice site and the lines show the possible nearest neighbor tunneling bonds.

less than 3%. If one assumes that the exact value $(J/U)_c$ actually lies between $(J/U)_c^{\text{even}}$ and $(J/U)_c^{\text{odd}}$, the error would even be less than 1%.

The study of the phase boundary determined with the process-chain approach and the ratio test is mostly done in Ref. [154]. There the phase boundary of orthogonal lattices with $2D$ nearest neighbors is calculated for various dimensionalities and filling factors. It is shown that for $D \rightarrow \infty$ the phase boundary converges to the phase boundary of the mean-field phase diagram [60],

$$2D \left(\frac{J}{U} \right)_{\text{pb}} = \frac{(\mu/U - g + 1)(g - \mu/U)}{\mu/U + 1}. \quad (5.4)$$

This is due to the effect that for $D \rightarrow \infty$ only one type of diagram contributes within the process-chain approach. These are the so-called one-way diagrams which never visit the same lattice site twice since the odds to do so is vanishing for infinite dimensionality.

Furthermore a scaling

$$\left(\frac{J}{U} \right)_c = \left(\frac{J}{U} \right)_c^{\text{mf}} + \frac{0.13}{\sqrt{g(g+1)}D^{2.5}} \quad (5.5)$$

was found which connects the critical hopping $(J/U)_c$ for given values of D and g to the critical hopping

$$\left(\frac{J}{U} \right)_c^{\text{mf}} = \frac{1}{2D} \left(2g + 1 - 2\sqrt{g(g+1)} \right) \quad (5.6)$$

of the mean-field solution.

It is also shown that one can render the critical hopping $(J/U)_c$ almost independent of the filling factor g with a scaling

$$\left(\frac{J}{U}\right)_c^{\text{sc}} = \sqrt{g(g+1)} \left(\frac{J}{U}\right)_c. \quad (5.7)$$

This scaling is further improved in Ref. [179] so that the scaled critical hopping

$$\left(\frac{J}{U}\right)_c^{\text{sc}} = \sqrt{g(g+1)} \left(\frac{1}{2} + \sqrt{\frac{1}{4} + \frac{1}{16g(g+1)}}\right) \left(\frac{J}{U}\right)_c \quad (5.8)$$

varies by less than 0.2% as a function of g . Finally a function

$$\begin{aligned} \left(\frac{J}{U}\right)_c &= \frac{1}{2D} \left(2g + 1 - 2\sqrt{g(g+1)}\right) \\ &\cdot \left(1 + 0.35\frac{1}{D} + 0.39\frac{1}{D^2} + 0.84\frac{1}{D^3}\right) \end{aligned} \quad (5.9)$$

was found numerically which gives the critical hopping as a function of the dimensionality and the filling factor with an accuracy of better than 0.15% in comparison to the results of the process-chain approach. This function also shows that the particle-hole asymmetry of the phase boundary vanishes in the limit $g \rightarrow \infty$.

Another advantage lies in the straight-forward adaption of this method to other lattice types. In Ref. [178] the phase boundaries of the two-dimensional triangular and hexagonal lattice as depicted in Fig. 5.3 were studied with the ratio test. These lattices differ from the square lattice in the number of nearest neighbors. Whereas each site of a two-dimensional square lattice has 4 nearest neighbors, the triangular lattice provides 6 and the hexagonal lattice only 3 nearest neighbors. This changes the respective diagrams of the process-chain approach so that these have to be evaluated separately for every lattice type.

5.2 Properties of effective potential

The condensate densities (4.21) and (4.22) as well as the superfluid density (4.26) depend on the coefficients

$$\alpha_2 = -\frac{1}{c_2}, \quad (5.10a)$$

$$\alpha_4 = \frac{c_4}{c_2^4}, \quad (5.10b)$$

$$\alpha_6 = \frac{c_6}{c_2^6} - \frac{4c_4^2}{c_2^7} \quad (5.10c)$$

of the effective potential

$$\Gamma(J/U, \mu/U, |\psi|^2) = \alpha_2 |\psi|^2 + \alpha_4 |\psi|^4 + \alpha_6 |\psi|^6 + \mathcal{O}(|\psi|^8), \quad (5.11)$$

where the sourceless part f_0 of the free energy is already subtracted as stated in (4.25). All coefficients are the result of a Taylor expansion so that they are given by series

$$\alpha_{2i}^{(\nu_m)} = \sum_{\nu=0}^{\nu_m \leq n-2i} a_{2i}^{(\nu)} (J/U)^\nu \quad \text{with } i = 1, 2, 3. \quad (5.12)$$

As already mentioned in Sec. 4.1, it is decisive for both densities up to which order the effective potential is expanded. This decision depends on the behavior of the coefficients (5.10) and particularly on the coefficient α_4 in (5.10b). If α_4 is greater than zero it should be sufficient to expand the effective potential up to $|\psi|^4$ according to the arguments given in Sec. 2.2.2. This would lead to the condensate density (4.22). If the coefficient α_4 is less than zero, one needs the coefficient α_6 of (5.10c) in order to guarantee a stable effective potential providing a minimum near $(J/U)_c$.

In what follows the coefficients of (5.10) will be examined in detail. It will be made clear that for $D = 2$ one has to consider two cases for the determination of the densities since the coefficient α_4 shows a behavior which depends on the parity of the order of the perturbation theory. That means it is always greater than zero for odd orders but it changes its sign from positive to negative for even orders. Moreover the case $D = 3$ is discussed for which the coefficient α_4 shows a similar behavior as for the dimensionality $D = 2$ but the zeros do not affect the region $J/U \approx (J/U)_c$ where the perturbation theory is valid.

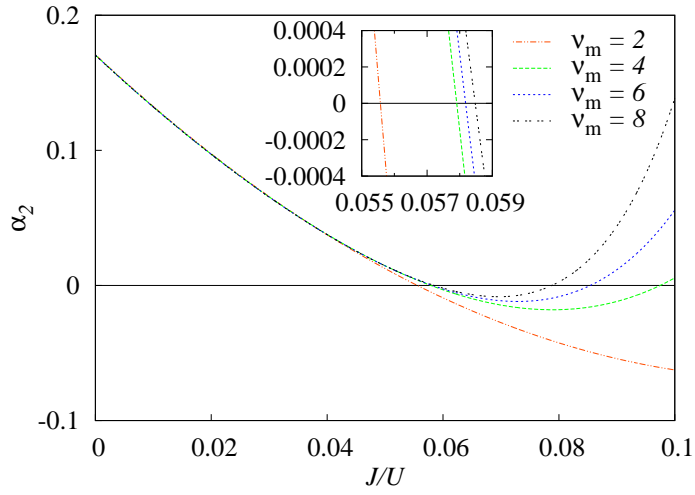
The coefficient α_2 has already been treated in Sec. 5.1 in the context of the phase boundary, where this boundary has been calculated by solving $\alpha_2 = 0$. But for the sake of completeness Fig. 5.4(a) and Fig. 5.5(a) show this coefficient depending on the maximal order ν_m as defined in (5.3) for $D = 2$. This and

all following coefficients are plotted for $\mu/U = (\mu/U)_c^{(\nu_m)}$. What is important to note is that α_2 changes its sign from positive to negative. The other zeros besides the first one can be explained by the finite Taylor expansion so that the perturbational expansion is not valid anymore for values $J/U \gtrsim 0.07$.

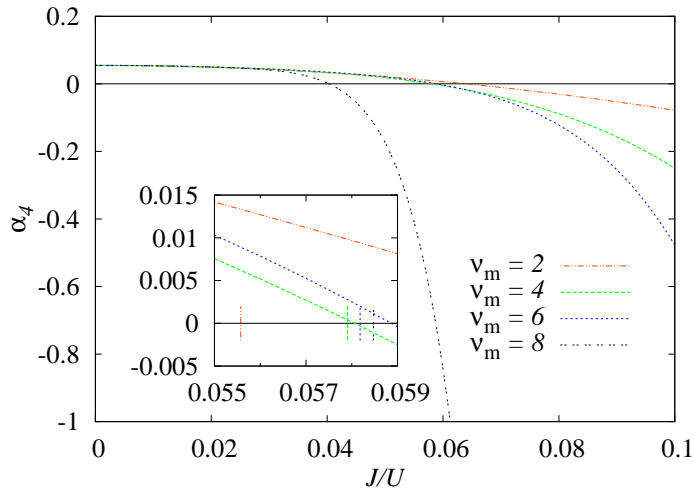
The behavior of α_4 is shown in Fig. 5.4(b) and Fig. 5.5(b). Whereas the odd orders are always positive, the even orders change their sign. This alternation of the behavior for different ℓ is also characteristic for the other coefficients as shown in Fig. 5.4 and Fig. 5.5. In order to illustrate this trend also

$$\alpha_8 = \frac{24c_4^3}{c_2^{10}} - \frac{12c_4c_6}{c_2^9} + \frac{c_8}{c_2^8} \quad (5.13)$$

is plotted. Since this coefficient is only known up to $\nu_m = 4$ which is equivalent to $n = 12$, it is not used to calculate the critical exponents later on.

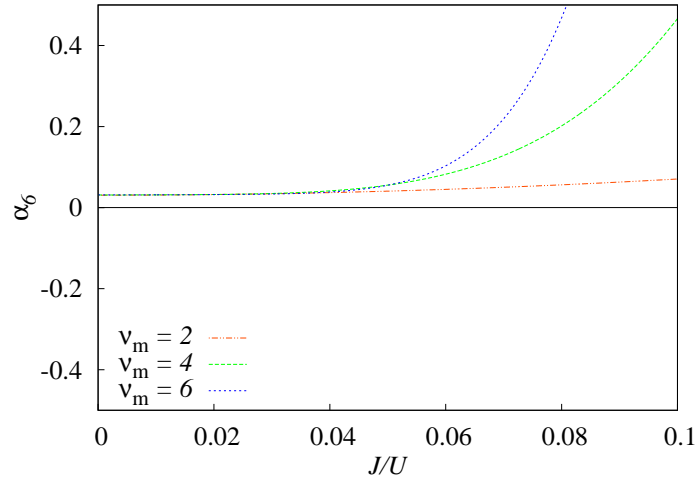


(a)

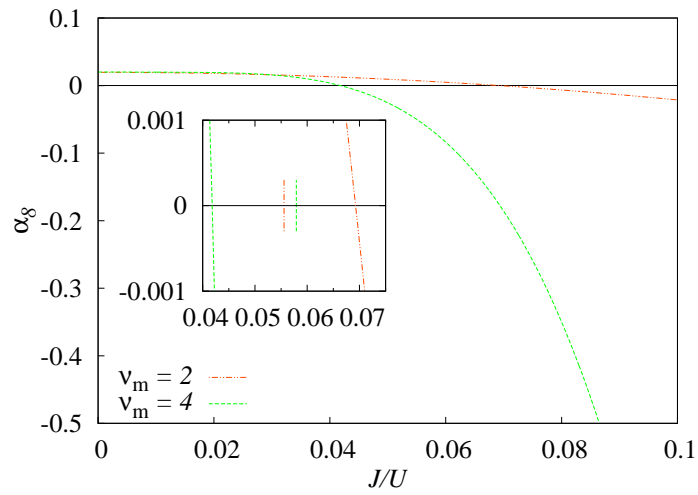


(b)

Figure 5.4: For details see the caption on the next page.

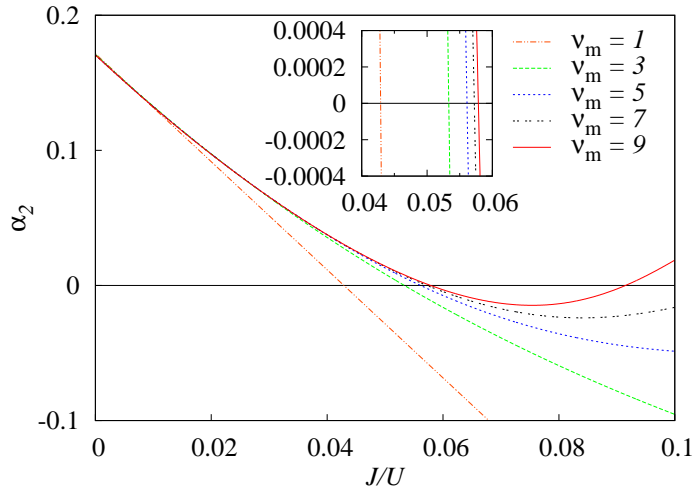


(c)

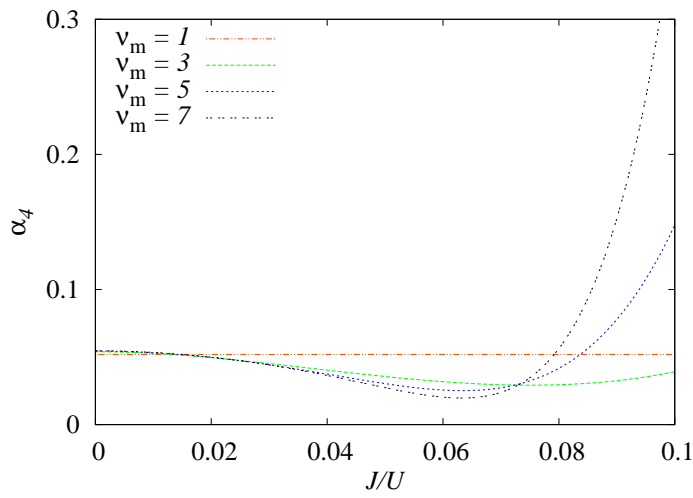


(d)

Figure 5.4: Coefficients α_{2i} given in (5.10) of the effective potential as defined in (5.11) for $D = 2$ with the critical chemical potential depending on ν_m as listed in Tab. 5.1. Here only even orders regarding the maximal order ν_m as defined in (5.12) are shown. The critical values of the respective orders are plotted in the inset of the plots as vertical lines.

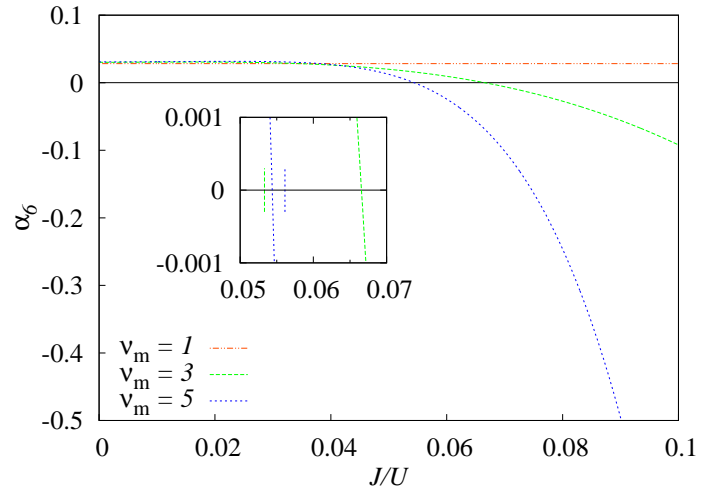


(a)

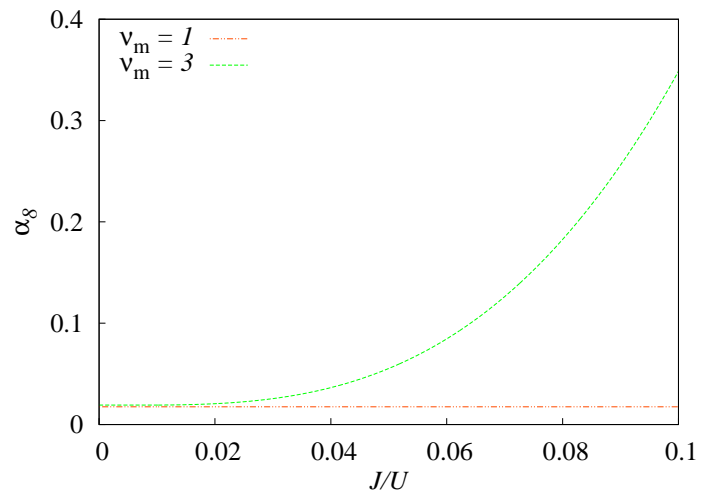


(b)

Figure 5.5: For details see the caption on the next page.



(c)



(d)

Figure 5.5: Coefficients $\alpha_{2i}(J/U, \mu/U)$ of the effective potential for odd orders and $D = 2$. More information is given in the caption of Fig. 5.4.

Now the question arises which form of the effective potential is valid for which set of coefficients α_{2i} . The alternation of positive and negative coefficients for values of the hopping $J/U > (J/U)_c$ must be considered in the effective potential. So the question is whether the effective potential guarantees a solution with a positive coefficient α_{2i} although the coefficient $\alpha_{2(i+1)}$ is negative. This would mean that there exists at least a local minimum of the effective potential in the vicinity of $(J/U)_c$ where the perturbation theory is valid.

Due to the self-consistency equation (4.19) with which the order parameter is determined, one would need the effective potential as a function of $|\psi|$ to determine this minimum. This is not possible since the effective potential is only known as a function of J/U and thus one cannot study the effective potential directly regarding the existence of a minimum. Thus the consequences of the properties of the coefficients will be clarified in the next section based on the behavior of the condensate and of the superfluid density.

In Fig. 5.6 the coefficients α_2 , α_4 , and α_6 for $D = 3$ are plotted for $D = 3$. The behavior is qualitatively similar to the behavior of the coefficients for $D = 2$ but especially the zeros of α_4 should not affect the perturbational results as significantly as do the zeros of the two-dimensional case, since α_4 is greater than zero in a sufficient range inside the superfluid region.

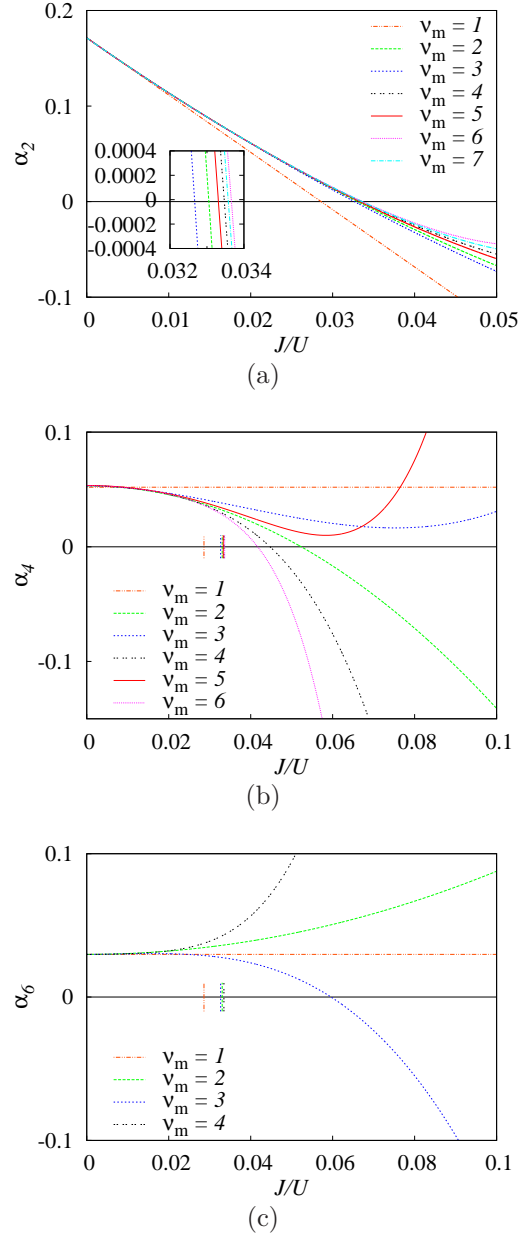


Figure 5.6: Coefficients $\alpha_{2i}(J/U, (\mu/U)_c^{(\nu_m)})$ of the effective potential for $D = 3$. The behavior is qualitatively similar to that for $D = 2$. The important difference is that for this dimensionality the zeros of α_4 are sufficiently far away from the critical hopping strengths, which are indicated by the vertical lines on the x -axis.

5.3 Particle number

If one knows the effective potential, one is also able to calculate the density $\langle n(\mu/U, J/U) \rangle$ of particles depending on the chemical potential μ/U and the hopping strength J/U . The particle density is in general given by

$$\langle n \rangle = -\frac{1}{M} \frac{\partial \mathcal{F}}{\partial \mu}, \quad (5.14)$$

which translates here to [180]

$$\langle n \rangle = -\frac{1}{M} \left(\frac{\partial \Gamma}{\partial (\mu/U)} \right)_{\psi=\psi_{0,\ell}} \quad (5.15)$$

since the free energy \mathcal{F} is substituted by the effective potential because of the use of the Legendre transformation. For ψ one must insert the self-consistent solution (4.21) for $\ell = 3$ or (4.22) for $\ell = 2$.

Inside the superfluid region one expects lines of constant density [60]. This is exemplarily shown in Fig. 5.7 for $D = 2$, $\nu_m = 7$ and $\ell = 2$. Starting from the tip of the Mott lobe one can see a line of constant density with $\langle n \rangle = 1$. Lines with $\langle n \rangle < 1$ and with $\langle n \rangle > 1$ converge to this line for $J/U \rightarrow \infty$. The lines which are inside the Mott lobe and the lines at the top and at the bottom of the plot are artifacts of the finite-order perturbation theory.

The dots on the line $\langle n \rangle = 1$ denote the phase boundary calculated by the zeros of α_2 as explained in Sec. 5.1. It is interesting to note that both phase boundaries are identical. That means the calculation of the particle number represents another method for determining the phase boundary of the Bose-Hubbard model. But both phase boundaries match each other perfectly only for the odd orders. For even orders the phase boundary determined by this method differs from that of Sec. 5.1 by approximately 1% at the tip of the lobe, but it converges to this phase boundary for $\mu/U \rightarrow 0$ and $\mu/U \rightarrow 1$, respectively.

5.4 Condensate and superfluid density

As stated in the previous section, for the determination of the densities two cases have to be considered. According to the behavior of the coefficients of

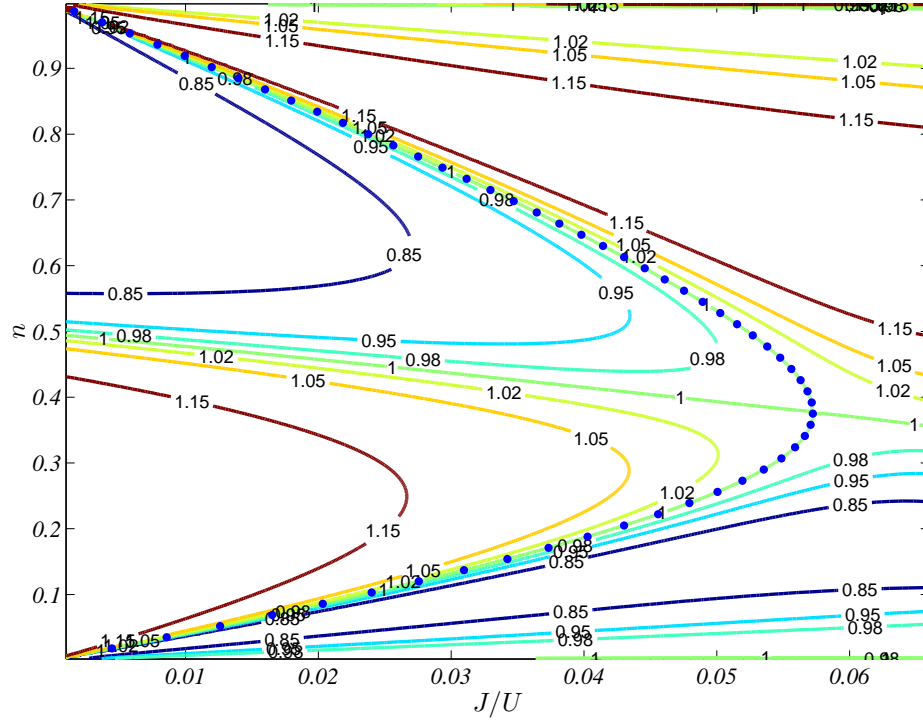


Figure 5.7: Lines of constant particle number $\langle n \rangle$ inside the superfluid region for $D = 2$. The lines inside the Mott lobe and the ones at the top and the bottom of the figure are relicts of the perturbational calculations where these are not valid. The dots on the line $\langle n \rangle = 1$ are determined by the condition $\alpha_2 = 0$ introduced in Sec. 5.1. The two phase boundaries are identical.

the effective potentials the even and odd orders should yield different estimates for the densities.

The condensate density

$$\rho_{c,3} = \frac{-\alpha_4 + \sqrt{\alpha_4^2 - 3\alpha_2\alpha_6}}{3\alpha_6} \quad (5.16)$$

has been introduced in (4.21) and results from (4.13) for $\ell = 3$, whereas for $\ell = 2$ one gets

$$\rho_{c,2} = -\frac{\alpha_2}{2\alpha_4}. \quad (5.17)$$

For $D = 2$ one should not expect a physical solution for $\rho_{c,2}$ if only even orders are considered due to the negative values of α_4 for $J/U > (J/U)_c$ since this would lead to negative values of $\rho_{c,2}$. This means one should only expect valid results of $\rho_{c,2}$ for odd orders.

Considering this case, the question remains how the coefficient α_6 or more specifically the change of its sign or even higher order coefficients influence the condensate density for odd orders for which α_4 is positive. If the perturbational results should be valid, higher order coefficients like α_6 or α_8 should change the density appreciable only for values of J/U significantly greater than the critical value. This will be proven in the following.

In Fig. 5.8(a) the densities $\rho_{c,2}$ and $\rho_{c,3}$ are plotted as a function of J/U at the respective critical chemical potential $(\mu/U)_c^{(\nu_m)}$. First of all it is noteworthy that both densities increase linearly in the vicinity of the critical hopping $(J/U)_c^{(\nu_m)}$. This is contrary to the expectations since for $D = 2$ the critical exponents of both densities of the Bose-Hubbard model with $N = 2$ should be approximately $2/3$ according to Tab. 2.4. This discrepancy is resolved in Sec. 5.5.1 where the critical exponents are calculated with the variational perturbation theory of Sec. 4.2.

Furthermore, one recognizes that the densities of the same order ν_m rapidly converge to each other for $J/U \rightarrow (J/U)_c^{(\nu_m)}$. This is illustrated more precisely in Fig. 5.8(b) where the ratios $\rho_{c,2}/\rho_{c,3}$ and $\rho_{c,2}/\rho_{c,4}$ as a function of $J/U - (J/U)_c^{(\nu_m)}$ are plotted. The density $\rho_{c,4}$ can be calculated just as the other two densities on page 66 by considering the coefficient α_8 defined in (5.13). One recognizes that, e.g., in the interval $(J/U)_c^{(\nu_m)} < J/U < (J/U)_c^{(\nu_m)} + 0.001$ the respective deviations are less than 3% which is less than the error one should expect due to the perturbational nature of the calculations.

The inset of Fig. 5.8(a) shows how the condensate densities of different orders can be transformed onto each other by plotting them as a function of $J/U - (J/U)_c^{(\nu_m)}$. Nonetheless this transformation does not lead to an extrapolation scheme for $\nu_m \rightarrow \infty$ since no convergence is recognizable and in addition one has too few data points.

Summarizing these considerations leads to the conclusion that for odd orders $\rho_{c,2}$ is a good approximation to the condensate density in the vicinity of the critical hopping since the deviation from higher order densities vanishes for

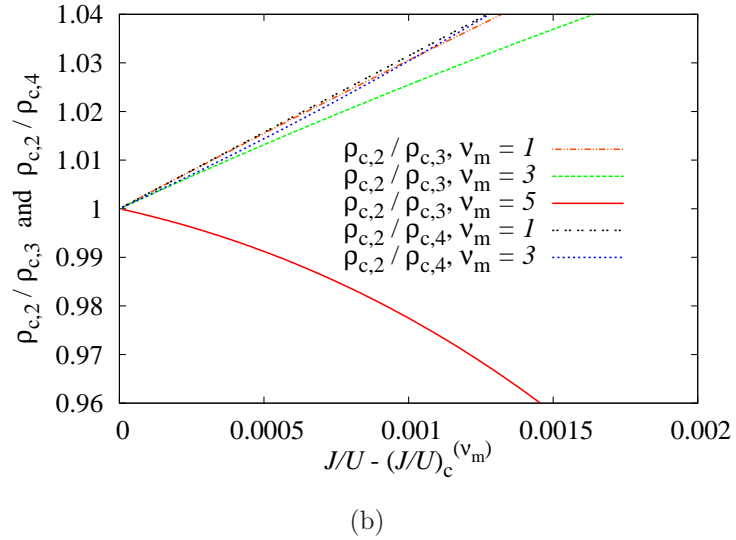
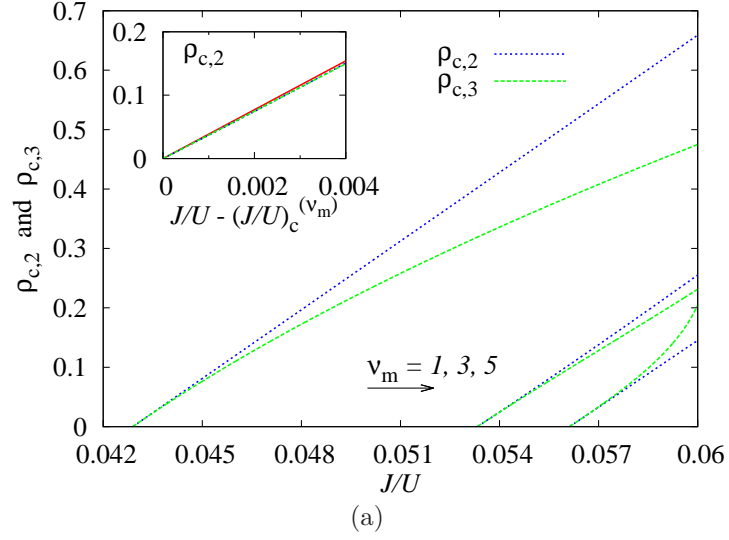


Figure 5.8: Properties of the condensate density for $D = 2$. (a) Comparison of the condensate densities $\rho_{c,2}$ and $\rho_{c,3}$ for odd orders. In a good approximation both densities increase linearly in the vicinity of $(J/U)_c^{(v_m)}$. The inset shows $\rho_{c,2}$ for the orders stated in the plot as a function of $J/U - (J/U)_c^{(v_m)}$. The curves conform so well that they can hardly be distinguished from each other. (b) The plot shows that the densities converge to each other remarkably well so that $\rho_{c,2}$ is sufficient to describe the condensate density for $J/U \approx (J/U)_c$.

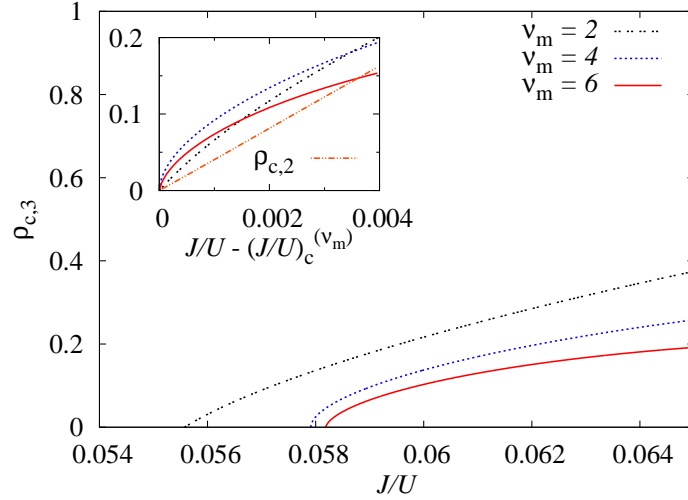
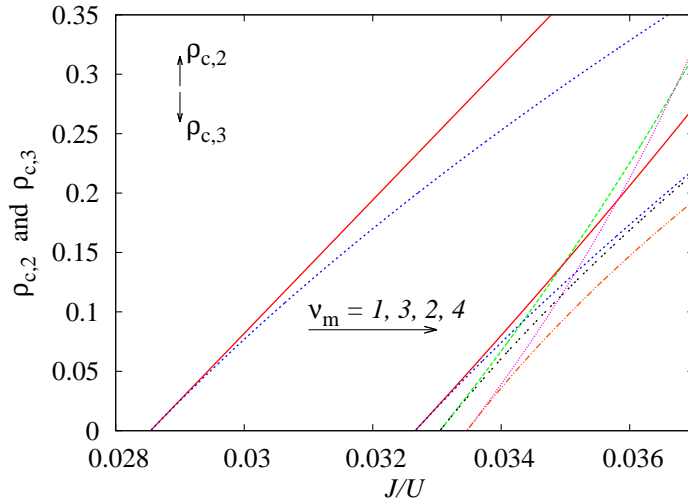

 (a) $D = 2$

 (b) $D = 3$

Figure 5.9: (a) Shown is the condensate density $\rho_{c,3}$ for even orders and $D = 2$ at the respective critical chemical potential. The plot shows that $\rho_{c,3}$ does not increase linearly like $\rho_{c,2}$ which is also illustrated in the inset. (b) Comparison of $\rho_{c,2}$ and $\rho_{c,3}$ for $D = 3$ and $\mu/U = 0.393$. The upper curve always belongs to $\rho_{c,2}$. Here no deviation from a critical exponent equal to one is observable neither for $\rho_{c,2}$ nor for $\rho_{c,3}$. Just like in the case $D = 2$ these densities also converge to each other for $J/U - (J/U)_c^{(v_m)} \rightarrow 0$.

$J/U = (J/U)_c^{(\nu_m)}$ which is crucial for the later determination of the critical exponent.

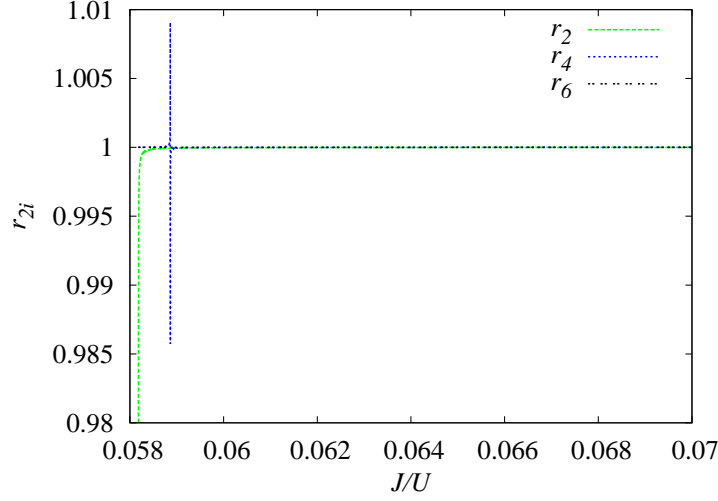
For the even orders the issue is more complicated. The density $\rho_{c,2}$ is not valid due to the arguments given at the beginning of this section regarding the sign of α_4 . The next order which could give physical results is $\ell = 3$ with the density $\rho_{c,3}$. This is shown in Fig. 5.9(a). Here the condensate density looks qualitatively different from that density obtained in odd orders. For example, the different curves do not fall onto each other if they are plotted as a function of $J/U - (J/U)_c^{(\nu_m)}$ as it is shown in the inset. But, more importantly, the density does not increase linearly but with a critical exponent less than one.

This is also illustrated in the inset where additionally $\rho_{c,2}$ with $\nu_m = 7$ is plotted. Apparently one has $\rho_{c,2} < \rho_{c,3}$ in the vicinity of the critical hopping. This observation will lead to a direct determination of the critical exponent of the condensate and of the superfluid density in Sec. 5.5.2.

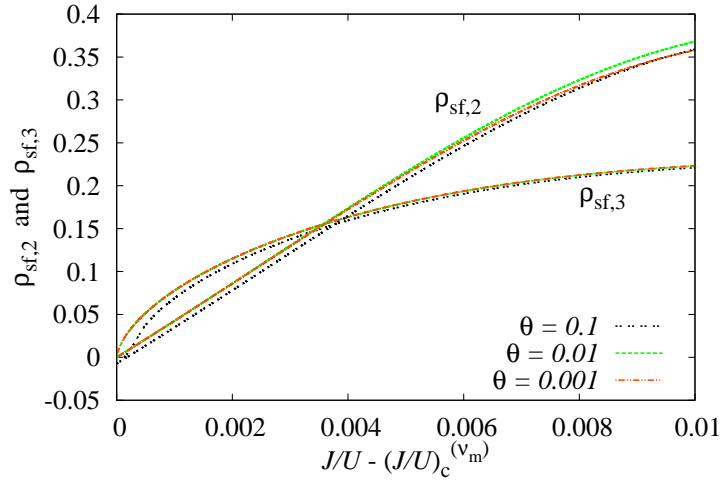
Fig. 5.9(b) shows the condensate density for $D = 3$ at the chemical potential $\mu/U = 0.393$ which is the extrapolated critical chemical potential. Both densities increase linearly so that here no difference between the cases $\ell = 2$ and $\ell = 3$ is observable. The convergence properties are like that for the densities of $D = 2$ which means that the two densities $\rho_{c,2}$ and $\rho_{c,3}$ converge to each other for $J/U \rightarrow (J/U)_c^{(\nu_m)}$. This behavior corresponds to the expected behavior since for the Bose-Hubbard model the dimension $D = 3$ is equal to the upper critical dimension so that here the mean-field critical exponents of Tab. 2.3 are valid.

The superfluid density (4.26) is determined with the help of the phase θ which is introduced in (4.28). As one can see in these equations, only the ratio θ/L of the phase θ and the length L of the system is crucial for the determination of the superfluid density. This ratio will from now on be called *twist*. In the following all coefficients c_{2i} and, therefore, also the coefficients α_{2i} depend on the twist.

All statements made for the condensate density are also valid for the superfluid density since the influence of the phase on the coefficients of the respective effective potential is only minimal. This is shown in Fig. 5.10(a), where the



(a)



(b)

Figure 5.10: Results for the superfluid density with $D = 2$: (a) Ratios r_{2i} defined in (5.18). As one can see the twist θ/L changes the coefficients only minimally. (b) Comparison of the superfluid densities for $\ell = 2$ with $\nu_m = 7$ and $\ell = 3$ with $\nu_m = 6$. Whereas the density for $\ell = 2$ increases linearly, the critical exponent for $\ell = 3$ must be less than 1.

ratios

$$r_{2i} := \frac{\alpha_{2i}(\theta/L = 0.001)}{\alpha_{2i}(\theta/L = 0)} \quad (5.18)$$

of the coefficients of the effective potential

$$\Gamma_\ell(\theta/L) = \sum_{i=1}^{\ell} \alpha_{2i}(\theta/L) |\psi_{0,\ell}(\theta/L)|^{2i} \quad (5.19)$$

with $|\psi_{0,\ell}(\theta/L = 0)|^2 = \rho_{c,\ell}$ are plotted. For $\theta/L = 0$ this effective potential is equal to that of (4.13), which is used for determining the condensate density. This plot shows that the twist does not change the qualitative behavior of the coefficients. The apparent divergence of r_2 at the beginning marks the point of the phase transition where α_2 changes its sign. Also the divergence of r_4 can be explained by a change of the sign of α_4 . The discrepancy of the coefficients at these points can be ascribed to numerical inaccuracies. The superfluid density itself is plotted in Fig. 5.10(b). This plot shows $\rho_{\text{sf},2}$ as well as $\rho_{\text{sf},3}$ and one can observe a linear behavior for $\ell = 2$ and a nonlinear behavior for $\ell = 3$, as it was already the case for the respective condensate densities. Besides, the very small influence of the twist is visible again.

Now the two densities can be compared to each other. Fig. 5.11 shows the condensate density and the superfluid density for $\ell = 2$ and $\ell = 3$, for $D = 2$ and $D = 3$ on a square lattice. Shown is in all cases the highest available order. For the superfluid density the chosen value of the twist is $\theta/L = 0.001$.

For $D = 2$ one observes once more that the superfluid density $\rho_{\text{sf},\ell}$ is greater than the condensate density $\rho_{c,\ell}$ which indicates that the critical exponent of the superfluid density is less than that of the condensate density. This is expected due to the Josephson relation $v = 2\beta - \eta\nu$ of (2.39) which connects the critical exponent ν of $\rho_{\text{sf},\ell}$ to the critical exponent $\beta_c = 2\beta$ of $\rho_{c,\ell}$.

Also the qualitative difference between the densities for $\ell = 2$ and $\ell = 3$ can be seen in this figure. Whereas for $\ell = 2$ both densities are linear over a wide range of the hopping, the densities for $\ell = 3$ are clearly not linear. In contrast, the densities for $D = 3$ are always linear in good approximation.

For three dimensions one observes only a slight difference between the two densities. Since in this case one expects the critical exponents of mean-field

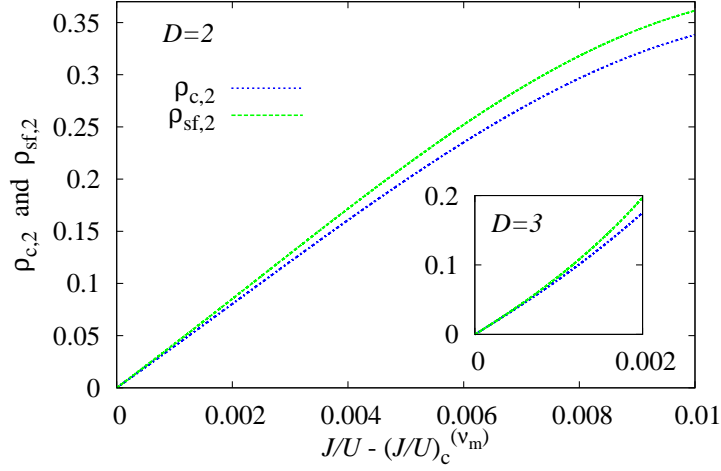
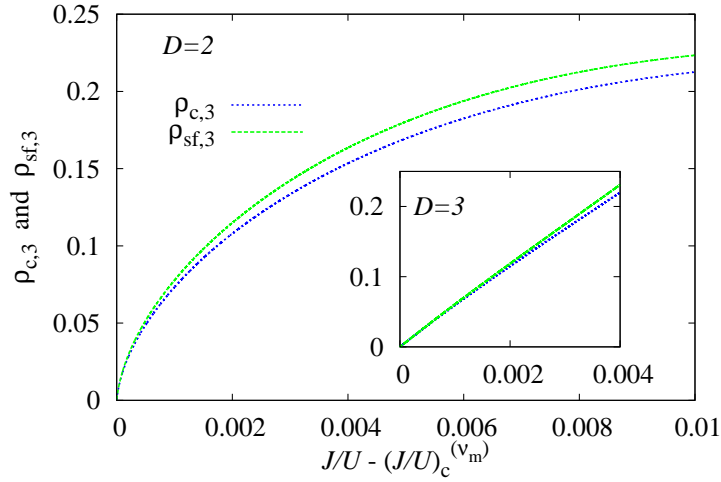

 (a) $\ell = 2$. $D = 2, 3$: $\nu_m = 7, 6$

 (b) $\ell = 3$. $D = 2, 3$: $\nu_m = 6, 5$

Figure 5.11: Superfluid density $\rho_{sf,\ell}$ and condensate density $\rho_{c,\ell}$ for $D = 2$ and $D = 3$. For the superfluid density the twist is set to $\theta/L = 0.001$. Whereas both densities shown in (a) increase linearly, the densities in (b) differ from each other, since only the densities for $D = 3$ show a linear behavior.

theory with $\eta = 0$, one can deduce $\nu = \beta_c$ from the Josephson relation (2.39), so that both densities should coincide in the critical region.

Since all these results are of finite order, they cannot compete with methods which calculate the condensate and superfluid density directly. But comparisons show that the densities calculated with the method of the effective action are at least in the vicinity of the critical point comparable to that obtained by other methods [181].

5.5 Critical exponents

In this section two methods for determining the critical exponents ν of the superfluid density and β_c of the condensate density of the Bose-Hubbard model are explained. The critical exponent of the condensate density is directly related to the critical exponent of the order parameter $|\psi_0|$ since the condensate density is given by $\rho_c = |\psi_0|^2$. Therefore the critical exponent of the order parameter is $\beta = \beta_c/2$.

The first method uses the effective potential only up to $\ell = 2$. This ansatz will be called $|\psi|^4$ -approach. The densities $\rho_{c,2}$ and $\rho_{sf,2}$ do not lead directly to the correct critical exponents since for $D = 2$ and $D = 3$ one just gets the critical exponents of mean-field theory, which are only valid for $D \geq 3$. Only after using the variational perturbation theory introduced in Sec. 4.2 one gets the predicted critical exponents for $D = 2$.

The second method is based on calculating the effective potential with $\ell = 3$ up to $|\psi|^6$, and analyzing the corresponding densities $\rho_{c,3}$ and $\rho_{sf,3}$. These densities permit a direct calculation of the critical exponents without further treatments. In the spirit of the first method, this ansatz will be called $|\psi|^6$ -approach.

The direct way to calculate the critical exponent of a certain variable is to use the following logarithmic derivative: Since both densities ρ scale like

$$\rho \propto (J/U - (J/U)_c)^x \quad (5.20)$$

for $(J/U - (J/U)_c) \ll 1$ as stated in (4.34), the logarithmic derivative

$$d \log \rho := \lim_{J/U - (J/U)_c \rightarrow 0} \frac{d \log \rho}{d \log (J/U - (J/U)_c)} = x \quad (5.21)$$

yields the critical exponent denoted here by x .

The Bose-Hubbard model on a D -dimensional cubic lattice is in the same universality class as the $D + 1$ -dimensional XY -model [60] for which one has $N = 2$. That means that for the two-dimensional Bose-Hubbard model one expects the critical exponents of Tab. 2.4 with $D = 3$ so that both critical exponents should be approximately $2/3$. To be more precise, the critical exponents of the two densities should be

$$\beta_c = 2\beta = 0.6962 \quad \text{and} \quad \nu = \beta_c - \eta\nu = 0.6697 \quad (5.22)$$

according to Ref. [97] for the condensate and for the superfluid density, respectively. Critical exponents calculated by other groups [98, 103] differ by less than 1% from these results so that the values of (5.22) function as reference values in the following. The second equation represents the Josephson relation of (2.39). For the Bose-Hubbard model the dimension $D = 3$ is equal to the upper critical dimension, so that in this case the mean-field critical exponents of Tab. 2.3 are valid. That means one should expect

$$\beta_c = 1 \quad \text{and} \quad \nu = 1. \quad (5.23)$$

5.5.1 $|\psi|^4$ -approach

As one can see in Fig. 5.12 the critical exponent for $D = 2$ of both densities, as calculated by the logarithmic derivative (5.21), is one. This conforms to the data shown in the previous section where this was already noticeable, e.g., in Fig. 5.11(a). But these are not the correct critical exponents for $D = 2$: Here one requires the values stated in (5.22).

Nonetheless variational perturbation theory permits an access to the critical exponents predicted by the ϕ^4 -theory. Starting point is the Taylor expansion

$$\alpha_{2i}^{(\nu_m)} = \sum_{\nu=0}^{\nu_m \leq n-2i} a_{2i}^{(\nu)} (J/U)^\nu \quad \text{with} \quad i = 1, 2, 3 \quad (5.24)$$

of the coefficients of the effective potential. For the following procedure it does not matter whether the coefficients depend on the twist θ/L so that this dependency is dropped during the discussion in this section. This expansion

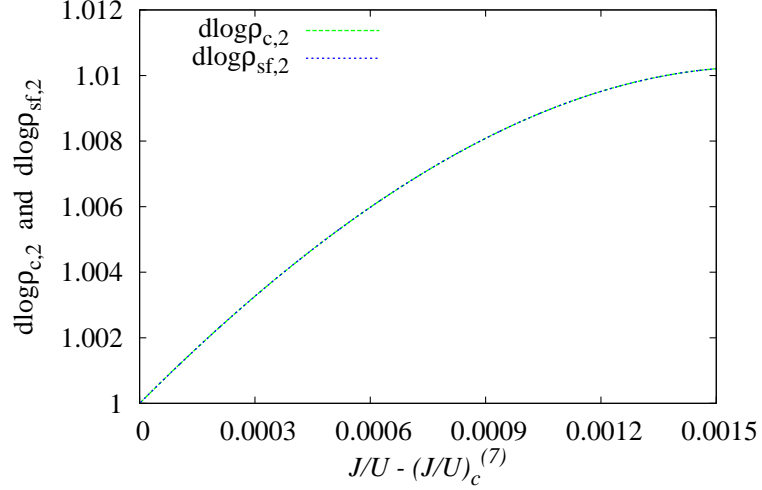


Figure 5.12: Logarithmic derivatives for $D = 2$ of the condensate density $\rho_{c,2}$ and the superfluid density $\rho_{sf,2}$ with $\theta/L = 0.001$. Both curves fall onto each other. As one can clearly see, according to (5.21) the critical exponents would be one in both cases.

(5.24) is transformed to a new variable $g = J/U - (J/U)_c^{(\nu_m)}$ so that one gets new coefficients $\tilde{a}_{2i}^{(\nu)}$. For example, in first order of the hopping the coefficients transform like

$$a_{2i}^{(0)} + a_{2i}^{(1)} J/U \longrightarrow a_{2i}^{(0)} + a_{2i}^{(1)} \left(g + (J/U)_c^{(\nu_m)} \right) = \tilde{a}_{2i}^{(0)} + \tilde{a}_{2i}^{(1)} g \quad (5.25)$$

with

$$\tilde{a}_{2i}^{(0)} = a_{2i}^{(0)} + a_{2i}^{(1)} (J/U)_c^{(\nu_m)} \quad \text{and} \quad \tilde{a}_{2i}^{(1)} = a_{2i}^{(1)}. \quad (5.26)$$

This transformation depends on the order n of the perturbational expansion so that for different n one gets different coefficients $\tilde{a}_{2i}^{(\nu)}$. This procedure leads to a new expansion

$$\tilde{\alpha}_{2i}^{(\nu_m)} = \sum_{\nu=0}^{\nu_m \leq n-2i} \tilde{a}_{2i}^{(\nu)} g^\nu \quad \text{with} \quad i = 1, 2, 3, \quad (5.27)$$

which just shifts the zero of the condensate and the superfluid density from $J/U = (J/U)_c^{(\nu_m)}$ to $g = 0$. With these new coefficients both the condensate

and the superfluid density can be expressed as series

$$\rho = \sum_{\nu=0}^{\nu_m} \hat{a}_\nu g^\nu \quad (5.28)$$

with coefficients \hat{a}_ν depending on the coefficients $\tilde{a}_{2i}^{(\nu)}$.

According to (4.66) the logarithmic derivative of (5.28) yields an expansion of the critical exponent. To this series variational perturbation theory is applied, leading to the estimate (4.67) which now depends on the two variational parameters \tilde{g} and the corresponding q . This parameter q must be determined by the first logarithmic derivative F_1 introduced in (4.68) or by the second logarithmic derivative F_2 introduced in (4.69), and by the conditions stated in (4.70).

It turns out that both logarithmic derivatives lead to a value for q . For the calculation of the critical exponents always that parameter q is chosen which is the closest to the reference value $q \approx 2.5$ stated in Ref. [81]. Since these parameters always lead to the best results for the critical exponents and due to the lack of further data points which could be used for an extrapolation, this procedure seems the best for a reliable choice of the optimal variational parameter q .

After applying the variational perturbation theory to F_2 , one has to look for the zeros \tilde{g}_{0,F_2} of $F_2^\infty(\tilde{g}, q) + 2/q$, which are simultaneously extrema or turning points due to the principle of minimum sensitivity. Fig. 5.13 shows the second derivative

$$F_2^{(2)} := \frac{d^2 F_2^\infty(\tilde{g}_{0,F_2}, q)}{d\tilde{g}_{0,F_2}^2} \quad (5.29)$$

for $\nu_m = 7$ in the case of the condensate density which has a zero at $q \approx 2.4615$. Besides this zero there is also a zero at $q \approx 2.817$. For lack of further zeros the smallest of these two values is taken as an approximation for the extrapolated q with $\nu_m \rightarrow \infty$. That means $q_c = 2.4615$ is taken as the value of the variational parameter q for the condensate density. The function F_1 leads in the same way to $q \approx 3.1$ but because of the arguments given above this estimate is not considered during the further calculations.

This value of q is now inserted in (4.67) so that the expansion of β only depends on \tilde{g} . The optimal \tilde{g} is determined by the extrema of (4.67). If there

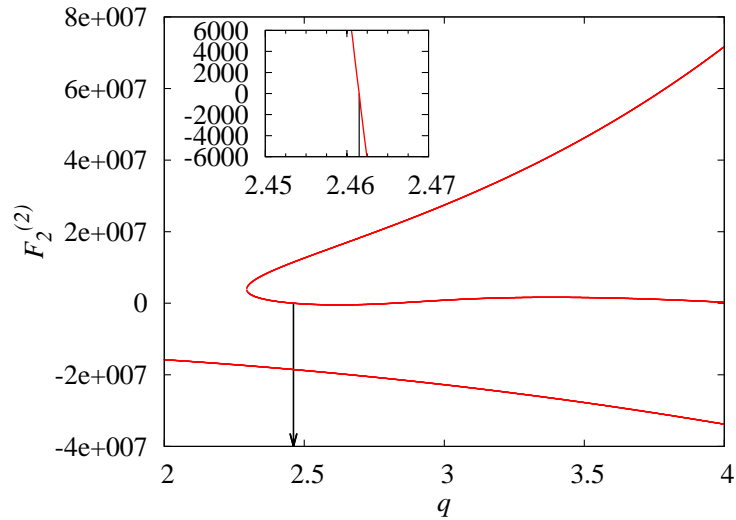


Figure 5.13: The second derivative of F_2 defined in (4.69). The zeros are possible solutions for the variational parameter q . That zero which is closest to $q = 2.5$ is taken as the optimal solution. The inset shows a magnification of this zero at $q \approx 2.4615$.

exists more than one zero of the derivative, always the smallest, nonnegative zero is taken as the optimal variational parameter \tilde{q} .

This procedure leads to the results stated in Tab. 5.2. Since only three data points are known, they are fitted linearly leading to the extrapolated critical exponent for $\nu_m \rightarrow \infty$ which is 0.7028 for the condensate density of a two-dimensional square lattice.

The calculation of the critical exponent ν of the superfluid density proceeds basically in the same way. Here one finds that the first logarithmic derivative F_1^∞ permits the determination of the best q in the same way as stated above.

Since the superfluid density depends on the twist θ/L , one more extrapolation for $\theta/L \rightarrow 0$ is necessary. This is done for $\theta/L = 0.001$ with $q_{0.001} = 2.7822$ and $\theta/L = 0.01$ with $q_{0.01} = 2.7857$. These two values are extrapolated linearly which leads to $q_{\text{sf}} = 2.7818$. One also gets the estimate $q \approx 3.4$ by using the function F_2 but as already said in the context of the condensate density this guess will not be considered furthermore.

The former value of q together with the coefficients of the superfluid density

ν_m	$\beta_c^{(\nu_m)}$	$\nu^{(\nu_m)}$	β	η	α	γ
3	1.3774	1.4291	-	-	-	-
5	1.0206	1.0836	-	-	-	-
7	1.0334	1.0221	-	-	-	-
∞	0.7028	0.6784	[0.3514]	[0.0360]	[-0.03533]	[1.33245]
Tab. 2.4	[0.6962]	0.6697	0.3481	0.0396	-0.01126	1.31045
[182]	[0.733]	0.699	[0.367]	0.049	[-0.097]	[1.364]

Table 5.2: The top of the table shows the critical exponents for $D = 2$ depending on the order ν_m , and the linear fit for $\nu_m \rightarrow \infty$. Critical exponents in square brackets are calculated via the hyperscaling relations (2.36) and the Josephson relation (2.39). The bottom of the table shows first the critical exponents as taken from the ϕ^4 -theory, see Tab. 2.4. The second reference values from Ref. [182] are critical exponents which were explicitly calculated for the Bose-Hubbard model by means of a renormalization group approach.

with $\theta/L = 0.001$ are used for the subsequent determination of the optimal variational parameter \tilde{g} and the resulting critical exponent. The determination of \tilde{g} differs slightly from that of the condensate density. Since there are no positive zeros always the smallest negative zero is taken as the variational parameter.

This procedure leads to the critical exponent ν stated in Tab. 5.2. The extrapolation for $\nu_m \rightarrow \infty$ is also done linearly here.

One is now able to calculate the other critical exponents with the help of the hyperscaling relations (2.36) and the Josephson relation (2.39). This leads to the rest of the exponents stated in Tab. 5.2. In the last row the reference values previously stated in Tab. 2.4 are listed again for comparison.

As one can see, the quality of the calculated critical exponents is very good if one considers the amount of data which is available for the extrapolation. It is also interesting to note that one actually finds values of q which are close to $q \approx 2.5$ as used in Ref. [81] for determining various critical exponents. But one has also to remark that the choice of the parameter q is in some way arbitrary since for the calculation of the critical exponents always the estimate closest

to $q = 2.5$ was chosen. This is only justified by the very good results, and by the lack of extrapolation points.

The error of the reference values is much smaller than that of our result due to the lack of extrapolation points. Since one needs a fit for the extrapolation of the variational parameter q and of the critical exponent itself, one should expect an error of at least approximately 5%.

For $D = 3$ the variational perturbation theory yields no unique results for the critical exponents. As in the case $D = 2$ one is not able to find a solution for the parameter q for the odd orders $\nu_m = 3$ and $\nu_m = 5$. Since with $\nu_m = 7$ no data are available for $D = 3$ due to the immense numerical effort, the question whether one can reproduce the expected mean-field results with the variational perturbation theory must remain open.

One can also apply the variational perturbation theory to the even orders for $D = 2$ and $D = 3$. This leads to results which are not consistent with the results for the odd orders and which do not lead to reliable values for the critical exponents. Possibly this can be traced back to the zeros of α_4 in the vicinity of the critical hopping, as shown in Fig. 5.4(b). Further research is necessary in order to clarify the properties of the even orders and the influence of the variational perturbation scheme on them.

5.5.2 $|\psi|^6$ -approach

The logarithmic derivative (5.21) is now applied to the condensate density $\rho_{c,3}$ and the superfluid density $\rho_{sf,3}$ shown in Fig. 5.11(b). Fig. 5.14 shows the derivatives for $D = 2$ and $\nu_m = 4, 6$ of the condensate density. As one recognizes, both functions behave differently depending on the distance to the respective critical hopping $(J/U)_c^{(\nu_m)}$. In the vicinity of $(J/U)_c^{(\nu_m)}$ the functions increase fast and converge to one. At a certain point the functions adopt a nearly linear behavior with a monotonic decrease. It is a remarkable observation that for specific extrapolations for $J/U - (J/U)_c^{(\nu_m)} \rightarrow 0$ of the segments with a linear behavior one is able to calculate the critical exponents, as will be demonstrated in the following.

In this Fig. 5.14 also the results for $D = 3$ are plotted. For this dimension the logarithmic derivatives behave differently from that for $D = 2$ and appar-

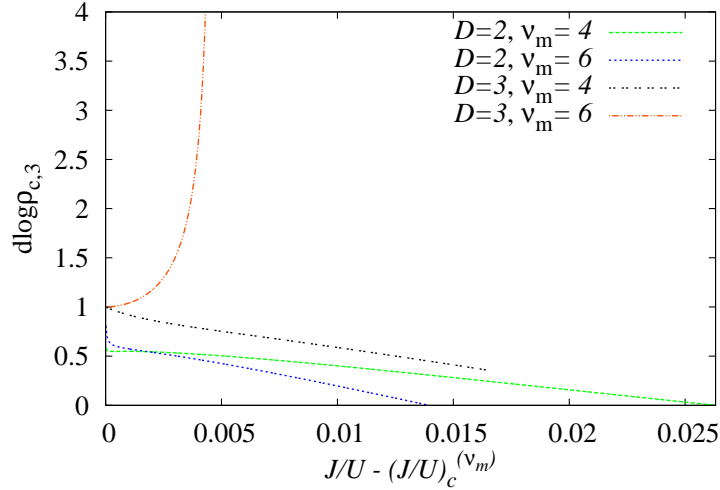


Figure 5.14: Logarithmic derivative $d \log \rho_{c,\ell}$ of the condensate density for various orders and dimensions $D = 2$ and $D = 3$. While the derivative for $D = 3$ converges to one, the linear part of the logarithmic derivative of $D = 2$ converges to a value less than one.

ently converge to one, which corresponds to the expected mean-field critical exponent.

For the condensate density the derivative

$$d \log \rho'_{c,3} := \frac{d}{dJ/U} d \log \rho_{c,3} \quad (5.30)$$

of the logarithmic derivative is shown in Fig. 5.15. All derivatives are plotted for those values of $J/U - (J/U)_c^{(\nu_m)}$ for which the condensate and the superfluid density are monotonically increasing. This is approximately the interval for which the perturbation theory is valid.

For $\nu_m = 6$ the derivative of $d \log \rho_{c,3}$ is monotonically decreasing so that a quadratic fit seems to be the best choice for an extrapolation. The horizontal black line underneath each curve shows which part of the respective curve is used for the fit. The derivative for $\nu_m = 4$ is not monotonically decreasing so that the minimum of the derivative is used as the boundary for the maximal value of J/U .

	$\beta_c^{(\nu_m)}$	$\nu^{(\nu_m)}$	
$\nu_m \setminus \theta/L$		0.001	0.01
4	0.5715	0.6446	0.6463
6	0.6153	0.6525	0.6541
∞	0.7029	0.6683	0.6697
$\theta/L \rightarrow 0$	-	0.6681	

Table 5.3: Shown are the results obtained when determining the critical exponents with the $|\psi|^6$ -approach for the two-dimensional Bose-Hubbard model on a square lattice.

The inset shows the derivative of $d \log \rho_{\text{sf},3}$. Both curves are decreasing after a maximum in the vicinity of the critical point until a minimum is reached after which both increase again. This behavior distinguishes them from that of the condensate density. Here a linear fit gives the best results. The values for which the logarithmic derivative is fitted is chosen by the maximal $(J/U)_{\text{max}}$ at the end of both curves and the respective point $(J/U)_{\text{min}}$ with the same value $d \log \rho'_{c,3}((J/U)_{\text{min}}) = d \log \rho'_{c,3}((J/U)_{\text{max}})$. This corresponds to an averaging of the slope by a linear fit.

To sum up, these arguments lead to the conclusion that the best fit of the logarithmic derivative of the condensate density is a quadratic fit and for the logarithmic derivative of the superfluid density one does get the best results with a linear fit. The results of this procedure are stated in Tab. 5.3. Again one needs an extrapolation for $\theta/L \rightarrow 0$ for the superfluid density, which is done linearly since only the two data points $\theta/L = 0.01$ and $\theta/L = 0.001$ are available.

These results agree with the reference values of Tab. 2.4 remarkably well. Both critical exponents, β_c and ν , differ from the reference values stated in Tab. 5.2 and Tab. 2.4 by less than 1%. But due to the various fitting schemes required to get this result one should expect an error between roughly 5% and 10%. Especially the choice of the interval used for the fit of the logarithmic derivatives $d \log \rho_{c,3}$ and $d \log \rho_{\text{sf},3}$, respectively, is crucial for the final result, but this interval is subject to a certain arbitrariness. Nonetheless both crit-

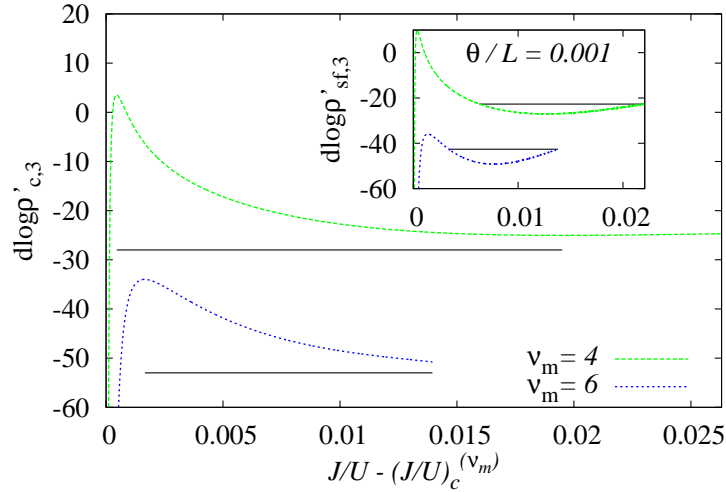


Figure 5.15: Shown is the derivative of $d \log \rho_{c,\ell}$ and $d \log \rho_{sf,\ell}$ with respect to J/U . The horizontal black line depicts which interval is used for the linear extrapolation of the logarithmic derivative. These derivatives are plotted for that range for which the densities are monotonically increasing.

ical exponents β_c and ν obtained from the present $|\psi|^6$ -approach, and from the $|\psi|^4$ -approach followed in the preceding subsection, agree significantly better with the previous values obtained by Kleinert and Schulte-Frohlinde [97] and by Guida and Zinn-Justin [98] from the ϕ^4 -theory than the values recently obtained from a renormalization group approach to the Bose-Hubbard model [182]. This indicates that the approaches put forward in this thesis have a high potential, and thus deserve to be studied further.

6 Summary

In this thesis critical properties of the two- and three-dimensional Bose-Hubbard model have been evaluated, using the method of the effective action. To this end, the coefficients α_i in the expansion (4.13) of the effective action with respect to the order parameter have been computed perturbatively with the help of the process-chain approach, which allows one to perform expansions in powers of the hopping strength numerically in high orders. These perturbative results have then been extended into the non-perturbative regime by means of variational perturbation theory as put forward by H. Kleinert.

- Knowledge of the coefficient α_2 provides the boundary between the Mott insulator and the superfluid phase. In Sec. 5.1 an extrapolation scheme has been established which provides an upper and a lower bound on the phase boundary, as depicted in Fig. 5.2. The results obtained in this manner are fully consistent with those of previous calculations.
- Inside the superfluid region, lines of constant density have been computed in Sec. 5.3, as shown in Fig. 5.7. In addition, both the condensate and the superfluid density have been computed in Sec. 5.4, see Fig. 5.11. These results demonstrate that the method of effective action actually enables one to calculate quantities which are defined only inside the superfluid region, although the underlying perturbative calculations start from the ground state of the Mott insulator. In contrast to other methods, this approach is particularly accurate in the vicinity of the phase boundary.
- Since $D = 3$ is the upper critical dimension of the Bose-Hubbard model, where the critical exponents coincide with those given by mean-field theory, a calculation of the critical exponents for $D = 2$ is of particular interest. In Sec. 5.5.1 the critical exponents β_c for the condensate density and

v for the superfluid density have been obtained from the coefficients α_2 and α_4 , combining the process-chain approach with variational perturbation theory. The results, listed in Tab. 5.2, indicate that this approach indeed is viable.

- In Sec. 5.5.2 the critical exponents have been obtained by evaluating also the coefficient α_6 ; see Fig. 5.14. The fact that the data obtained in this manner, listed in Tab. 5.3, agree quite well with those of the previous approach is a quite important confirmation of consistence, since variational perturbation theory is not used here.

It might be interesting to ask whether the methods developed in this thesis can be refined and extended such that they yield the critical properties of the Bose-Hubbard model with even higher accuracy. It should also be emphasized that these methods are not restricted to the Bose-Hubbard model, but should be adaptable in a straightforward manner to other models.

Bibliography

- [1] M. H. Anderson, J. R. Ensher, M. R. Matthews, C. E. Wieman, and E. A. Cornell. Observation of Bose-Einstein condensation in a dilute atomic vapor. *Science*, **269**(198), 1995.
- [2] K. B. Davis, M.-O. Mewes, M. R. Andrews, N. J. van Druten, D. S. Durfee, D. M. Kurn, and W. Ketterle. Bose-Einstein condensation in a gas of sodium atoms. *Phys. Rev. Lett.*, **75**(3969), 1995.
- [3] B. DeMarco and D. S. Jin. Onset of Fermi degeneracy in a trapped atomic gas. *Science*, **285**(1703), 1999.
- [4] F. Schreck, L. Khaykovich, K. L. Corwin, G. Ferrari, T. Bourdel, J. Cubizolles, and C. Salomon. Quasipure Bose-Einstein condensate immersed in a Fermi sea. *Phys. Rev. Lett.*, **87**(080403), 2001.
- [5] A. G. Truscott, K. E. Strecker, W. I. McAlexander, G. B. Partridge, and R. Hulet. Observation of Fermi pressure in a gas of trapped atoms. *Science*, **291**(2570), 2001.
- [6] M. Greiner, O. Mandel, T. Esslinger, T. W. Hänsch, and I. Bloch. Quantum phase transition from a superfluid to a Mott insulator in a gas of ultracold atoms. *Nature*, **415**(39), 2002.
- [7] R. P. Feynman. Simulating physics with computers. *Int. J. Theor. Phys.*, **21**(467), 1982.
- [8] I. Bulita and F. Nori. Quantum simulators. *Science*, **326**(108), 2009.
- [9] S. Lloyd. Universal quantum simulators. *Science*, **273**(1073), 1996.
- [10] D. S. Abrams and S. Lloyd. Simulation of many-body systems on a universal quantum computer. *Phys. Rev. Lett.*, **79**(2586), 1997.

- [11] D. P. DiVincenzo. Quantum Computation. *Science*, **270**(255), 1995.
- [12] T. D. Ladd, F. Jelezko, R. Laflamme, Y. Nakamura, C. Monroe, and J. L. O'Brien. Quantum computers. *Nature*, **464**(45), 2010.
- [13] W. D. Phillips, P. L. Gould, and P. D. Lett. Cooling, stopping, and trapping Atoms. *Science*, **239**(878), 1988.
- [14] C. S. Adams and E. Riis. Laser cooling and trapping of neutral atoms. *Prog. Quant. Electron*, **21**(1), 1997.
- [15] M. Lewenstein, A. Sanpera, V. Ahufinger, B. Damski, A. Sen De, and U. Sen. Ultracold atomic gases in optical lattices: mimicking condensed matter physics and beyond. *Advances in Physics*, **56**(243), 2007.
- [16] I. Bloch, J. Dalibard, and W. Zwerger. Many-body physics with ultracold gases. *Rev. Mod. Phys.*, **80**(885), 2008.
- [17] S. Chu. The manipulation of neutral particles. *Rev. Mod. Phys.*, **70**(685), 1998.
- [18] C. N. Cohen-Tannoudji. Manipulating atoms with photons. *Rev. Mod. Phys.*, **70**(707), 1998.
- [19] W. D. Phillips. Laser cooling and trapping of neutral atoms. *Rev. Mod. Phys.*, **70**(721), 1998.
- [20] H. Metcalf and P. van der Straten. Cooling and trapping of neutral atoms. *Phys. Rep.*, **244**(203), 1994.
- [21] C. E. Wieman, D. E. Pritchard, and D. J. Wineland. Atom cooling, trapping, and quantum manipulation. *Rev. Mod. Phys.*, **71**(S253), 1999.
- [22] C. J. Pethick and H. Smith. *Bose-Einstein condensation in dilute gases*. Cambridge University Press, 1. edition, 2002.
- [23] S. Bose. Plancks Gesetz und Lichtquantenhypothese. *Z. Phys.*, **26**(178), 1924.
- [24] A. Einstein. Quantentheorie des einatomigen idealen Gases. *Sitzungsber. Preuss. Akad. Wiss.*, (261), 1924.

-
- [25] A. Einstein. Quantentheorie des einatomigen idealen Gases. 2. Abhandlung. *Sitzungsber. Preuss. Akad. Wiss.*, (3), 1925.
- [26] W. Pauli. The connection between spin and statistics. *Phys. Rev.*, **58** (716), 1940.
- [27] V. Bagnato, D. E. Pritchard, and D. Kleppner. Bose-Einstein condensation in an external potential. *Phys. Rev. A*, **35**(4354), 1987.
- [28] K. Huang. *Statistical Mechanics*. John Wiley, 2. edition, 1987.
- [29] D. S. Durfee and W. Ketterle. Experimental studies of Bose-Einstein condensation. *Opt. Exp.*, **2**(299), 1998.
- [30] C. C. Bradley, C. A. Sackett, J. J. Tollett, and R. G. Hulet. Evidence of Bose-Einstein Condensation in an Atomic Gas with Attractive Interactions. *Phys. Rev. Lett.*, **75**(1687), 1995.
- [31] C. C. Bradley, C. A. Sackett, J. J. Tollett, and R. G. Hulet. Erratum: Evidence of Bose-Einstein Condensation in an Atomic Gas with Attractive Interactions [Phys. Rev. Lett. **75**(1687), 1995]. *Phys. Rev. Lett.*, **79** (1170), 1997.
- [32] C. C. Bradley, C. A. Sackett, and R. G. Hulet. Bose-Einstein Condensation of Lithium: Observation of Limited Condensate Number. *Phys. Rev. Lett.*, **78**(985), 1997.
- [33] P. A. Ruprecht, M. J. Holland, K. Burnett, and Mark Edwards. Time-dependent solution of the nonlinear Schrodinger equation for Bose-condensed trapped neutral atoms. *Phys. Rev. A*, **51**(4704), 1995.
- [34] J. M. Gerton, D. Strekalov, I. Prodan, and R. G. Hulet. Direct observation of growth and collapse of a Bose-Einstein condensate with attractive interactions. *Nature*, **408**(692), 2000.
- [35] C. A. Sackett and R. G. Hulet. Dynamics of Bose-Einstein condensation in a gas with attractive interactions. *J. Opt. B: Quantum Semiclass. Opt.*, **3**(R1), 2001.
- [36] T. Fukuhara, S. Sugawa, and Y. Takahashi. Bose-Einstein condensation of an ytterbium isotope. *Phys. Rev. A*, **76**(051604(R)), 2007.

- [37] S. Sugawa, R. Yamazaki, S. Taie, and Y. Takahashi. Bose-Einstein condensate in gases of rare atomic species. *Rev. Rev. A*, **84**(011610(R)), 2011.
- [38] A. E. Leanhardt, T. A. Pasquini, M. Saba, A. Schirotzek, Y. Shin, D. Kielpinski, D. E. Pritchard, and W. Ketterle. Cooling Bose-Einstein condensates below 500 picokelvin. *Science*, **301**(1513), 2003.
- [39] J. Klaers, J. Schmitt, F. Vewinger, and M. Weitz. Bose-Einstein condensation of photons in an optical microcavity. *Nature*, **468**(545), 2010.
- [40] J. Klaers, J. Schmitt, T. Damm, F. Vewinger, and M. Weitz. Statistical physics of Bose-Einstein-condensed light in a dye microcavity. *Phys. Rev. Lett.*, **108**(160403), 2012.
- [41] C. J. Myatt, E. A. Burt, R. W. Ghrist, E. A. Cornell, and C. E. Wieman. Production of two overlapping Bose-Einstein condensates by sympathetic cooling. *Phys. Rev. Lett.*, **78**(586), 1997.
- [42] E. Timmermans and R. Côté. Superfluidity in sympathetic cooling with atomic Bose-Einstein condensates. *Phys. Rev. Lett.*, **80**(3419), 1998.
- [43] Z. Idziaszek, L. Santos, and M. Lewenstein. Laser cooling of trapped Fermi gases far below the Fermi temperature. *Phys. Rev. A*, **64**(051402(R)), 2001.
- [44] C. A. Regal and D. S. Jin. Measurement of positive and negative scattering lengths in a Fermi gas of atoms. *Phys. Rev. Lett.*, **90**(230404), 2003.
- [45] C. Chin and R. Grimm. Feshbach resonances in ultracold gases. *Rev. Mod. Phys.*, **82**(1225), 2010.
- [46] C. A. R. Sá de Melo, M. Randeria, and J. R. Engelbrecht. Crossover from BCS to Bose superconductivity: Transition temperature and time-dependent Ginzburg-Landau theory. *Phys. Rev. Lett.*, **71**(3202), 1993.
- [47] M. Randeria, C. A. R. Sá de Melo, and J. R. Engelbrecht. Crossover from BCS to Bose superconductivity: A functional integral approach. *Physica B*, **194**(1409), 1994.

-
- [48] R. Haussmann, W. Rantner, S. Cerrito, and W. Zwerger. Thermodynamics of the BCS-BEC crossover. *Phys. Rev. A*, **75**(023610), 2007.
- [49] C. A. Regal, C. Ticknor, J. L. Bohn, and D. S. Jin. Creation of ultracold molecules from a Fermi gas of atoms. *Nature*, **424**(47), 2003.
- [50] K. E. Strecker, G. B. Partridge, and R. G. Hulet. Conversion of an Atomic Fermi Gas to a Long-Lived Molecular Bose Gas. *Phys. Rev. Lett.*, **91**(080406), 2003.
- [51] J. Cubizolles, T. Bourdel, S. J. J. M. F. Kokkelmans, G.V. Shlyapnikov, and C. Salomon. Production of Long-Lived Ultracold Li_2 Molecules from a Fermi Gas. *Phys. Rev. Lett.*, **91**(240401), 2003.
- [52] M. Greiner, C. A. Regal, and D. S. Jin. Emergence of a molecular Bose-Einstein condensate from a Fermi gas. *Nature*, **426**(537), 2003.
- [53] S. Jochim, M. Bartenstein, A. Altmeyer, G. Hendl, S. Riedl, C. Chin, J. Hecker Denschlag, and R. Grimm. Bose-Einstein condensation of molecules. *Science*, **302**(2101), 2003.
- [54] M. W. Zwierlein, C. A. Stan, C. H. Schunck, S. M. F. Raupach, S. Gupta, Z. Hadzibabic, and W. Ketterle. Observation of Bose-Einstein condensation of molecules. *Phys. Rev. Lett.*, **91**(250401), 2003.
- [55] J. Bardeen, L. N. Cooper, and J. R. Schrieffer. Microscopic theory of superconductivity. *Phys. Rev.*, **106**(162), 1957.
- [56] J. Bardeen, L. N. Cooper, and J. R. Schrieffer. Theory of superconductivity. *Phys. Rev.*, **108**(1189), 1957.
- [57] M. Imada, A. Fujimori, and Y. Tokura. Metal-insulator transitions. *Rev. Mod. Phys.*, **70**(1039), 1998.
- [58] R. Peierls and N. F. Mott. Discussion of the paper by de Boer and Verwey. *Proc. Phys. Soc.*, **49**(72), 1937.
- [59] J. Hubbard. Electron Correlations in Narrow Energy Bands. *Proc. R. Soc. London, Ser. A*, **276**(238), 1963.

- [60] M. P. A. Fisher, P. B. Weichman, G. Grinstein, and D. S. Fisher. Boson localization and the superfluid-insulator transition. *Phys. Rev. B*, **40**(546), 1989.
- [61] S. Sachdev. *Quantum Phase Transitions*. Cambridge University Press, 1999.
- [62] D. Jaksch, C. Bruder, J. I. Cirac, C. W. Gardiner, and P. Zoller. Cold bosonic atoms in optical lattices. *Phys. Rev. Lett.*, **81**(3108), 1998.
- [63] G. H. Wannier. The Structure of Electronic Excitation Levels in Insulating Crystals. *Phys. Rev.*, **52**(191), 1937.
- [64] G. H. Wannier. Dynamics of Band Electrons in Electric and Magnetic Fields. *Rev. Mod. Phys.*, **34**(645), 1962.
- [65] R. Grimm, M. Weidemüller, and Y. B. Ovchinnikov. Optical dipole traps for neutral atoms. *Adv. At., Mol., Opt. Phys.*, **42**(95), 2000.
- [66] P. Navez and R. Schützhold. Emergence of coherence in the Mott-insulator-superfluid quench of the Bose-Hubbard model. *Phys. Rev. A*, **82**(063603), 2010.
- [67] C. N. Yang. Concept of off-diagonal long-range order and the quantum phases of liquid He and of superconductors. *Rev. Mod. Phys.*, **34**(694), 1962.
- [68] A. J. Legget. *Quantum Liquids*. Oxford University Press, 2006.
- [69] P. Braun-Munzinger and J. Stachel. The quest for the quark-gluon plasma. *Nature*, **448**(302), 2007.
- [70] K. Aamodt et al. Elliptic Flow of Charged Particles in Pb-Pb Collisions at $\sqrt{s_{NN}} = 2,76 \text{ TeV}$. *Phys. Rev. Lett.*, **105**(252302), 2010.
- [71] G. Aad et al. Observation of a Centrality-Dependent Dijet Asymmetry in Lead-Lead Collisions at $\sqrt{s_{NN}} = 2,76 \text{ TeV}$ with the ATLAS Detector at the LHC. *Phys. Rev. Lett.*, **105**(252303), 2010.
- [72] J. D. van der Waals. *Over de Continuïteit van den Gas- en Vloeistoof-toestand*. Dissertation, University of Leiden, 1873.

-
- [73] E. A. Guggenheim. The principle of corresponding states. *J. Chem. Phys.*, **13**(253), 1945.
- [74] J. M. Yeomans. *Statistical Mechanics of Phase Transitions*. Oxford University Press, 1992.
- [75] C. N. Yang and T. D. Lee. Statistical Theory of Equations of State and Phase Transitions. I. Theory of Condensation. *Phys. Rev.*, **87**(404), 1952.
- [76] W. Nolting. *Grundkurs Theoretische Physik 6: Statistische Physik*. Springer-Verlag, 4. edition, 2002.
- [77] L. P. Kadanoff. More is the Same; Phase Transitions and Mean Field Theories. *J. Stat. Phys.*, **137**(777), 2009.
- [78] P. Weiss. L'hypothèse du champ moléculaire et la ferromagnétique. *J. Phys. Theor. Appl.*, **6**(661), 1907.
- [79] P. Weiss. Molekulares Feld und Ferromagnetismus. *Physikalische Zeitschrift*, **9**(358), 1908.
- [80] M. Blasone, G. Vitiello, and P. Jizba. *Quantum Field Theory And Its Macroscopic Manifestations*. Imperial College Press, 2011.
- [81] H. Kleinert and V. Schulte-Frohlinde. *Critical Properties of ϕ^4 -Theories*. World Scientific, 2001.
- [82] M. Cyrot. Ginzburg-Landau theory for superconductors. *Rep. Prog. Phys.*, **36**(103), 1973.
- [83] L. D. Landau. *Phys. Z. Sow.*, **11**(26), 1937. English translation: Collected Papers of Landau, L.D., ter Haar, D. (eds.), 193-215. Pergamon Press, (1965).
- [84] T. H. Berlin and M. Kac. The spherical model of a Ferromagnet. *Phys. Rev*, **86**(821), 1952.
- [85] H. E. Stanley. Spherical model as the limit of infinite spin dimensionality. *Phys. Rev.*, **176**(718), 1968.

- [86] P. G. de Gennes. Exponents for the Excluded Volume Problem as Derived by the Wilson Method. *Phys. Lett.*, **38A**(339), 1972.
- [87] J. J. Binney, N. J. Dowrick, A. J. Fisher, and M. E. J. Newman. *The Theory of Critical Phenomena*. Oxford University Press, 1998.
- [88] R. Balian and G. Toulouse. Critical Exponents for Transition with $n = -2$ Components of the Order Parameter. *Phys. Rev. Lett.*, **30**(544), 1973.
- [89] M. E. Fisher. Classical, n -Component Spin Systems or Fields with Negative Even Integral n . *Phys. Rev. Lett.*, **30**(679), 1973.
- [90] M. E. Fisher. The renormalization group in the theory of critical behavior. *Rev. Mod. Phys.*, **4**(597), 1974.
- [91] P. A. Fleury. Phase Transitions, Critical Phenomena, and Instabilities. *Science*, **211**(125), 1981.
- [92] C. Domb and M. S. Green. *Phase Transitions and Critical Phenomena*, volume 6. Academic Press, 1976.
- [93] K. G. Wilson and J. Kogut. The renormalization group and the ϵ Expansion. *Phys. Rep.*, **12**(75), 1974.
- [94] K. G. Wilson. The renormalization group and critical phenomena. *Rev. Mod. Phys.*, **55**(583), 1983.
- [95] M. Strösser, S.A. Larin, M. Mönnigmann, and V. Dohm. Renormalization-group predictions of universal critical-point amplitude ratios. 1998. Proceedings of the 1998 NASA/JPL Workshop on Fundamental Physics in Microgravity.
- [96] J. Zinn-Justin. *Quantum Field Theory And Critical Phenomena*. Oxford University Press, 4. edition, 2002.
- [97] H. Kleinert and V. Schulte-Frohlinde. Critical exponents from five-loop strong-coupling ϕ^4 theory in $4 - \epsilon$ dimensions. *J. Phys. A*, **34**(1037), 2001.

-
- [98] R. Guida and J. Zinn-Justin. Critical exponents of the \mathbf{N} -vector model. *J. Phys. A*, **31**(8103), 1998.
- [99] H. Kleinert. Variational interpolation algorithm between weak- and strong-coupling expansions - application to the polaron. *Phys. Lett. A*, **207**(133), 1995.
- [100] H. Kleinert. Strong-coupling behavior of ϕ^4 theories and critical exponents. *Phys. Rev. D*, **57**(2264), 1998.
- [101] H. Kleinert. Addendum to "Strong-coupling behavior of ϕ^4 theories and critical exponents". *Phys. Rev. D*, **58**(107702), 1998.
- [102] H. Kleinert. Theory and satellite experiment for critical exponent α of λ -transition in superfluid helium. *Phys. Lett. A*, **277**(205), 2000.
- [103] M. Campostrini, M. Hasenbusch, A. Pelissetto, P. Rossi, and E. Vicari. Critical behavior of three-dimensional XY universality class. *Phys. Rev. B*, **63**(214503), 2001.
- [104] L. Onsager. Crystal statistics. I. A two-dimensional model with an order-disorder transition. *Phys. Rev.*, **65**(117), 1944.
- [105] B. Kaufman. Crystal statistics. II. Partition function evaluated by spinor analysis. *Phys. Rev.*, **76**(1232), 1949.
- [106] N. D. Mermin and H. Wagner. Absence of Ferromagnetism or antiferromagnetism in one- or two-dimensional isotropic Heisenberg models. *Phys. Rev. Lett.*, **17**(1133), 1966.
- [107] P. C. Hohenberg. Existence of long-range order in one and two dimensions. *Phys. Rev.*, **158**(383), 1966.
- [108] A. Gelfert and W. Nolting. The absence of finite-temperature phase transitions in low-dimensional many-body models: a survey and new results. *J. Phys.:Condens. Matter*, **13**(R505), 2001.
- [109] L. D. Landau and E. M. Lifshitz. *Statistical Physics, Part 1*, volume 5. Pergamon Press, 3. edition, 1980.

- [110] N. Theodorakopoulos. Phase transitions in one dimensions: Are they all driven by domain walls? *Physica D*, **216**(185), 2006.
- [111] J. Goldstone, A. Salam, and S. Weinberg. Broken Symmetries. *Phys. Rev.*, **127**(965), 1962.
- [112] J. M. Kosterlitz and D. J. Thouless. Ordering, metastability and phase transitions in two-dimensional systems. *J. Phys. C*, **6**(1181), 1973.
- [113] Z. Hadzibabic, P. Krüger, M. Cheneau, B. Battelier, and J. Dalibard. Berezinskii-Kosterlitz-Thouless crossover in a trapped atomic gas. *Nature*, **441**(1118), 2006.
- [114] J. M. Kosterlitz. The critical properties of the two dimensional xy model. *J. Phys. C*, **7**(1046), 1974.
- [115] J.-K. Kim. Phase transitions in the two-dimensional classical XY model. *Phys. Lett. A*, **223**(261), 1996.
- [116] K. J. Strandburg. Two-dimensional melting. *Rev. Mod. Phys.*, **60**(161), 1988.
- [117] J. Corson, R. Mallozzi, J. Orenstein, J. N. Eckstein, and I. Bozovic. Vanishing of phase coherence in underdoped $Bi_2Sr_2CaCu_2O_{8+\delta}$. *Nature*, **398**(221), 1999.
- [118] H. W. J. Blöte, W. Guo, and H. J. Hilhorst. Phase transition in a two-dimensional Heisenberg model. *Phys. Rev. Lett.*, **88**(047203), 2002.
- [119] S. Caracciolo and A. Pelissetto. Two-dimensional Heisenberg model with nonlinear interactions. *Phys. Rev. E*, **66**(016120), 2002.
- [120] G. S. Rushbrooke. On the thermodynamics of the critical region for the Ising problem. *J. Chem. Phys.*, **39**(842), 1963.
- [121] B. D. Josephson. Relation between the superfluid density and the order parameter for superfluid He near T_c . *Phys. Lett.*, **21**(608), 1966.
- [122] J. A. Tyson and D. H. Douglass, Jr. Superfluid density and scaling laws for liquid Helium near T_λ . *Phys. Rev. Lett.*, **17**(472), 1966.

-
- [123] J. Rudnick and D. Jasnow. Renormalization-group proof of Josephson's relation and ϵ expansion for helicity modulus (superfluid density). *Phys. Rev. B*, **16**(2032), 1977.
- [124] C. Domb and M. S. Green. *Phase Transitions and Critical Phenomena*, volume 3. Academic Press, 1974.
- [125] A. M. Kahn and G. Ahlers. Thermal conductivity of ^4He near the superfluid transition in a restricted geometry. *Phys. Rev. Lett.*, **74**(944), 1994.
- [126] D. Murphy, E. Genio, G. Ahlers, F. Liu, and Y. Liu. Finite-size scaling and universality of the thermal resistivity of liquid ^4He near T_λ . *Phys. Rev. Lett.*, **90**(025301), 2003.
- [127] J. Mayers. Bose-Einstein condensation and two fluid behavior in ^4He . *Phys. Rev. B*, **74**(014516), 2006.
- [128] G. B. Hess and W. M. Fairbank. Measurements of angular momentum in superfluid helium. *Phys. Rev. Lett.*, **19**(216), 1967.
- [129] J. A. Lipa, J. A. Nissen, and D. A. Stricker. Specific heat of liquid helium in zero gravity very near the lambda point. *Phys. Rev. B*, **68**(174518), 2003.
- [130] D. S. Greywall and G. Ahlers. Second-sound velocity and superfluid density in ^4He under pressure near T_λ . *Phys. Rev. A*, **7**(2145), 1973.
- [131] D. M. Ceperley and E. L. Pollock. Path-integral computation of the low-temperature properties of liquid ^4He . *Phys. Rev. Lett.*, **56**(351), 1986.
- [132] M. Barmatz, I. Hahn, J. A. Lipa, and R. V. Duncan. Critical phenomena in microgravity: Past, present, and future. *Rev. Mod. Phys.*, **79**(1), 2007.
- [133] F. Wegner. Corrections to Scaling Laws. *Rev. Rev. B*, **5**(4529), 1972.
- [134] H. R. Glyde, R. T. Azuah, and W. G. Stirling. Condensate, momentum distribution, and final-state effects in liquid ^4He . *Phys. Rev. B*, **62**(14337), 2000.

- [135] T. Donner, S. Ritter, T. Bourdel, A. Öttl, M. Köhl, and T. Esslinger. Critical behavior of a trapped interacting Bose gas. *Science*, **315**(1556), 2007.
- [136] I. Bloch, T. W. Hänsch, and T. Esslinger. Measurement of the spatial coherence of a trapped Bose gas at the phase transition. *Nature*, **403**(166), 2000.
- [137] O. Morsch and M. Oberthaler. Dynamics of Bose-Einstein condensates in optical lattices. *Rev. Mod. Phys.*, **78**(179), 2006.
- [138] N. Gemelke, X. Zhang, C.-L. Hung, and C. Chin. In situ observation of incompressible Mott-insulating domains in ultracold atomic gases. *Nature*, **460**(995), 2009.
- [139] P. Würtz, T. Langen, T. Gericke, A. Koglbauer, and H. Ott. Experimental demonstration of single-site addressability in a two-dimensional optical lattice. *Phys. Rev. Lett.*, **103**(080404), 2009.
- [140] W. S. Bakr, A. Peng, M. E. Tai, R. Ma, J. Simon, S. Fölling, L. Pollet, and M. Greiner. Probing the superfluid to Mott-insulator transition at the single-atom level. *Science*, **329**(547), 2010.
- [141] J. F. Sherson, C. Weitenberg, M. Endres, M. Cheneau, I. Bloch, and S. Kuhr. Single-atom-resolved fluorescence imaging of an atomic Mott insulator. *Nature*, **467**(68), 2010.
- [142] E. Kapit and E. Mueller. Even-odd correlation functions on an optical lattice. *Phys. Rev. A*, **82**(013644), 2010.
- [143] W. Greiner. *Quantum Mechanics*. Springer, 4. edition, 2000.
- [144] I. Hubač and S. Wilson. On the use of Brillouin-Wigner perturbation theory for many-body systems. *J. Phys. B: At. Mol. Opt. Phys.*, **33**(365), 2000.
- [145] T. Kato. On the convergence of the perturbation method. I. *Progress of Theoretical Physics*, **4**(514), 1949.
- [146] T. Kato. *Perturbation Theory for Linear Operators*. Springer-Verlag, 1976.

-
- [147] M. Langemeyer. Störungstheorie in hohen Ordnungen: Automatisierung und Anwendung auf das eindimensionale, homogene Bose-Hubbard-Modell. Diploma thesis, University of Oldenburg, 2008.
- [148] V. Steenhoff. Automatisierung der Störungsreihe. Seminar paper, University of Oldenburg, 2007.
- [149] A. Eckardt. Process-chain approach to high-order perturbation calculus for quantum lattice models. *Phys. Rev. B*, **79**(195131), 2009.
- [150] R. P. Feynman. Forces in molecules. *Phys. Rev.*, **56**(340), 1939.
- [151] C. Heil and W. von der Linden. Strong coupling expansion for the Bose-Hubbard and the Jaynes-Cummings lattice model. *J. Phys.: Condens. Matter*, **24**(295601), 2012.
- [152] N. Teichmann, D. Hinrichs, M. Holthaus, and A. Eckardt. Bose-Hubbard phase diagram with arbitrary integer filling. *Phys. Rev. B*, **79**(100503(R)), 2009.
- [153] M. P. Gelfand, R. R. P. Singh, and D. A. Huse. Perturbation Expansions for Quantum Many-Body Systems. *J. Stat. Phys.*, **59**(1093), 1990.
- [154] N. Teichmann, D. Hinrichs, M. Holthaus, and A. Eckardt. Process-chain approach to the Bose-Hubbard model: Ground-state properties and phase diagram. *Phys. Rev. B*, **79**(224515), 2009.
- [155] B. Damski and J. Zakrzewski. Mott-insulator phase of the one-dimensional Bose-Hubbard model: A high-order perturbative study. *Phys. Rev. A*, **74**(043609), 2006.
- [156] D. Hinrichs. Diagrammatische Störungstheorie und Anwendung auf das Bose-Hubbard Modell. Diploma thesis, University of Oldenburg, 2009.
- [157] F. E. A. dos Santos and A. Pelster. Quantum phase diagram of bosons in optical lattices. *Phys. Rev. A*, **79**(013614), 2009.
- [158] A. J. Legget. Superfluidity. *Rev. Mod. Phys.*, **71**(S318), 1999.

- [159] B. S. Shastry and B. Sutherland. Twisted boundary conditions and effective mass in Heisenberg-Ising and Hubbard rings. *Phys. Rev. Lett.*, **65**(243), 1990.
- [160] M. E. Fisher, M. N. Barber, and D. Jasnow. Helicity modulus, superfluidity, and scaling in isotropic systems. *Phys. Rev. A*, **8**(1111), 1973.
- [161] R. Roth and K. Burnett. Superfluidity and interference pattern of ultracold bosons in optical lattices. *Phys. Rev. A*, **67**(031602(R)), 2003.
- [162] G. A. Baker and P. Graves-Morris. *Padé approximants*. Oxford University Press, 1981.
- [163] P. M. Stevenson. Optimized perturbation theory. *Phys. Rev. D*, **23**(2916), 1981.
- [164] J. K. Freericks and H. Monien. Strong-coupling expansions for the pure and disordered Bose-Hubbard model. *Phys. Rev. B*, **53**(2691), 1996.
- [165] N. Elstner and H. Monien. Dynamics and thermodynamics of the Bose-Hubbard model. *Phys. Rev. B*, 59(12184), 1999.
- [166] G. G. Batrouni and R. T. Scalettar. World-line quantum Monte Carlo algorithm for a one-dimensional Bose model. *Phys. Rev. B*, **46**(9051), 1992.
- [167] S. Wessel, F. Alet, M. Troyer, and G. G. Batrouni. Quantum Monte Carlo simulations of confined bosonic atoms in optical lattices. *Phys. Rev. A*, **70**(053615), 2004.
- [168] B. Capogrosso-Sansone, N. V. Prokof'ev, and B. V. Svistunov. Phase diagram and thermodynamics of the three-dimensional Bose-Hubbard model. *Phys. Rev. B*, **75**(134302), 2007.
- [169] B. Capogrosso-Sansone, Ş. G. Söyler, N. Prokof'ev, and B. Svistunov. Monte Carlo study of the two-dimensional Bose-Hubbard model. *Phys. Rev. A*, **77**(015602), 2008.
- [170] T. D. Kühner and H. Monien. Phases of the one-dimensional Bose-Hubbard model. *Phys. Rev. B*, **58**(14741(R)), 1998.

-
- [171] S. Rapsch, U. Schollwöck and W. Zwerger. Density matrix renormalization group for disordered bosons in one dimension. *Europhys. Lett.*, **46** (559), 1999.
- [172] C. Kollath, U. Schollwöck, J. von Delft, and W. Zwerger. Spatial correlations of trapped one-dimensional bosons in an optical lattice. *Phys. Rev. A*, **69**(031601(R)), 2004.
- [173] C. Kollath, A. M. Läuchli, and E. Altman. Quench Dynamics and Nonequilibrium Phase Diagram of the Bose-Hubbard Model. *Phys. Rev. Lett.*, **98**(180601), 2007.
- [174] M. Knap, E. Arrigoni, and W. von der Linden. Benchmarking the variational cluster approach by means of the one-dimensional Bose-Hubbard model. *Phys. Rev. B*, **81**(2351223), 2010.
- [175] M. Knap, E. Arrigoni, and W. von der Linden. Variational cluster approach for strongly correlated lattice bosons in the superfluid phase. *Phys. Rev. B*, **83**(134507), 2011.
- [176] C. Becker, P. Soltan-Panahi, J. Kronjäger, S. Dörscher, K. Bongs, and K. Sengstock. Ultracold quantum gases in triangular optical lattices. *New J. Phys.*, **12**(065025), 2010.
- [177] G.-B. Jo, J. Guzman, C. K. Thomas, P. Hosur, A. Vishwanath, and D. M. Stamper-Kurn. Ultracold Atoms in a Tunable Optical Kagome Lattice. *Phys. Rev. Lett.*, **108**(045305), 2012.
- [178] N. Teichmann, D. Hinrichs, and M. Holthaus. Reference data for phase diagrams of triangular and hexagonal bosonic lattices. *Europhysics Letters*, **91**(10004), 2010.
- [179] N. Teichmann and D. Hinrichs. Scaling property of the critical hopping parameters for the Bose-Hubbard model. *Eur. Phys. J. B*, **71**(219), 2009.
- [180] B. Bradlyn, F. Ednilson A. dos Santos, and A. Pelster. Effective action approach for quantum phase transitions in bosonic lattices. *Phys. Rev. A*, **79**(013615), 2009.

- [181] E. Arrigoni, M. Knap, and W. von der Linden. Extended self-energy functional approach for strongly correlated lattice bosons in the superfluid phase. *Phys. Rev. B*, **84**(014535), 2011.
- [182] A. Rançon and N. Dupuis. Nonperturbative renormalization group approach to strongly correlated lattice bosons. *Phys. Rev B*, **84**(174513), 2011.

Erklärung gemäß Promotionsordnung

Hiermit versichere ich, dass ich diese Arbeit selbständig verfasst habe und keine anderen als die angegebenen Quellen und Hilfsmittel benutzt habe.

Dennis Hinrichs

Lebenslauf

Persönliche Daten

Dennis Hinrichs
geboren am 27. Juli 1982 in Sögel
Staatsangehörigkeit: deutsch

Schulbildung

1989 – 1993 Bernhardschule Sögel
1993 – 1995 Orientierungsstufe Sögel
1995 – 2002 Hümmling Gymnasium Sögel,
abgeschlossen mit Abitur

Zivildienst

2002 – 2003 Deutsches Rotes Kreuz, Rettungsdienst Sögel

Studium

2003 – 2005 Studium der Physik an der Universität Bielefeld,
abgeschlossen mit Vordiplom
2005 – 2009 Studium der Physik an der Carl von Ossietzky Universität
Oldenburg, Diplomarbeit in der Arbeitsgruppe *Theorie der
kondensierten Materie* unter der Leitung von Prof. Dr. Mar-
tin Holthaus mit dem Titel *Diagrammatische Störungstheorie
und Anwendung auf das Bose-Hubbard Modell*,
abgeschlossen mit Diplom

Promotion

2009 – 2012 Wissenschaftlicher Mitarbeiter an der Carl von Ossietzky Uni-
versität Oldenburg
seit 2009 Doktorand an der Fakultät für Mathematik und Naturwissen-
schaften der Carl von Ossietzky Universität Oldenburg

Publikationen

- Niklas Teichmann, Dennis Hinrichs, and Martin Holthaus:
Reference data for phase diagrams of triangular and hexagonal bosonic lattices,
Europhysics Letters **91**, 10004 (2010).
- Niklas Teichmann and Dennis Hinrichs:
Scaling property of the critical hopping parameters for the Bose-Hubbard model,
Eur. Phys. J. B **71**, 219 (2009).
- Niklas Teichmann, Dennis Hinrichs, Martin Holthaus, and André Eckardt:
Process-chain approach to the Bose-Hubbard model: Groundstate properties and phase diagram,
Phys. Rev. B **79**, 224515 (2009).
- Niklas Teichmann, Dennis Hinrichs, Martin Holthaus, and André Eckardt:
Bose-Hubbard phase diagram with arbitrary integer filling,
Phys. Rev. B **79**, 100503(R) (2009).
- Dave J. Boers, Benjamin Goedeke, Dennis Hinrichs, and Martin Holthaus:
Mobility edges in bichromatic optical lattices,
Phys. Rev. A **75**, 063404 (2007).

Danksagung

Ganz besonders möchte ich mich bei Prof. Dr. Martin Holthaus bedanken. Dadurch, dass er mir immer die Freiheit gelassen hat, selbständig zu forschen, schuf er die für mich optimalen Bedingungen für ein kreatives und motiviertes Arbeiten. Er hatte immer ein offenes Ohr für meine Probleme und nur durch seine Unterstützung und Förderung ist diese Arbeit möglich geworden.

Ferner möchte ich mich herzlich bei Priv.-Doz. Dr. Axel Pelster bedanken. Er hat durch zahlreiche Diskussionen diese Arbeit maßgeblich beeinflusst und viel zu einem erfolgreichen Gelingen meiner Promotion beigetragen. Sein Engagement ging weit über die einer Forschungskoooperation hinaus. Nicht zuletzt hat er sich bereit erklärt, das Koreferat dieser Arbeit zu übernehmen, wofür ich mich gesondert bedanken möchte.

Besonders viel Glück hatte ich bei der Zusammenstellung meiner Kollegen. Die viel zu kurze Zusammenarbeit mit Niklas Teichmann war nicht nur sehr erfolgreich, sie war auch immer mit viel Spaß verbunden. Beim Wettrennen mit Stephan Arlinghaus, Bettina Gertjerenken und Matthias Langemeyer zur Promotion bin ich zwar nur Zweiter geworden, die vielen lustigen Stunden, die wir insbesondere auf den Tagungen hatten, machen das aber mehr als wett. Außerdem möchte ich mich bei den CondMatlern Svend-Age Biehs, André Eckardt, Oliver Huth, Felix Rüting und Maria Tschikin für viele wertvolle Diskussionen und die gemeinsam gemachten Erfahrungen bedanken.

Von ganzem Herzen möchte ich meiner Familie für ihren uneingeschränkten Rückhalt danken. Insbesondere meine Eltern Egon und Marlies Hinrichs haben mich immer bedingungslos unterstützt.